INFLUENCE OF CELLULAR LOCALIZATION ON ACTIVITY OF

HYDROXYSTEROID DEHYDROGENASES

APPROVED BY SUPERVISORY COMMITTEE

_____

Richard Auchus, M.D. Ph.D.

_____

Joel Goodman, Ph.D.

_____

Margaret Phillips, Ph.D.

_____

Joyce Repa, Ph.D.

_____

Diana Tomchick, Ph.D.

To my parents, Patricia and Michael Wooding, and wife, Catherine Wooding,

for all your love, and support.

In fond memory of my inspirational friend, Adam Oneto.

INFLUENCE OF CELLULAR LOCALIZATION ON ACTIVITY OF HYDROXYSTEROID DEHYDROGENASES

by

KERRY MICHAEL WOODING

DISSERTATION

Presented to the Faculty of the Graduate School of Biomedical Sciences

The University of Texas Southwestern Medical Center at Dallas

In Partial Fulfillment of the Requirements

For the Degree of

DOCTOR OF PHILOSOPHY

The University of Texas Southwestern Medical Center at Dallas

Dallas, Texas

July, 2011

Acknowledgements

As I finish my graduate school education and transition into a postdoctoral position, I reflect back to the beginning, and am humbled by the number of individuals who have helped, educated, guided, aided, and encouraged me during the long and arduous process to successfully complete my Ph.D. The list of individuals is too long to accurately document but to all who have helped me during my time in graduate school; I am forever grateful to you and offer a heartfelt and sincere "Thank You!" I can never repay you for your efforts but can honor you by paying it forward in helping aspiring scientists succeed.

First and foremost, I thank my mentor, Richard Auchus. Your infectious enthusiasm for science was always apparent and invigorating. I am forever grateful to you for all the time, hard work and effort you gave in mentoring me. I appreciate the encouragement and guidance when experiments did not turn out as expected. I have tried to emulate your presentation style of pure joy and excitement but will always come up short when compared to you. My success is a direct reflection of your efforts. I am honored to be your first Ph.D. student and will reflect fondly on my experiences with you.

I would like to thank my dissertation committee, Joel Goodman, Margaret Phillips, Joyce Repa and Diana Tomchick, for their genuine interest, support, and guidance during the course of my dissertation project. Your constructive criticism was always paired with encouragement. I appreciate the input from all of you and

regret not utilizing your expertise more. It has been a real pleasure to learn from all of you during committee meetings, journal clubs, courses and WIPS.

I am deeply indebted to my wonderful lab members. Dario Mizrachi spent much time guiding me through experimental design, troubleshooting, and engaging in numerous intellectually stimulating conversations. You enlightened me to a different perspective and approach in addressing scientific problems. I am thankful for the time I spent with you and will greatly miss you. I wish you the best of luck in your future scientific endeavors in Israel. I need to thank Mahoubeh Papari-Zareei for patiently teaching me numerous cell culture and PCR techniques. You were a wonderful lab manager who kept the daily lab operations running smoothly. We did not fully realize and appreciate all you did until you left! I would like to thank David Vance and Team Chemie, Francis Yoshimoto and Kamalesh Sharma, for being wonderful lab mates, and enlightening me to the worlds of small molecule mass spectrometry, synthetic chemistry and steroid hormone purification. I am thankful to Francis for his time and energy in teaching me the difficult task of radiolabeled steroid hormone purification. His efforts allowed us to synthesize and purify our own radiolabeled cortisone, which was used in a number of important experiments. I need to thank former lab member Melissa Rasar Young for helping with some rather troublesome cloning.

I thank my close friend, former roommate, groomsman, and best friend in graduate school Juan Mendoza for all of his help with troubleshooting Quickchange PCR reactions. Before Juan helped me, we struggled to optimize the reaction conditions. After Juan helped, we generated more clones than we could

assess! I am incredibly thankful for all the time spent with you in and out of lab. I reflect back and smile at all the fun times we shared. I am also honored and thankful to have gone through qualifying exam and stressful committee meetings with you. I know you have worked hard and the Dean's Discretionary Award you received is testament to that.

I also need to especially thank Hyeilin Ham of the Orth Lab for generating all of the cellular fractionation data. Thank you for your patience and due diligence in performing all those fractionations! Those qualities will take you far in science. Kate Luby-Phelps and Abhijit Bugde were a godsend in helping us generate fluorescence microscopy images. I also need to thank Chris Broberg for his fluorescence microscopy slide-preparation protocols. I need to thank Anil Agarwal for giving cells and various constructs whenever we requested them.

Anyone that knows me well, knows about my passion for volleyball. I have thoroughly enjoyed being a part of the Dallas volleyball community. I would like to thank Charlie Nigrelli for numerous on and off the court memories, especially for introducing me to my wife, Catherine. I thank Zachary Matzen for being a steadfastly loyal teammate since I arrived in Dallas. I thank Jenny Barker for taking me under her wing and introducing me to the world of coaching adolescent girls' club volleyball. It was a wonderful experience I will never forget. I would also like to thank the 900 Volleyball Club directors, Meredith and Ryan Grady, for the opportunity to coach with Jenny as well as play in Adult Nationals! I would like to thank all those that I have played with and against since I arrived in Dallas. It has been a real pleasure to play with all of you!

I thank Brad and Scott Mezei for their wonderful friendship over the years. I speed skated with them in our grade school days and reconnected with them upon my arrival in Dallas. The two of you have provided a much needed retreat from graduate school. I am thankful for all that the two of you have given me.

I am grateful to Yohan Lee for all of his encouragement and support during our undergraduate and graduate school days. You have been a wonderful friend over the years, providing an ear for me whenever I needed it. I am thankful and blessed to have you as a close friend.

I thank my parents, Patricia and Michael Wooding, for all of their love and support during the trials and tribulations graduate school presented. I appreciate the numerous sacrifices repeatedly made over the years and am forever indebted to both of you for the selfless love you showed me. Without your love and support over my lifetime, I would not have the opportunities that I do. I can never repay you but I potentially offset some of the debt with grandchildren…someday.

Last, but certainly not least, I would like to thank my wife, Catherine Wooding. I know that I am incredibly blessed to be married to you and that has become readily apparent as I write this. You have loved me unconditionally and believed in me before I ever did. You believed that I could finish graduate school, despite the obstacles put in my way. You stood by my side and weathered life's storms with me. I am forever thankful and blessed beyond my wildest dreams to be married to you.

INFLUENCE OF CELLULAR LOCALIZATION ON ACTIVITY OF HYDROXYSTEROID DEHYDROGENASES

KERRY MICHAEL WOODING

The University of Texas Southwestern Medical Center at Dallas, GRADUATION YEAR

RICHARD J. AUCHUS, M.D. Ph.D.

Hydroxysteroid dehydrogenases (HSDs) catalyze the interconversion of inactive steroids and active hormones. HSDs use nicotinamide cofactors in the cytosol and endoplasmic reticulum (ER) lumen to either reduce or oxidize their steroid substrates. Our lab has extensively studied the 17β-HSDs types 1, 2 and 3 of the short-chain oxidoreductase family, particularly human 17β-HSD1, which favors estrone reduction to estradiol. Rat AKR1C9 has also been thoroughly studied as a model HSD of the aldo-keto reductase family; AKR1C9 catalyzes the reduction of dihydrotestosterone to androstanediol. These two enzymes provide a

basis for comparative studies with 11β-HSD1, which catalyzes the reduction of cortisone to cortisol.

Most mammalian cells supplied with adequate glucose and oxygen maintain cytoplasmic high nicotinamide concentration gradients, [NADPH] >> [$NADP^+$] and [NAD^+] >> [NADH], and in the strongly oxidizing environment of the ER lumen, both these gradients are shifted to more oxidized cofactor. Whereas 17βHSD types 1, 2, 3 and AKR1C9 catalyze their respective reactions in a thermodynamically predictable manner based on cofactor gradients, 11β-HSD1 does the opposite. 17β-HSD1, 17β-HSD3, and AKR1C9 favor reduction in the cytosol using NADPH, and 17β-HSD2 favors oxidation in the ER lumen using NAD^+. In contrast, 11β-HSD1 reduces cortisone to cortisol in the highly oxidative ER lumen but requires hexose-6-phosphate-dehydrogenase (H6PD) to regenerate NADPH in the ER lumen. We hypothesize that H6PD directly channels NADPH to 11β-HSD1 through specific interactions.

To test this hypothesis, we have targeted 17β-HSD1 and AKR1C9 to the ER lumen rather than the cytosol. Conversely, we have targeted 11β-HSD1 to the cytoplasmic surface of the ER. In addition, we have engineered point mutations in 17β-HSD1, AKR1C9, 11β-HSD1 and H6PD, designed to attenuate the directional preferences by altering cofactor binding. Targeting and retaining 17β-HSD1 in the ER lumen proved troublesome; regardless of the transfection conditions, ER-targeted 17β-HSD1 was always detected in the cytosol. We conclude that either 17β-HSD1's activity or structure causes its translocation to the cytosol.

Table of Contents

Prior Publications

Mizrachi D, **Wooding KM**, Tomchick D, and Auchus RJ "Crystal structure of an abortive complex of mutant 17βHSD1 (R38G) with NAD^+ and estrone sheds light on cofactor affinity" *In Preparation*

Liu CW, Li X, Thompson D, **Wooding K**, Chang TL, Tang Z, Yu H, Thomas PJ, DeMartino GN, "ATP Binding and ATP Hydrolysis Play Distinct Roles in the Function of 26S Proteasome." Molecular Cell, Oct 6, 2006; 24(1):39-50

Loo JA, Berhane B, Kaddis CS, **Wooding KM**, Xie Y, Kaufman SL and Chernushevich IV, "Electrospray Ionization Mass Spectrometry and Ion Mobility Analysis of the 20S Proteasome Complex", Journal of the American Society for Mass Spectrometry, July 2005 16(7): 998-1008

LIST OF FIGURES

LIST OF TABLES

List of Abbreviations

11β-HSD1 - 11 Beta Hydrozysteroid Dehydrogenase Type 1

17β-HSD1 - 17 Beta Hydroxysteroid Dehydrogenase Type 1

17β-HSD2 - 17 Beta Hydroxysteroid Dehydrogenase Type 2

17β-HSD3 - 17 Beta Hydroxysteroid Dehydrogenase Type 3

2-DG - 2-Deoxyglucose

Adiol - Androstanediol

AKR - Aldo-Keto Reductase

AKR1C9 - Aldo-Keto Reductase Type 1C9

CHO - Chinese Hamster Ovary Cells

CM : Complete Media

DHT - Dihydrotestosterone

E1 - Estrone

E2 - Estradiol

ER - Endoplasmic Reticulum

ERAD : Endoplasmic Reticulum Associated Degradation

-F - FLAG

G6PD - Glucose-6-Phosphate Dehydrogenase

GFP - Green Fluorescent Protein

H6PD - Hexose-6-Phosphate Dehydrogenase

HEK293 - Human Embryonic Kidney Cells

HEK293T - Human Embryonic Kidney Cells with Overexpressed Large T-antigen

HIF-2α - Hypoxia-Inducible Factor 2α

hrs - Hours

HSD - Hydroxysteroid Dehydrogenase

K - KDEL

MW - Molecular Weight

NAD+ - Nicotinamide Adenine Dinucleotide, Oxidized Form

NADH - Nicotinamide Adenine Dinucleotide, Reduced Form

NADP+ - Nicotinamide Adenine Dinucleotide Phosphate, Oxidized Form

NADPH - Nicotinamide Adenine Dinucleotide Phosphate, Reduced Form

P1 : Pellet 1

P2 : Pellet 2

P3: Pellet 3

RFP - Red Fluorescent Protein

S3: Supernatant 3

SDR - Short-chain Dehydrogenase / Reductase

SHBG - sex-hormone binding protein

ss - signal sequence

TLC - Thin Layer Chromatography

μM - Micromolar

WT - Wild-type

α-PDI - Alpha Protein Disulfide Isomerase

Chapter 1

Introduction

Steroid hormones are potent signaling molecules important for organism homeostasis and maturation (Griffin 2004). Their importance is highlighted through deficiencies in regulation; they have been associated with breast cancer (Chen 2008), prostate cancer (Bosland 2000), metabolic syndrome and obesity (Fortunati 2010). Understanding steroid hormone regulation has the potential to positively impact a number of people and improve their lives.

Cholesterol serves as the starting material for all steroid hormone synthesis, known as steroidogenesis (Miller 2011). After cholesterol is converted to pregnenolone by cytochrome P450scc in the first committed step of steroidogenesis, a number of different enzyme cascades, consisting of cytochrome P450s and hydroxysteroid dehydrogenase (HSD) enzymes, produce different steroid hormones (FIGURE 1.1, Miller 2011). The steroid hormones are released into the blood stream where they circulate largely bound to plasma proteins and are either further metabolized or transported to target tissues (Attanasov 2010, Rosner 2010). In order for a cell to respond to the steroid hormone, a hormone receptor must be present. Once the steroid hormone binds to a nuclear hormone receptor, transcription cascades are initiated, and the effect of the steroid hormone is observed (FIGURE 1.2, Griffin 1992). HSD enzymes are vital in maintaining

the active/inactive state of the steroid hormone; one mechanism for protecting cells that are not intended to respond to the steroid hormone is an HSD that inactivates said hormone. The inactive hormone either diffuses or is transported out of the cell and back into circulation where it can be either excreted or transported to tissues that it is intended for; these target tissues have HSDs that regenerate the active form of the steroid hormone.

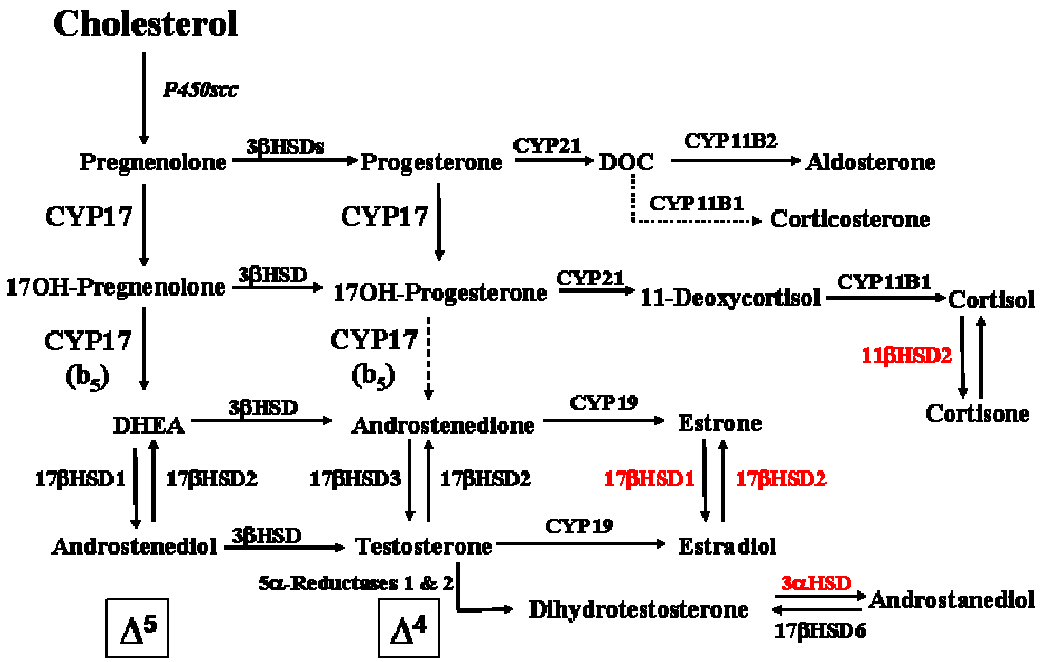

FIGURE 1.1. Major Steroid Biosynthetic Pathways in Human Beings. Note the first and rate-limiting step of steroidogenesis, the conversion of cholesterol to pregnenolone by P450scc in the mitochondria. The red enzymes are the focus of the dissertation research. Note they are at the terminal steroidogenic step of their respective steroid hormones. Slide courtesy of Richard Auchus M.D. Ph.D.

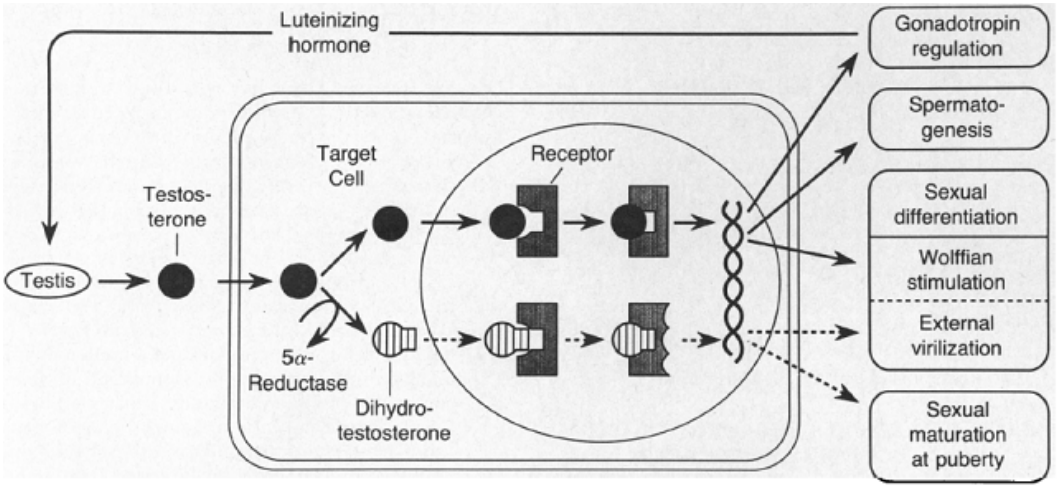

FIGURE 1.2. Steroid Hormone Mechanism of Action. Steroid hormones are synthesized in their respective tissue and secreted into the bloodstream. They are taken to their respective tissues where they bind to a hormone receptor (in this case androgens and their receptor) in either the nucleus or cytosol for transport into the nucleus. Once in the nucleus, the receptor-hormone pair act as a transcription factor and initiate gene transcription accordingly. Figure taken from Griffen 1992 illustrating testosterone's mechanism of action.

HSDs can be classified by either their structure or function (FIGURE 1.3). HSDs belong to two major structural classes: short-chain dehydrogenase / reductase (SDR) or aldo-keto reductase (AKR) (Mizrachi 2009). The SDRs share a β-α-β Rossman fold where a beta sheet is sandwiched between alpha helices (Rossman 1972); this is a common structural motif among enzymes binding nicotinamide cofactors (Ma 2008). SDR HSDs are membrane bound and either dimers or tetramers (Mizrachi 2009). The TIM barrel, an α-β pattern resulting in a barrel structure, provides the defining structural motif for AKR enzymes (Banner 1975). AKRs are monomeric and soluble (Mizrachi 2009).

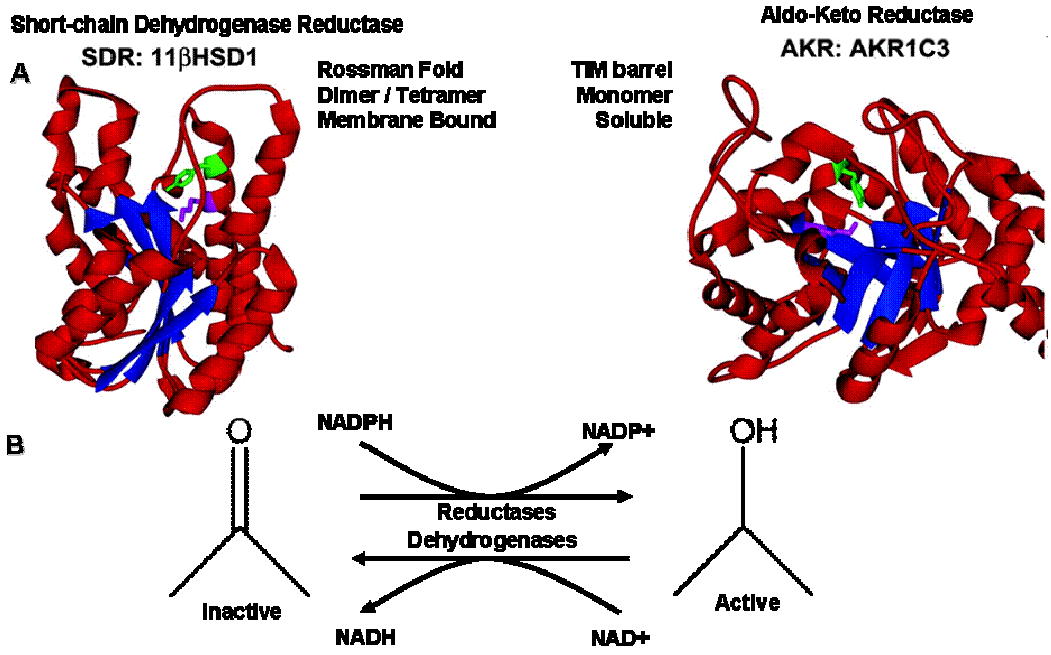

FIGURE 1.3. HSD Classification. HSDs can be classified either structurally or functionally. **A**. The two major HSD structure classes are short-chain dehydrogense / reductase (SDR) or aldo-keto reductase (AKR). Several defining characteristics of each structural family are listed beside the example structure; note the blue beta-sheet and barrel defining the Rossman Fold and TIM barrel. **B.** HSDs are considered reductases if they reduce an inactive ketosteroid to an active hydroxysteroid; conversely, they are considered dehydrogenases if they catalyze the reverse oxidative reaction. Figure adapted from Agarwal and Auchus 2005.

HSDs are traditionally considered as "reductases" if they reduce an inactive ketosteroid to an active hydroxysteroid; they are classified as a "dehydrogenase" if they oxidize an active hydroxysteroid to an inactive ketosteroid (Mizrachi 2009). This classification is not straightforward; many HSD enzymes can catalyze either the reduction or oxidation reaction *in vitro* depending on the reaction's starting conditions, but exhibit a strong directional preference *in*

vivo (Khan 2004). What dictates the direction of this strong directional preference? The concentrations of the two substrates in these reactions are significantly different; cytoplasmic nicotinamide cofactors have been measured in concentrations at the mM range (Veech 1969) while circulating steroid hormones are mostly in the nM-fM range (Griffin 2004). Among the nicotinamide cofactors, there is an uneven distribution with [NADPH and NAD^+] exceeding [$NADP^+$ and NADH] by orders of magnitude (Veech 1969, Williamson 1967, Hwang 1992, Mizrachi 2009). The pentose phosphate pathway maintains high [NADPH] in a well-fed state, while high [NAD^+] results from continuous NADH consumption in numerous cellular processes such as ATP generation and fatty acid oxidation (Agarwal 2005). It has been noted that HSDs using NADPH can also accept NADH, while HSDs utilizing NAD^+ apparently cannot accept $NADP^+$. It has been suggested that a negatively charged glutamic acid residue in the binding pocket presumably repels the negative phosphate group in NADPH for most HSDs (Sherbet 2009). A sequence alignment of several HSDs shows a conserved arginine while others have a conserved glutamic acid instead (TABLE 1.1). The crystal structures of two reductases, 17β-HSD1 and AKR1C9, show this conserved arginine to form a salt-bridge with the phosphate group of NADPH (Sawicki 1999, Bennett 1996). Could this arginine be important for *in vivo* directional preference?

TABLE 1.1 Conserved HSD Nicotinamide Cofactor Binding Residues

		Cofactor	LOOP4
17β-HSD1	Reductase	NADPH	DV**R**DS
17β-HSD2	Dehydrogenase	NAD^+	LN**E**NG
11β-HSD1	Reductase	NADPH	TA**R**SK
11β-HSD2	Dehydrogenase	NAD^+	VL**E**LN

Table courtesy of Dario Mizrachi, Ph.D.

To test this hypothesis, two well-studied enzymes were used, 17β-HSD1 and AKR1C9. 17β-HSD1 catalyzes the reduction of inactive estrone (E1) to the active estradiol (E2) using NADPH *in vivo* (Luu-The 1995). The crystal structure of human 17β-HSD1 shows R38 coordinating the phosphate group of NADPH (Sawicki 1999). AKR1C9 catalyzes the reduction of dihydrotestosterone (DHT) to androstanediol (Adiol) with NADPH (Cooper 2007). The crystal structure of AKR1C9 shows R276 coordinating NADPH's phosphate group (Bennett 1996). HEK293 cells were transfected with expression constructs of 17β-HSD1 WT and R38 mutants to assess the effect of R38 on the strong *in vivo* directional preference (Sherbet 2009); replacement of the positively charged arginine with a neutral or negative amino acid resulted in a lower E2/E1 ratio at steady-state. An analogous result was observed with AKR1C9; when R276 was mutated glutamate, the mutation favored Adiol oxidation to 90% DHT (Papari-Zareei 2006). Replacing high-glucose media with low-glucose media causes a reduction

in E2 and Adiol production in cells transfected with 17β-HSD1 or AKR1C9 expression constructs. Thus, these two enzymes behave as expected: when the ability of the enzyme to bind NADPH is compromised, a decrease in reductive activity is observed.

Do these same principles apply to all HSDs? 17β-HSD1 and AKR1C9 are cytosolic enzymes that utilize the high cytosolic [NADPH] to catalyze a reductive reaction. In the oxidative environment of the ER lumen, 11β-HSD1 catalyzes a reductive reaction; it reduces cortisone to cortisol (TABLE 1.2 for comparison of all three enzymes). Other HSD enzymes reside in the ER lumen, but these favor oxidation as predicted, e.g. 17β-HSD2 oxidizes estradiol to estrone using NAD^+. How can a reductive enzyme catalyze its reaction in an oxidative environment?

TABLE 1.2 Comparison of 17β-HSD1 , AKR1C9 and 11β-HSD1

	17β-HSD1	**AKR1C9**	**11β-HSD1**
Structural Fold	SDR	AKR	SDR
Multimer	Dimer	Monomer	Dimer
Molecular Weight	34kDa	37kDa	34kDa
Soluble / Membrane Bound	Soluble	Soluble	Membrane Bound
Cellular Location	Cytosol	Cytosol	ER lumen
Km NADPH	2.1μM (Heyns 1974)	0.08μM (Cooper 2007)	0.1-0.3μM (Moore 1993)
***In vivo* Reaction**	E1 Reduction	DHT Reduction	Cortisone Reduction
Reaction Mechanism	Random Sequential (Negri 2010)	Ordered Bi-Bi (Cooper 2007)	?

SDR: Short-Chain Dehydrogenase / Reductase

AKR: Aldo-Keto Reductase

Hexose-6-phosphate dehydrogenase (H6PD) regenerates NADPH in the ER lumen using glucose 6-phosphate; the ER and cytosolic nicotinamide cofactor pools do not mix, requiring separate regenerating mechanisms (Lavery 2006). H6PD has been shown to co-localize with 11β-HSD1 through immunoprecipitation and fluorescence microscopy experiments (Kotelevtsev 1997, Atanasov 2008). Furthermore, most patients diagnosed with cortisone reductase deficiency have wild-type 11β-HSD1 but present mutations in H6PD (Lavery 2008).

Substrate channeling occurs when the product of one reaction is transferred directly to another enzyme (Geck 1999, FIGURE 1.4). This has been observed for reaction cascades with unstable intermediates. One way to test for substrate channeling is the use of a catalytically inactive enzyme. For example, in a two step reaction, a catalytically inactive enzyme for the second step which still forms a complex with the first-step enzyme would be titrated into a mixture of active first-step enzyme and active second-step enzyme. If channeling occurs in this two enzyme pathway, the amount of final product observed will decrease with increasing inactive enzyme. If channeling is not required, the inactive enzyme will have no bearing on the rate of product formation. Several prominent examples have been characterized enzymatically and structurally (Huang 2001). Carbamoyl phosphate synthetase is a large protein complex catalyzing the formation of carbamoyl phosphate from bicarbonate, magnesium, ATP and glutamine (Thoden 1999). The unstable metabolic intermediates are channeled between several catalytic sites to protect them from the environment (FIGURE

1.5). Numerous approaches have been used to assess the carbamoyl phosphate synthetase reaction scheme, including the use of point mutations in the proposed hydrophobic tunnels to block passage of intermediates, failure to incorporate various radiolabeled intermediates, and the failure to detect reaction intermediates in the bulk fluid (Huang 2001).

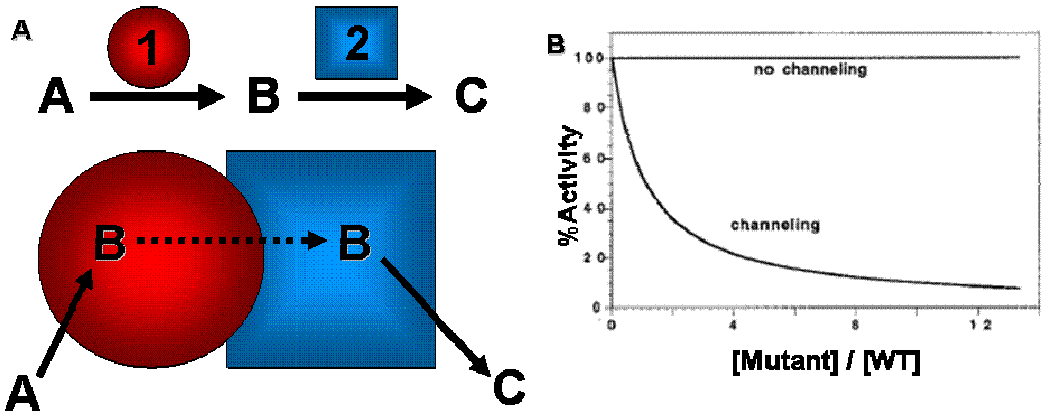

FIGURE 1.4. Substrate Channeling. **A**. Schematic for an enzymatic reaction using channeling. In this example, B never equilibrates with the bulk solvent. **B**. One way to test whether a reaction sequence uses channeling or not is with a catalytically inactive enzyme. In the above example, if the red enzyme was incubated with active blue enzyme and increasing concentrations of inactive blue enzyme, a channeling mechanism would show a decrease in the rate because the red enzymes are being sequestered by inactive blue enzymes. If channeling does not occur, the increase in inactive blue enzyme will have no impact on the reaction rate.

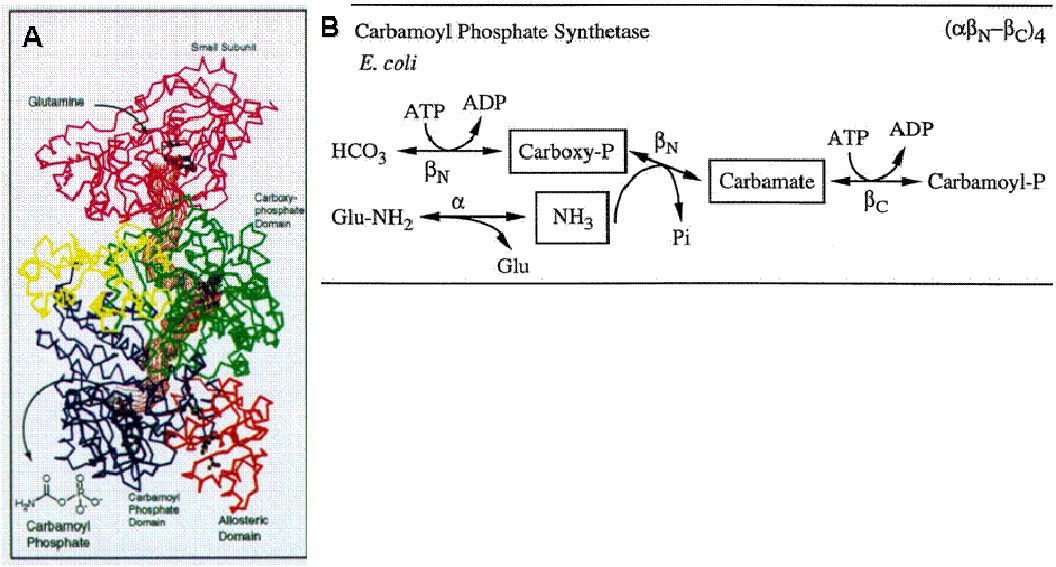

FIGURE 1.5. Carbamoyl Phosphate Synthetase. A. Crystal structure of carbamoyl phosphate synthetase showing several active sites as well as a hydrophobic tunnel (orange) (Figure taken from Thoden 1997). **B**. Reaction scheme for carbamoyl phosphate synthetase (Figure taken from Miles 1999).

We hypothesized that H6PD channels NADPH to 11β-HSD1 in the ER lumen through specific interactions. Several predictions derive from this hypothesis which might be tested experimentally. For example, artificially translocating 11β-HSD1 to the cytosol tests whether 11β-HSD1 can continue to reduce cortisone to cortisol by either utilizing the high cytosolic [NADPH] or forms a complex with glucose-6-phosphate dehydrogenase (G6PD), the major cytosolic NADPH regenerating enzyme of the pentose phosphate pathway. If 11β-HSD1 fails to reduce cortisone to cortisol in the cytosol, this result points towards the importance of complex formation with H6PD for appreciable cortisone reduction activity. In contrast, targeting other reductive HSDs into the ER lumen might result in a reversal to oxidative preference, because these enzymes are

governed by their affinity for cofactors and the free nicotinamide cofactor concentration accessible *in vivo.*

To address these predictions, we used a model of tissue culture HEK293 cells, which have very low basal steroid metabolism. Our laboratory has used this approach in the past to determine steroid equilibrium distributions as well as steady state kinetics in intact cells. An intact cell system is essential to address the questions posed by our research, because purified HSDs catalyze both oxidative and reductive reactions *in vitro* depending on the cofactors supplied to the incubation. In order to interpret our results, we must determine enzyme activity but also demonstrate that the enzymes were targeted to the appropriate intracellular location. These experiments are the topic of this dissertation.

Chapter 2

17β-HSD1 Results

Tagging 17β-HSD1 with FLAG and GFP

To determine the location of 17β-HSD1 constructs, GFP and the FLAG epitope were employed to permit fluorometric and immunometric detection as monoclonal antibodies are now available for both GFP and FLAG (Day 2008). The first constructs made were GFP-17β-HSD1 and GFP-17β-HSD2. To assess whether GFP negatively affected enzyme activity, we transfected HEK293 cells with expression constructs for GFP-17β-HSD1 and GFP-17β-HSD2 and compared their activities to untagged 17β-HSD1 and 17β-HSD2 (FIGURE 2.1). Under conditions where cells expressing wild-type 17β-HSD1 or 17β-HSD2 almost completely converted substrate to product, only partial conversion was observed for cells expressing the GFP-fusion proteins. These data suggest that GFP fused to the N-terminus of both 17β-HSD1 and 17β-HSD2 hinders steroid metabolism when compared to the non-tagged wild-type constructs.

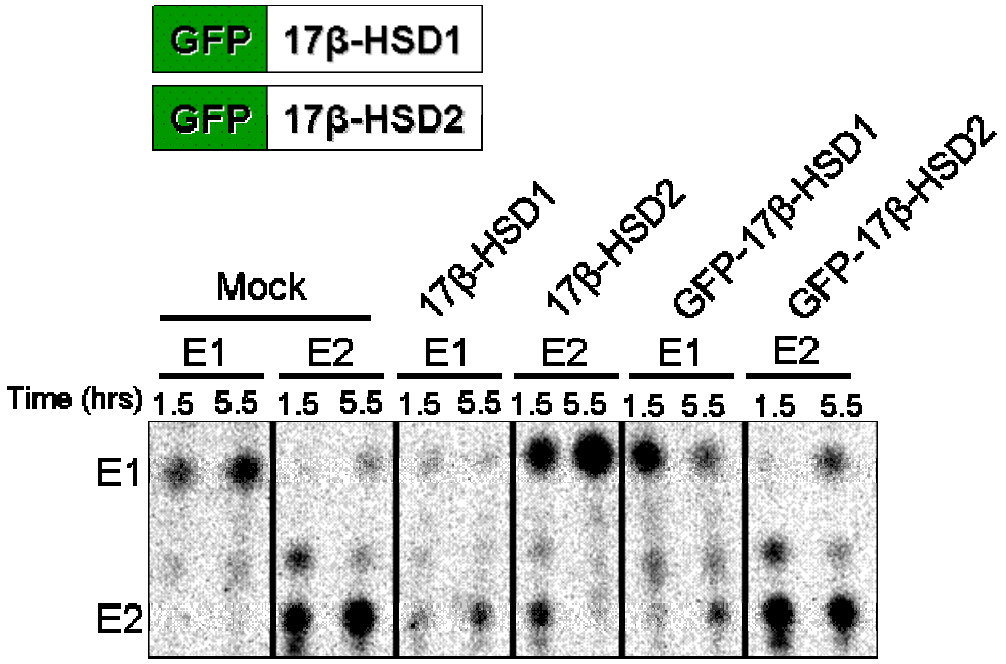

FIGURE 2.1. Assessing GFP-17β-HSD1 and GFP-17β-HSD2 Activity. HEK293 cells were transfected with expression vectors containing the cDNA of 17β-HSD1 WT, 17β-HSD2 WT, GFP-17β-HSD1 WT, GFP-17β-HSD2 WT. Cells were then incubated with 100nM E1 (Mock, 17β-HSD1, GFP-17β-HSD1) or 100nM E2 (Mock, 17β-HSD2, GFP-17β-HSD2). Aliquots were removed at 1.5 and 5.5hrs, extracted, separated on a TLC plate and imaged with a phosphoscreen.

Since GFP fused to the N-terminus of 17β-HSD1 and 17β-HSD2 appeared to interfere with activity, the next set of constructs fused GFP and FLAG to the C-terminus of 17β-HSD1. To assess whether GFP or FLAG negatively affected 17β-HSD1 activity, we likewise transfected HEK293 cells with expression constructs. FIGURE 2.2 shows that GFP or FLAG fused to the C-terminus of 17β-HSD1 has no discernible negative impact on activity.

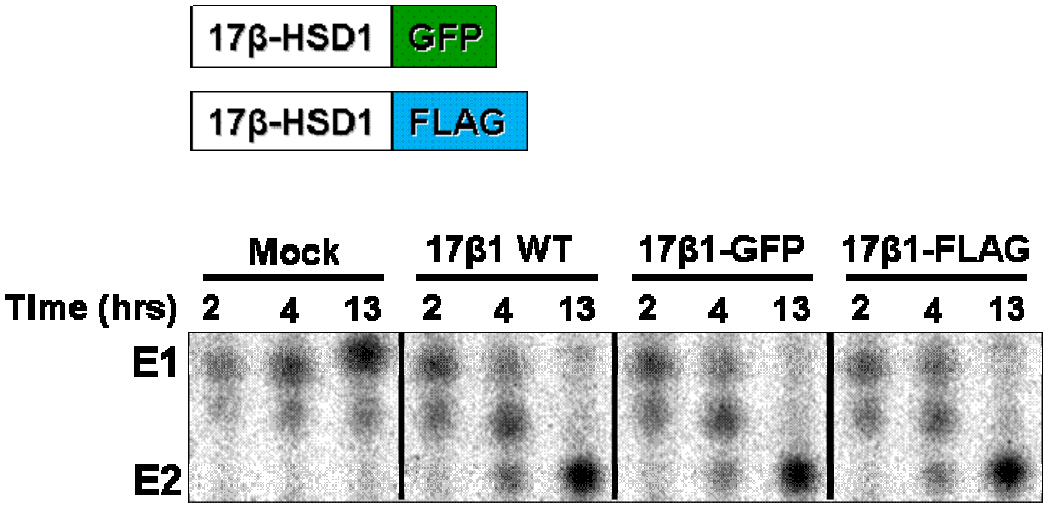

FIGURE 2.2 Assessing 17β-HSD1-GFP and 17β-HSD2-GFP Activity. HEK293 cells were transfected with expression vectors containing the cDNA of 17β-HSD1 WT, 17β-HSD1-GFP WT, 17β-HSD1-FLAG WT. Cells were then incubated with 100nM E1. Aliquots were removed at 2, 4 and 13hrs, extracted, separated on a TLC plate and imaged with a phosphoscreen.

To assess the influence of GFP and FLAG tags on 17β-HSD1 constructs with a BiP signal sequence for ER targeting, we transfected HEK293 cells with ss-17βHSD1-GFP-KDEL and ss-17βHSD1-FLAG-KDEL and assessed their activity. Since we did not know the activity of either ER targeted construct, 17β-HSD1 was used as a positive control. FIGURE 2.3 shows that GFP and FLAG constructs are active, and contrary to our predictions give similar final steroid proportions as 17β-HSD1 WT.

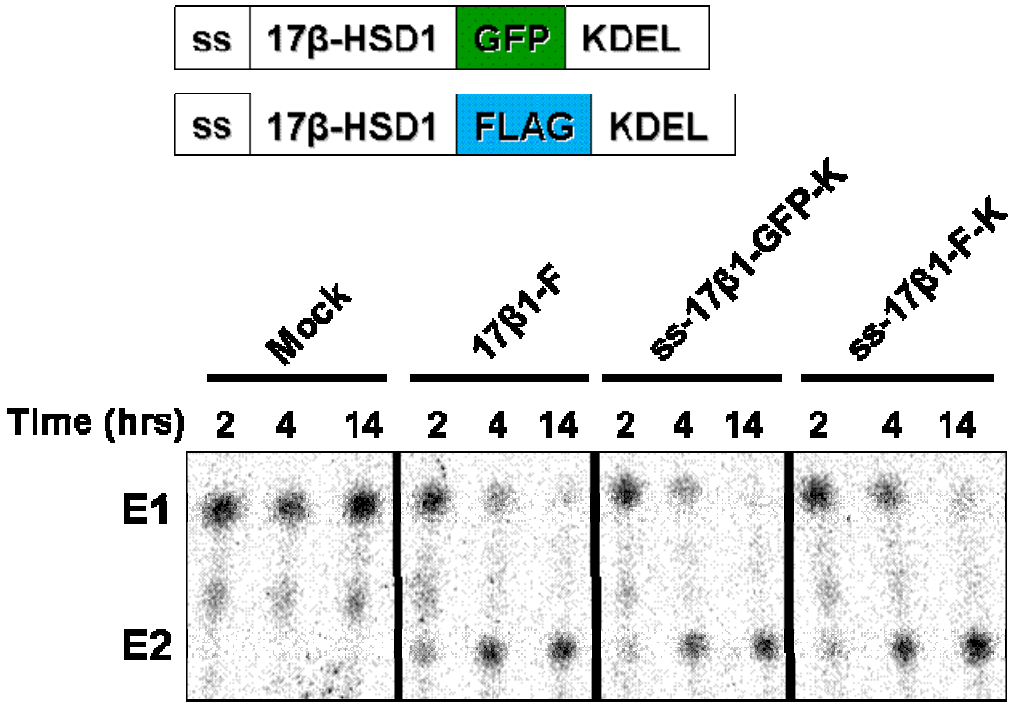

FIGURE 2.3. Assessing ER-targeted FLAG and GFP Tagged 17β-HSD1 for Activity. HEK293 cells were transfected with expression vectors containing the cDNA of 17β-HSD1-FLAG WT, ss-17β-HSD1-GFP-KDEL WT, ss-17β-HSD1-FLAG-KDEL WT. Cells were then incubated with 100nM E1. Aliquots were removed at 2, 4 and 14hrs, extracted, separated on a TLC plate and imaged with a phosphoscreen.

Previous work in our laboratory (Sherbet 2009) indicated an attenuated directional preference when arginine (R)38 of 17β-HSD1 is mutated to an aspartic acid (D), glutamic acid (E), and glycine (G) but not to lysine (K). The crystal structure of human 17β-HSD1 shows R38 coordinating the 2'-phosphate group of $NADP^+$ (FIGURE 2.4). To determine how the R38 mutation plus a change in cellular environment effects 17β-HSD1's activity, we made R38 FLAG-tagged mutant constructs targeted to the cytosol or ER. To confirm that the constructs

were active, we transfected HEK293 cells and assayed for activity (FIGURE 2.5). The R38 mutant constructs behave as expected compared to the WT constructs, but again, the ER-targeting did not shift the directional preference. To further assess our constructs, we performed a Western Blot of whole cell lysates (FIGURE 2.6). Robust expression of all constructs was observed.

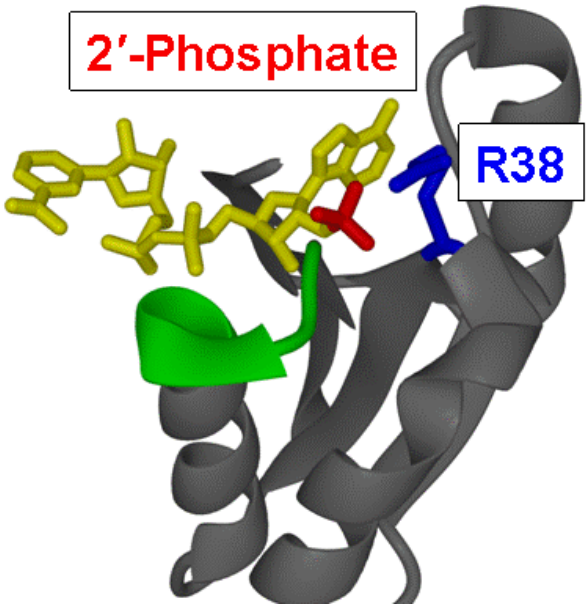

FIGURE 2.4 Crystal Structure of Human 17β-HSD1 with $NADP^+$. A partial view of human 17β-HSD1 (grey) coordinating $NADP^+$ (yellow). 17β-HSD1's R38 (blue) forms a salt bridge with the 2'-phosphate group (red) of $NADP^+$. Disruption of this salt bridge results in altered steroid distributions. Figure adapted from Mizrachi 2009.

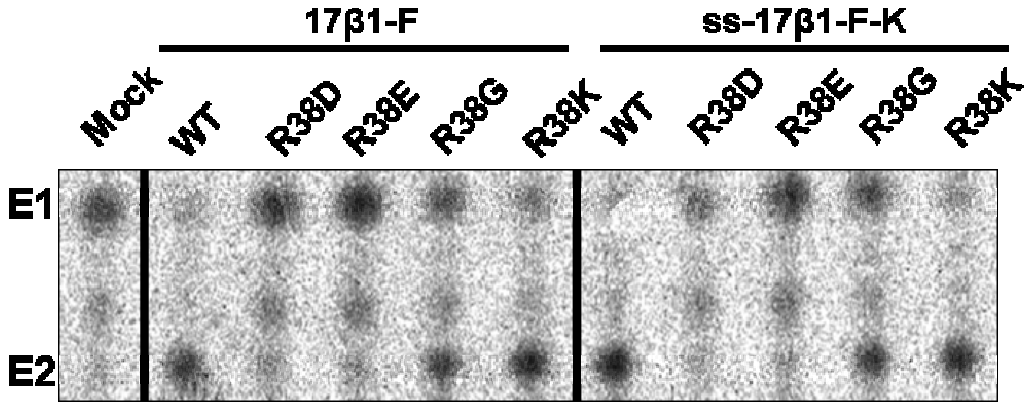

FIGURE 2.5. Testing R38 Mutations for Activity. HEK293 cells were transfected with expression vectors containing the cDNA of 17β-HSD1-FLAG WT or R38 mutations, ss-17β-HSD1-GFP-KDEL WT or R38 mutations. Cells were then incubated with 100nM E1. Aliquots were removed after 24hrs, extracted, separated on a TLC plate and imaged with a phosphoscreen.

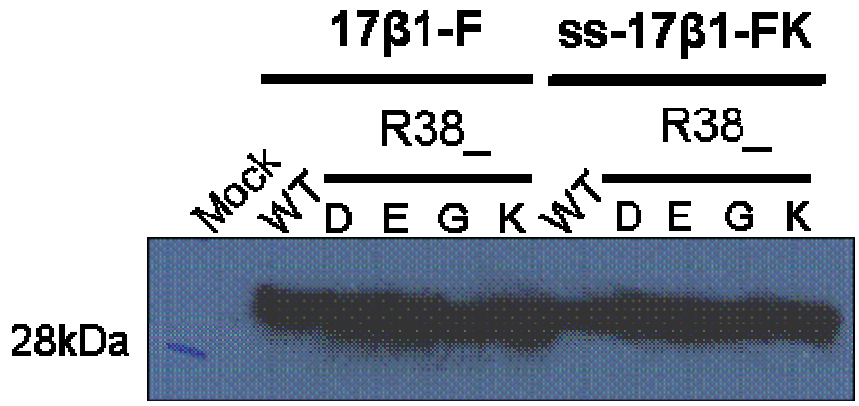

FIGURE 2.6. Protein Expression. HEK293 cells were transfected with expression vectors containing the cDNA of 17β-HSD1-FLAG WT or R38 mutations, ss-17β-HSD1-GFP-KDEL WT or R38 mutations. Cells were lysed, centrifuged at low speed, electrophoresed on SDS-PAGE and Western blotted for the FLAG epitope with α-FLAG M2.

Stable Cell Lines

To eliminate transfection efficiency as a variable and to expedite further experiments, we sought to make stable cell lines to study the effect of cellular location and cofactor affinity. Stable cell lines also have a greater signal to noise ratio than transient transfections. Stable cell lines were generated as previously mentioned (Sherbet 2009, Papari-Zareei 2006) to quantitatively assess the affect of cellular location (ER vs. cytosol) and cofactor affinity on steroid metabolism. Briefly, cells were transfected, transferred to a larger plate and selected on complete media containing G418. Colonies were picked and expanded in two plates (an assay plate and a propagation plate). FIGURES 2.7 and 2.8 show the metabolism of seventeen 17β-HSD1 colonies (six WT, six R38G, five R38E); all colonies assayed catalyzed E1 to E2 conversion resembling previously published results with FLAG-less constructs (Sherbet 2009).

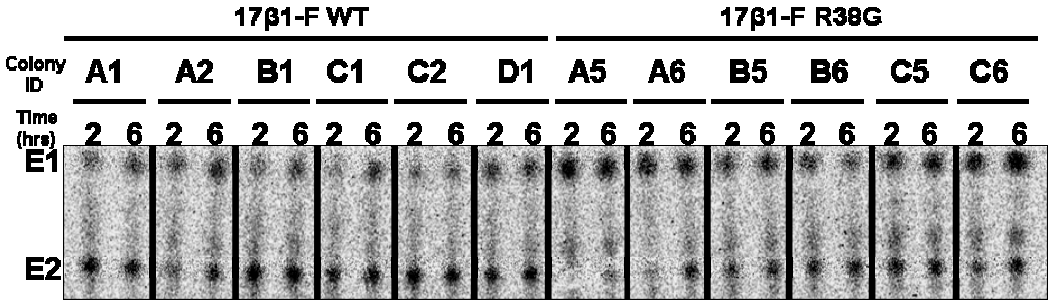

FIGURE 2.7. Stable HEK293 Cell Lines Expressing 17β-HSD1-FLAG WT or R38G. Viable colonies are indicated by their alpha-numerical identification. Cells were incubated with 100nM E1. Aliquots were removed after 2 and 6hrs, extracted, separated on a TLC plate and imaged with a phosphoscreen. All lines metabolized E1 to E2.

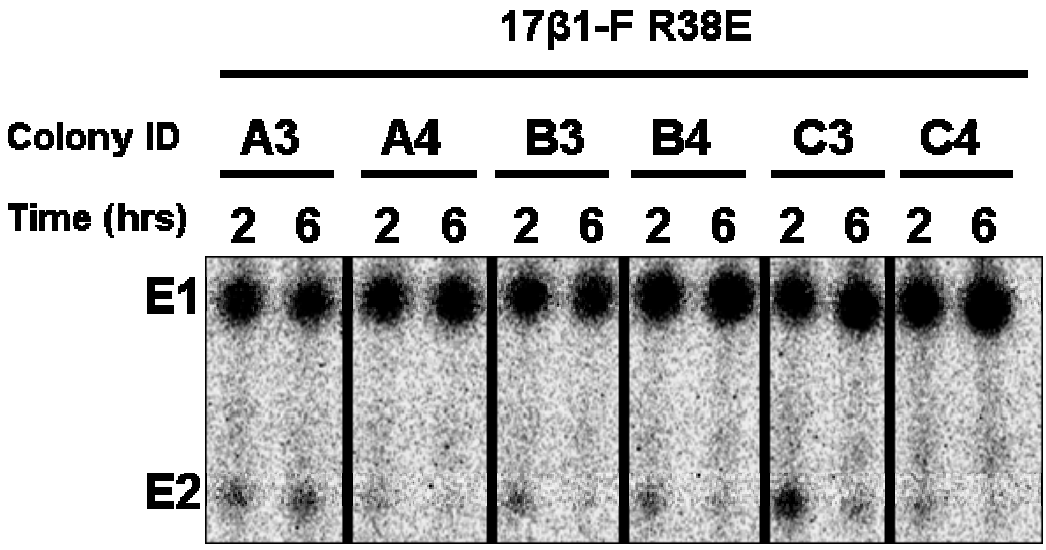

FIGURE 2.8. HEK293 Cell Lines Expressing 17β-HSD1-FLAG R38E Mutation. Viable colonies are indicated by their alpha-numerical identification. Cells were incubated with 100nM E2. Aliquots were removed after 2 and 6hrs, extracted, separated on a TLC plate and imaged with a phosphoscreen. Nearly complete conversion is observed by 6h in all lines.

We generated stable cell lines using the ER-targeted constructs but encountered numerous problems. In the generation of these clonal lines, we observed that all ER-targeted constructs resulted in very few clones surviving G418 selection, on average 3-8 compared to 25-40 for 17β-HSD1 WT line generation. We altered the above protocol and used a 6-well plate for transfection instead of a 100mm dish, picked colonies, and split them into assay and propagation plates. FIGURES 2.9 and 2.10 show the results of several colonies obtained using ER-targeted constructs, demonstrating negligible steroid metabolism and few surviving cells. To rule out any sort of systematic bias between the cytosolic and ER targeted stable cell lines, a control experiment was

performed where the WT cytosolic 17β-HSD1 and WT ER 17β-HSD1 construct were transformed at the same time, with the same cells and reagents. The same result was observed several times: the cytosolic targeted constructs resulted in numerous viable colonies with high estrogen metabolisms whereas the ER targeted constructs resulted in few viable clones with no detectable activity.

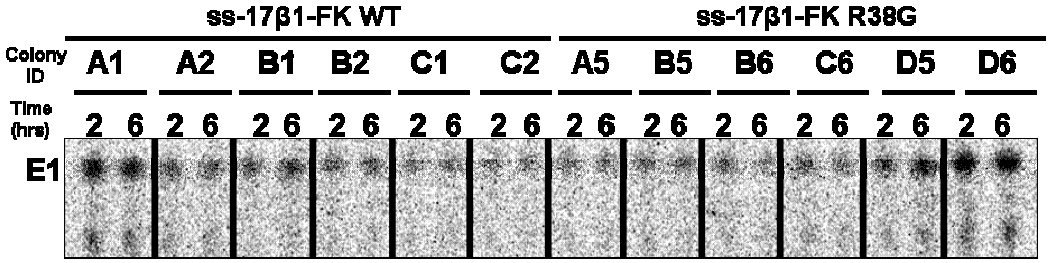

FIGURE 2.9. HEK293 Cell Lines Expressing ss-17β-HSD1-FLAG-KDEL WT or R38G Mutation. Colonies selected on G418 are indicated by their alpha-numerical identification. Cells were incubated with 100nM E1 for 6h. Aliquots were removed after 2 and 6hrs, extracted, separated on a TLC plate and imaged with a phosphoscreen. No convincing metabolism was observed for any clone.

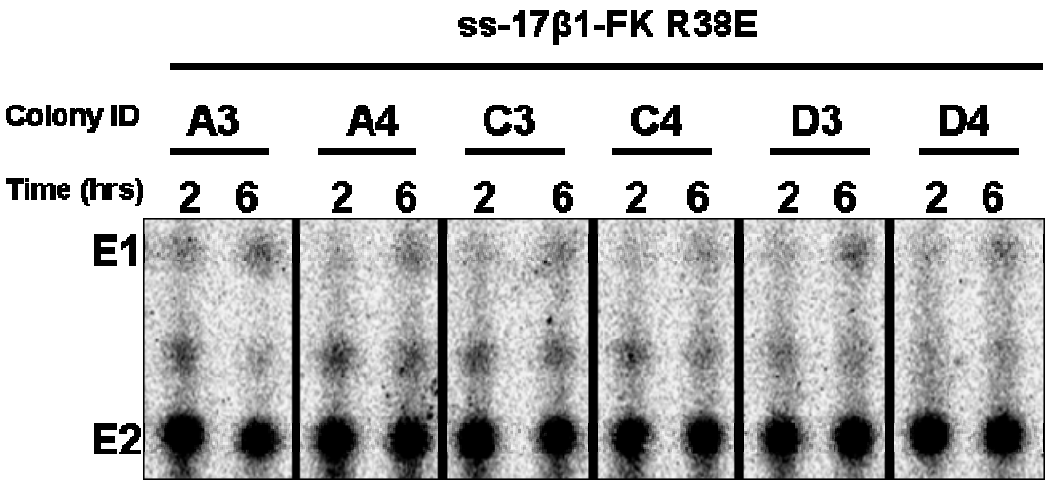

FIGURE 2.10. HEK293 Cell Lines Expressing ss-17β-HSD1-FLAG-KDEL R38E Mutation. Viable colonies are indicated by their alpha-numerical identification. Cells were incubated with 100nM E2 for 6h. Aliquots were removed after 2 and 6hrs, extracted, separated on a TLC plate and imaged with a phosphoscreen.

Our efforts to study the effect of location on 17β-HSD1 activity by generating stable cell lines constitutively expressing 17β-HSD1 using our conventional protocol were unsuccessful, and we sought to understand why and to find a successful approach. We suspected that chronic over-expression of a foreign protein not normally found in the ER might be toxic to our cells. This theory would explain why so few viable clones were generated with ER-targeted constructs. Perhaps the only surviving cells lacked the full-length cDNA, consistent with the lack of enzyme activity. Therefore, we decided to pursue making 17β-HSD1 (WT, R38G, R38E) and ss17β-HSD1-FK (WT, R38G, R38E) using Invitrogen's Flp-In T-REx system for inducible protein expression (FIGURE 6.1). This system employs Invitrogen's pcDNA5 vector, which flanks the cDNA of interest with the appropriate Flp recombinase sites. We first tested

these new constructs by transfecting them into our HEK293 cells, using the same estrogen metabolism assay. FIGURE 2.11 indicates that all six constructs are active as were their pcDNA3 counterparts. Thus, the constructs that we are using to make stable cell lines encode active proteins.

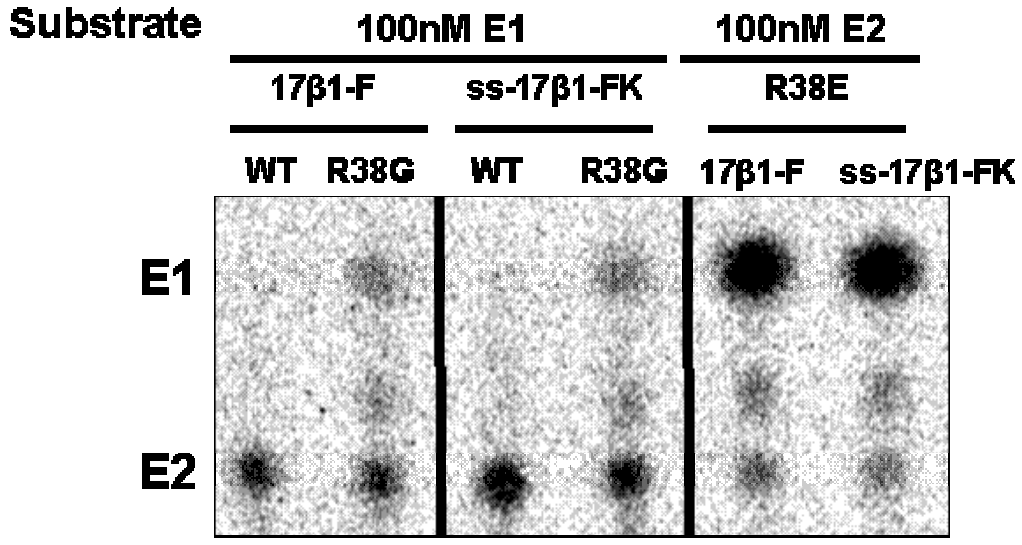

FIGURE 2.11. Screening 17β-HSD1 pcDNA5 Constructs for Activity. HEK293 cells were transfected with pcDNA5 expression vectors containing the cDNA of 17β-HSD1 WT and R38 mutations, or ss-17β-HSD1-FLAG-KDEL WT and R38 mutations. Cells were then incubated with 100nM E1 (WT and R38G) or 100nM E2 (R38E). Aliquots were removed after 28hrs, extracted, separated on a TLC plate and imaged with a phosphoscreen.

We proceeded to transfect our active pcDNA5 constructs into Invitrogen's Flp-In HEK293 cells along with the vector coding for Flp-Recombinase, per Invitogen's established protocol (FIGURE 6.1). Invitrogen's Flp-In HEK293 cells have a Flp-In site in their genome whereas the HEK293 cells previously used do not. After several weeks in the hygromycin selection media, numerous large colonies were picked and grown in assay and propagation plates per our standard procedure. We induced protein expression with a 16hour incubation with tetracycline, followed by a time course to assay for enzyme activity. FIGURE 2.12 shows that the two colonies assayed have no activity. To rule out simple artifacts, more colonies were picked and assayed in FIGURE 2.13. Again, little if any activity was observed. Since we knew that the pcDNA5 constructs gave active enzyme when expressed in HEK293 cells, the absence of activity suggested either failed cDNA integration and/or failure to induce with tetracycline. Consequently, we conducted a time course of protein induction with various concentrations of tetracyline for 24 or 48 hours (FIGURE 2.14). The resultant phosphoscreen image indicates no activity under any of these induction conditions. To assess whether protein was expressed but inactive, we lysed the cells used for the assay and assessed protein expression with a Western Blot against the FLAG epitope (FIGURE 2.14). The Western Blot shows no discernible band of ~40kDa. To further confirm that we have successfully transfected our construct and incorporated it into the host genome, a "kill assay" was employed. A successfully transformed cell line will be sensitive to Zeocin and resistant to hygromycin. The Zeocin resistance conferring protein expression

is repressed by the TetR protein but not the hygromycin resistance conferring protein expressed from the same pcDNA5 vector our cDNA is in (FIGURE 6.1). To ensure that our antibiotics were active, we used standard HEK293 cells and observed 100% cell death within two weeks; we also added hygromycin to the original untransformed Flp-In T-REx HEK293 cells and also observed complete cell death within two weeks. We introduced Zeocin to our cells as well as the untransformed Flp-In T-REx HEK293 cells and observed cell death with transfected Flp-In T-REx cells but not the untransformed cells, indicating that our cells are indeed sensitive to Zeocin and resistant to hygromycin. We concluded that our cells have been transfected successfully; however, this result does not explain the lack of enzyme activity.

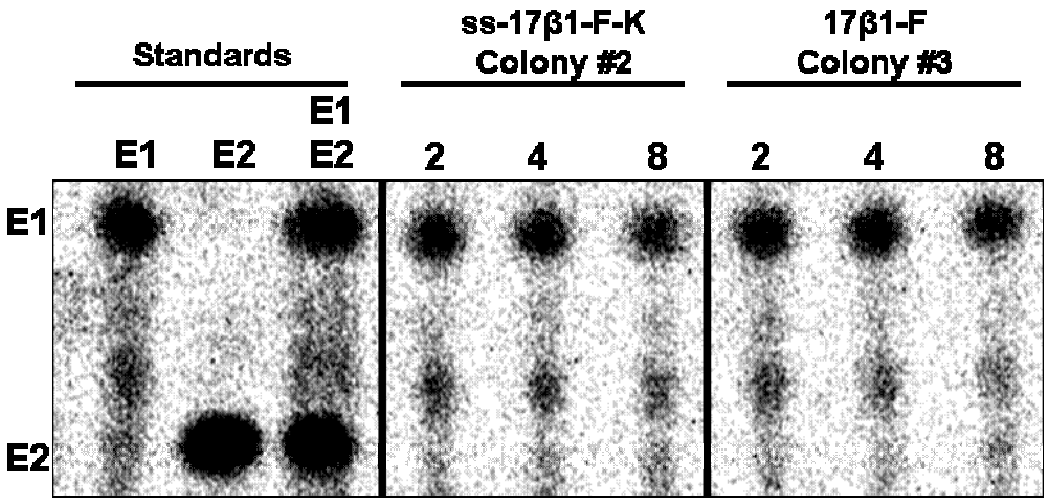

FIGURE 2.12. Testing Two Tetracycline induced Colonies for Activity. Colonies were picked and split into an assay and propagation 6-well plates. When the assay plate reached ~75% confluency, a final concentration of 1μg/ml tetracycline was added and incubated with the cells for 16hrs. Fresh media and fresh 1ug/ml tetracycline were added along with 100nM E1. Aliquots were taken at indicated time points; and activity was assessed by TLC and phosphoscreen exposure. The dark spot above E2 is a contaminant from the E1 starting material.

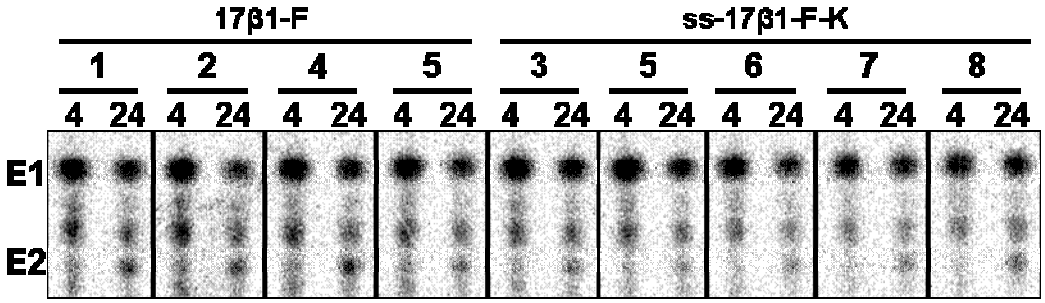

FIGURE 2.13. Screening WT 17β1-F and ss17β1-F-K Colonies for Activity. Colonies were picked and split into an assay and propagation 6-well plate. When the assay plate reached ~75% confluency, a final concentration of 1µg/ml tetracycline was added and incubated with the cells for 24hrs. Fresh media and fresh 1µg/ml tetracycline were added along with 100nM E1. Aliquots were taken at indicated time points; activity was assessed by TLC and phosphoscreen exposure.

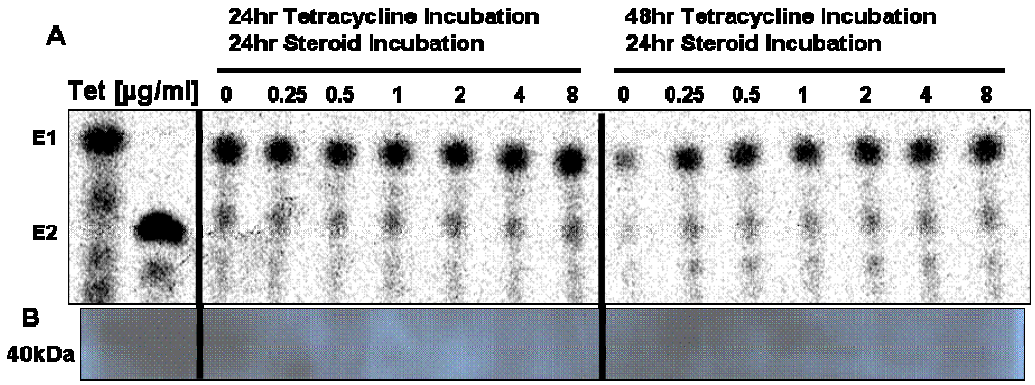

FIGURE 2.14. Induction Optimization. Colony 17β1-F #3 was used for the optimization of protein expression. Cells were grown to approximately 75% confluency, induced with increasing tetracyline concentrations for either 24 or 48hrs, and assayed with 100nM E1. **A**. Samples were separated by TLC and exposed to a phosphoscreen overnight. **B.** After the assay, cells were gently washed with PBS buffer, lysed, electrophoresed on a SDS-PAGE gel, transferred to a PVDF membrane and Western Blotted with anti-FLAG to assess protein expression.

To eliminate the possibility that we are not using enough tetracycline or that it is degrading before full protein induction, a 48hour time course with increasing tetracycline (10µg/ml up to 320µg/ml) was attempted. All of these treatments were toxic, either from the amount of ethanol vehicle added or the high concentrations of tetracycline. A control plate with just ethanol and no tetracycline gave the same toxicity, suggesting that ethanol was the cause. Due to the poor solubility of tetracycline, we reasoned that we could not use higher concentrations.

To overcome the protein induction problem, we first contacted Dr. Frank S. Lee (University of Pennsylvania) and requested he send his Flp-In T-Rex HEK293 FLAG-HIF-2α –P531A cell line (Percy 2008) for us to use as a positive control. We chose his cell line because it is the same parental cell type, HEK293, and because they used the same FLAG epitope to tag their protein, HIF-2α. Second, we employed doxycycline, a more stable tetracycline analog; tetracycline has a 24hour half-life, whereas doxycycline's half-life is reported to be 48hrs (Invitrogen T-REx System Manual). We incubated the HIF-2α-P531A cells with increasing amounts of doxycycline for 24 hours, lysed the cells, and ran the whole cell lysate on a gel for Western blot analysis (FIGURE 2.15). A band appears at 96.5kDa corresponding to the correct MW of HIF-2α upon doxycycline addition (0.1-0.5µg/ml) but appears to fade with higher doxycycline concentrations. This result indicates that we can use doxycycline to induce protein expression in HIF-2α-P531A HEK293 cells, so we performed similar induction experiments with our 17β-HSD1 cell lines. When doxycycline was used on a Flp-In T-REx

HEK293 cell line with integrated 17β-HSD1, no steroid metabolism was observed (FIGURE 2.16); this experiment was repeated, and the same result was observed numerous times.

FIGURE 2.15. Induction Troubleshooting with HIF-2α-P531A Flp-In T-REx HEK293 Cells. Cells were incubated with increasing amounts of doxycycline for 24hours, lysed and blotted for protein expression. A band running at approximately 95kDa indicates the presence of HIF-2α-P531A protein.

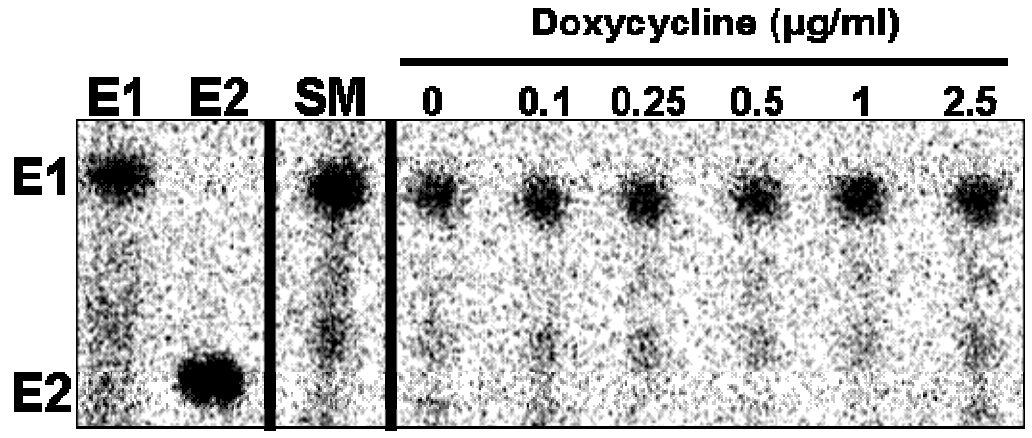

FIGURE 2.16. Doxycycline Induction with 17β1-F Cell Line. Stable cell line Flp-In T-REx HEK293 17β1-F was incubated with increasing concentrations of doxycyline for 24hrs followed by 24hrs of 100nM E1 substrate incubation. SM, Starting Material (E1).

To determine if the full-length 17β-HSD1 cDNA was incorporated in the genome of the Flp-In T-REx cell lines, genomic DNA was isolated and PCR was used to identify host DNA that could be amplified with CMV and BGH primers indicating the presence of the pcDNA5 sequence as well as the TetR sequence (FIGURE 2.17). CMV and BGH primers amplified one band in Flp-In T-REx HEK293 host cells and two bands in HIF-2α -P531A, 17β-HSD1-F #3, 17β-HSD1-F #4; Regular HEK293 cells were used as a negative control, 17β-HSD1-F pcDNA5 and FRT TO CAT as positive controls. HIF-2α-P531A (2610bp) appears faintly because the PCR conditions were optimized for amplifying the 17β-HSD1 coding regions. A 1 kb band appears in all three transfected Flp-In T-REx HEK293 cell lines but not untransfected Flp-In T-REx HEK293. To confirm that the 1kb band observed was 17β-HSD1, we used 17β-HSD1 sequence specific primers. We did not observe a band in the 17β-HSD1 transfected cell lines. We conclude that we did not incorporate 17β-HSD1 cDNA into the Flp-In T-REx HEK293 genome.

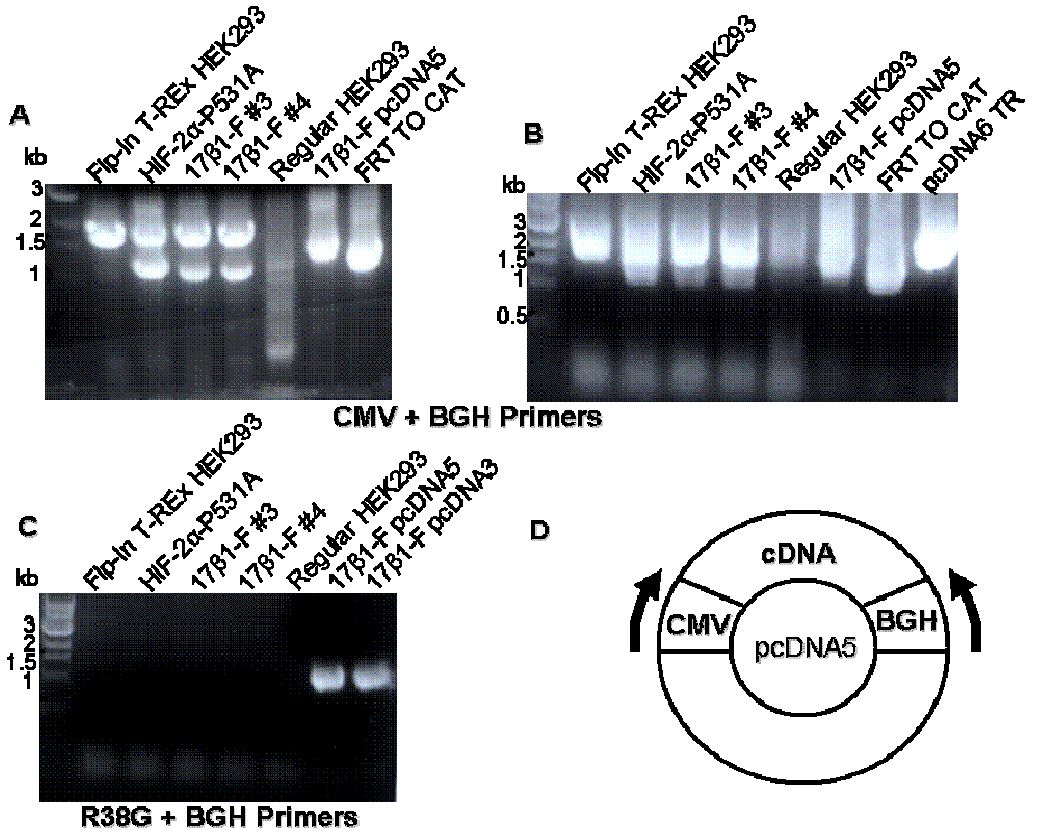

FIGURE 2.17. PCR Reactions with Genomic DNA. A. PCR reactions using the CMV and BGH primers along with purified Genomic DNA from the following cell lines: Flp-In T-REx HEK293 (untransfected Flp-In T-REx HEK293, HIF-2α-P531A, 17β1-F #3 + #4), Regular HEK293. 17β1-F pcDNA5 and FRT TO CAT served as positive controls. **B.** PCR reactions identical to A but done at a later time. pcDNA6 TR was added as a control to aid in the identification of the 2kb band. **C**. PCR reactions were repeated but with R38G and BGH primers. **D.** Map of pcDNA5. The map of TetR construct is identical but has a blasticidin resistance marker instead of hygromycin (FIGURE 6.1 for greater detail).

Transient Transfections

At the same time we were troubleshooting our tetracycline inducible cell line, we reasoned that if the main reasons for using a stable cell line were consistency and higher signal to noise ratio, we could achieve comparable results using transient transfections in a 6-well plate using optimal technique and DNA loading for high transfection efficiency. HEK293T cells have a high transfection efficiency as well as high protein expression from vectors with CMV promoters due to the presence of the SV-40 large T-antigen. To test the feasibility of our approach, we transfected 17β-HSD1-F (WT, R38E, R38G) expression vectors into HEK293 cells, added E1 or E2 and measured a time course for metabolism. We compared our data against previously published work from our lab (Sherbet 2009) and found our data to be comparable when either E1 or E2 was added. We also observed that our ER targeted constructs exhibited similar activity to the cytosolic versions.

We compared the activity of our transient transfections with 0.5-7.5µg DNA after 48 hours of transfection and 6 hours of incubation with E1 (FIGURE 2.18). All transient transfections had the same activity and were very comparable to the equilibrium achieved with a previously published stably expressing cell line. Of note, the background activity of the HEK293T cells was very low, further aiding our ability to distinguish activity from the expression constructs and the host cell line.

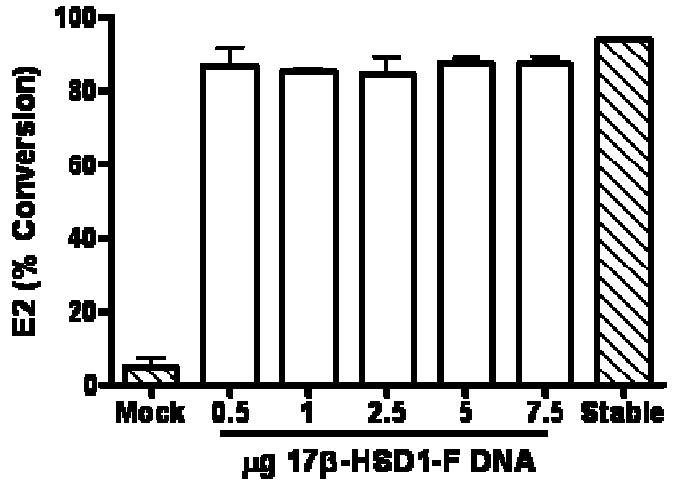

FIGURE 2.18. HEK293T Cell Transient Transfection Optimization. HEK293T cells were transfected with increasing amounts of expression vector containing the cDNA of 17β-HSD1-FLAG WT. Cells were then incubated with 100nM E1. Aliquots were removed at 6hrs, extracted, separated on a TLC plate. Conversion was measured by cutting plate regions containing E1 and E2 and scintillation counting. Each bar represents the mean + S.D. of at least three independent experiments. Previously published (Sherbet 2009) data from a cell line expressing 17β-HSD1 WT is represented by hatched bar on the far right for comparison.

To validate our earlier finding of similar activities between cytosolic and ER 17β-HSD1-F expression constructs, we ran a time course with WT and the mutants R38G or R38E, and we observed nearly identical equilibrium ratios between our transiently transfected cells and previously reported stable cell lines (FIGURE 2.19). We compared our cytosolic targeted expression constructs to our ER targeted expression constructs, and contrary to our predictions, we observed nearly identical steroid distribution at equilibrium (FIGURE 2.20, TABLE 2.1).

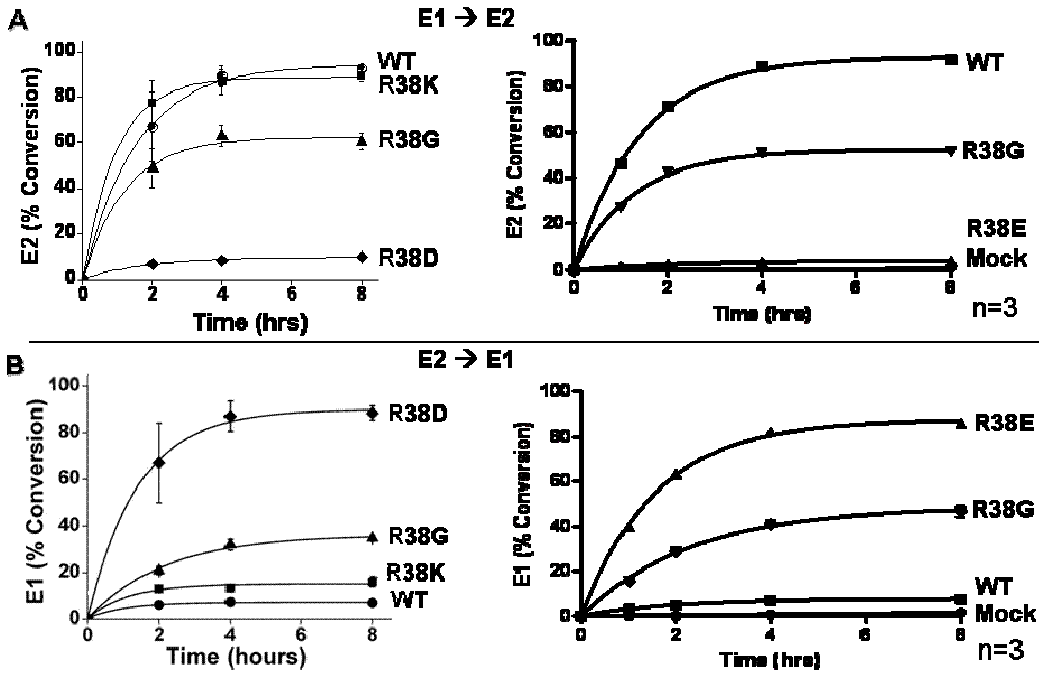

FIGURE 2.19. Comparing Activity of Stable Cell Lines and Transient Transfections. Comparison of E1 and E2 metabolism between HEK293 cell lines expressing 17β-HSD1 WT or R38 mutations (left hand side of panels from Sherbet 2009) and transient transfections with expression vectors containing cDNA of 17β-HSD1-FLAG WT and R38 mutations (right hand side of panels). **A.** Conversion of E1 (100nM) to E2 by indicated 17β-HSD1-FLAG expression vectors is plotted as a function of time. **B.** Conversion of E2 (100nM) to E1 by the same vectors. Data points are means $\pm$ SD of at least three assays; curves are fit to the equation $f(t)=A(1-e^{-kt})$. Equilibrium steroid distributions are derived by setting $t = \infty$ and summarized in TABLE 2.1.

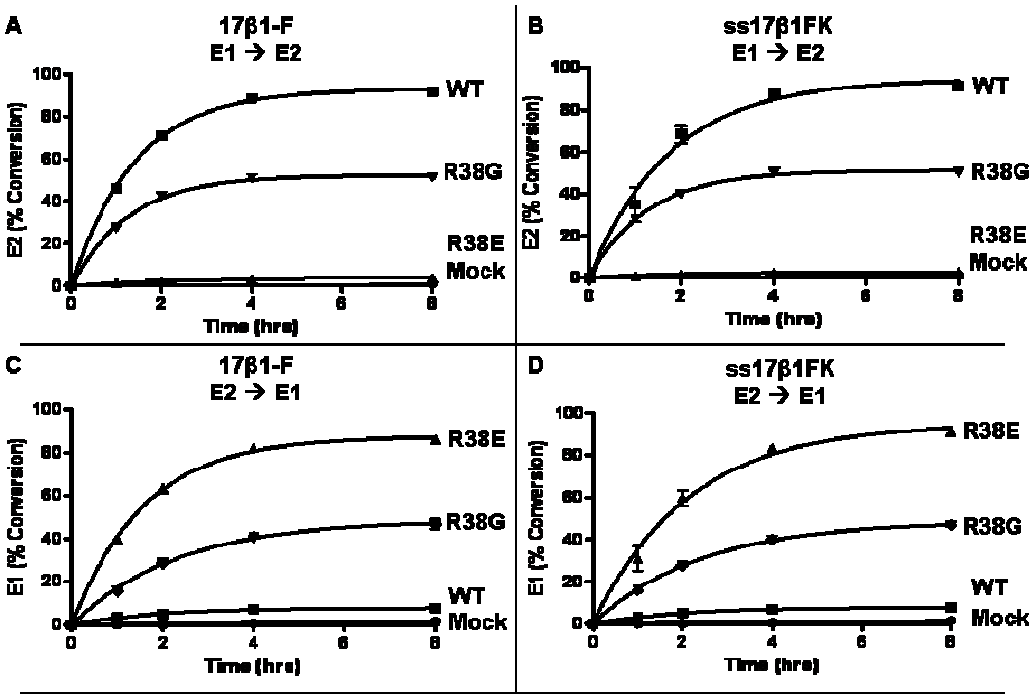

FIGURE 2.20. Activity of Cytosolic and ER-Targeted 17β-HSD1-F Constructs in High-Glucose Medium. Comparison of E1 and E2 metabolism in high-glucose medium between transient transfections with expression vectors containing cDNA of 17β-HSD1-FLAG WT and R38 mutations (left hand side of panels) or ss17B1FK WT and R38 mutations (right hand side of panels). **A.** Conversion of E1 (100nM) to E2 by indicated expression vectors is plotted as a function of time. **B.** Conversion of E2 (100nM) to E1 by the same vectors. Data points are means $\pm$ SD of at least three assays; curves are fit to the equation $f(t)=A(1-e^{-kt})$. Equilibrium steroid distributions are derived by setting $t = \infty$ and summarized in TABLE 2.2.

TABLE 2.1 Comparison of Steroid Distributions at Pseudo-Equilibrium in Transiently Transfected HEK-293T Cells and Stably Expressing HEK293 Cells

		E1 → E2 (%)		**E2 → E1 (%)**	
	Enzyme	**E1**	**E2**	**E1**	**E2**
Transient Transfections in HEK293T cells	17β1F WT	7	93	8	92
	R38E	96	4	88	12
	R38G	48	52	49	51
Stably expressing HEK293 cells (Sherbet 2009)	17β1F WT	6	94	7	93
	R38D	90	10	90	10
	R38G	38	62	36	67

Because the data with transiently transfected cells matched our prior results with stable cell lines, we performed all subsequent experiments using transient transfections. To compare the steroid distribution in low glucose conditions, we repeated the previous experiment but used glucose-free, serum-free media with 2-deoxyglucose (2-DG) to lower intracellular [NADPH]. Again, we observed nearly identical steroid distributions between the cytosolic expression vectors and the ER expression vectors (FIGURE 2.21) similar to previous studies (Sherbet 2009), with lower E2/E1 ratios in 2DG than in high-glucose medium.

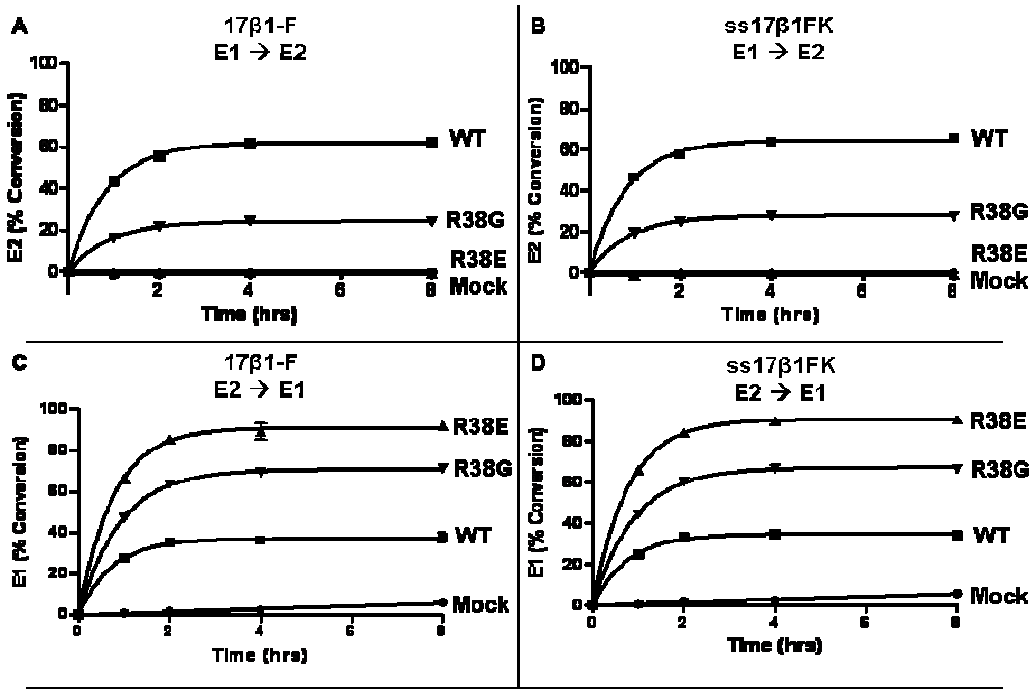

FIGURE 2.21. Activity of Cytosolic and ER-Targeted 17β-HSD1-F Constructs in Low-Glucose Medium. Comparison of E1 and E2 metabolism in 2-deoxyglucose medium between transient transfections with expression vectors containing cDNA of 17β-HSD1-FLAG WT and R38 mutations (left hand side of panels) or ss17B1FK WT and R38 mutations (right hand side of panels). **A & B.** Conversion of E1 (100nM) to E2 by indicated expression vectors is plotted as a function of time. **C & D.** Conversion of E2 (100nM) to E1 by the same vectors. Data points are means $\pm$ SD of at least three assays; curves are fit to the equation $f(t)=A(1-e^{-kt})$. Equilibrium steroid distributions are derived by setting $t = \infty$ and summarized in TABLE 2.2.

These data showed no discernible difference in directional preference for reactions catalyzed by cells transfected with WT or ER-targeted 17β-HSD1 expression vectors (TABLE 2.2). Perhaps the final steroid distribution is the same but the rates of conversion are different in different cellular locations. To determine the rates of estrogen metabolism by cells expressing cytosolic and ER targeted 17β-HSD1-F WT constructs at equilibrium, we used a double-isotope scrambling experiment (Khan 2004). In these experiments, the equilibrium steroid distribution is added to cells (CM 6:94% E1:E2, 2-DG 36:64% E1:E2), but two different isotope labels (^{14}C E1, ^{3}H E2) are used instead of one; this design us to follow the reaction in both directions and to calculate true rates of conversion. Again, there was no discernible difference in the rates of conversion between the cells expressing ER and cytosolic 17β-HSD1-F WT (FIGURE 2.22 and TABLE 2.3).

TABLE 2.2 Steroid Distributions at Pseudo-Equilibrium in HEK-293T Cells

	E1 → E2 (%)				E2 → E1 (%)			
	High Glucose		2-Deoxyglucose		High Glucose		2-Deoxyglucose	
Enzyme	E1	E2	E1	E2	E1	E2	E1	E2
17β1F WT	7	93	38	62	8	92	37	63
R38E	96	4	>99	<1	88	12	91	9
R38G	48	52	76	24	49	51	71	29
ss17β1FK WT	5	95	35	65	8	92	35	65
R38E	97	3	>99	<1	95	5	91	9
R38G	49	51	72	28	49	51	67	33

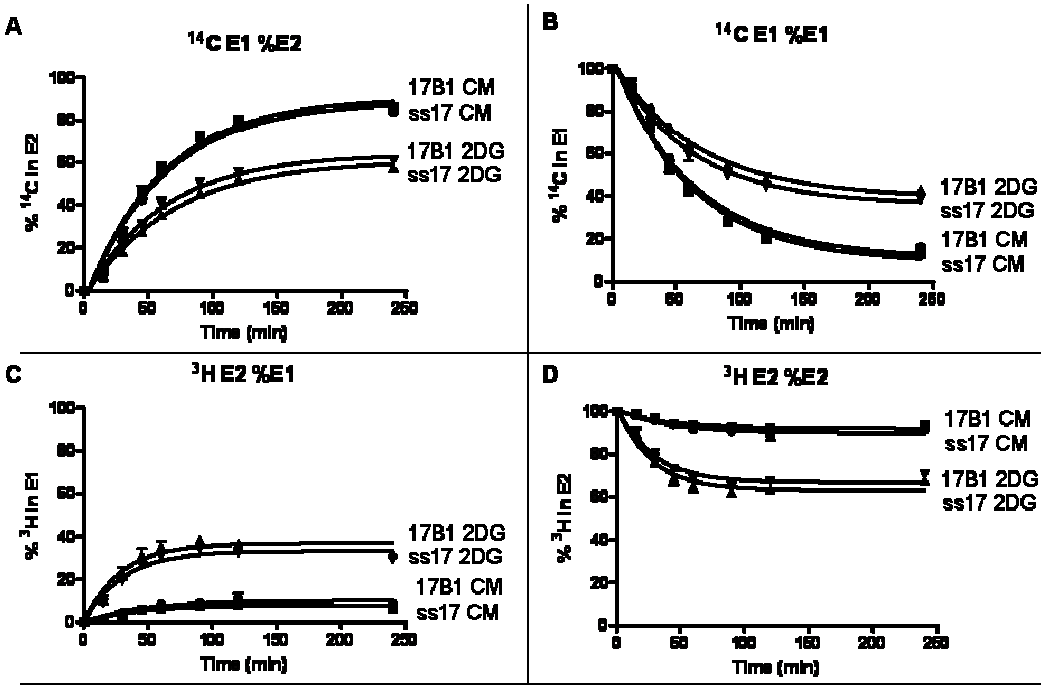

FIGURE 2.22. Double-Isotope Scrambling Experiments. Double-isotope scrambling experiments to determine kinetics of E1 and E2 metabolism by 17β1-FLAG WT and ss-17β1-FLAG-KDEL WT. Metabolism of [^{14}C]-E1 is shown in panels **A** and **B** while [^{3}H]-E2 is shown in panels **C** and **D**. Data from plots **B & D** are fitted to one phase exponential decay curves ($f(t) = Ae^{-kt} + C$); rates are shown in Table 2.3.

TABLE 2.3 E2 Oxidation Reaction Rates at Steady State Steroid Distribution

	^{14}C E1	
	CM	2DG
17β1F WT	21.95	34.92
ss17β1FK WT	24.06	32.90

Rates (pmol/min) derived from plots in FIGURE 2.22.

The data using transiently-transfected cells suggested that ER-targeting does not change the directional preference of 17β-HSD1. We considered two explanations: either the ER environment has a similar NADPH/$NADP^+$ ratio as the cytosol, yielding similar estrogen metabolism, or ER-targeted constructs upon over-expression in this system failed to target all of the enzyme to the ER lumen. To determine the cellular location of cytosolic and ER-targeted 17β-HSD1-F protein, we used fluorescence microscopy with our FLAG- and GFP-tagged constructs. FIGURE 2.23 shows the 17β-HSD1-GFP to be diffusely and evenly spread in the cell, consistent with cytosol localization, and no overlap with a published ER protein marker (ss-RFP-KDEL, Altan-Bonnet 2006). The ER targeted version, ss-17β-HSD1-GFP-KDEL, appears to be in the ER as evidenced by co-localization with ss-RFP-KDEL (FIGURE 2.24). Using the FLAG-tagged constructs, 17β-HSD1-FLAG and ss-17β-HSD1-FLAG-KDEL, we probed the cellular localization using immunofluorescence microscopy with anti-FLAG after permeabilizing with Triton X-100. Both the ER and the cytosolic vectors give similar images (FIGURE 2.25). Immunofluorescence microscopy was repeated several times with the FLAG constructs, giving the same result every time. This result can be attributed to the cytosolic protein being partially associated with the ER membrane, and the ER targeted protein being not isolated to the ER.

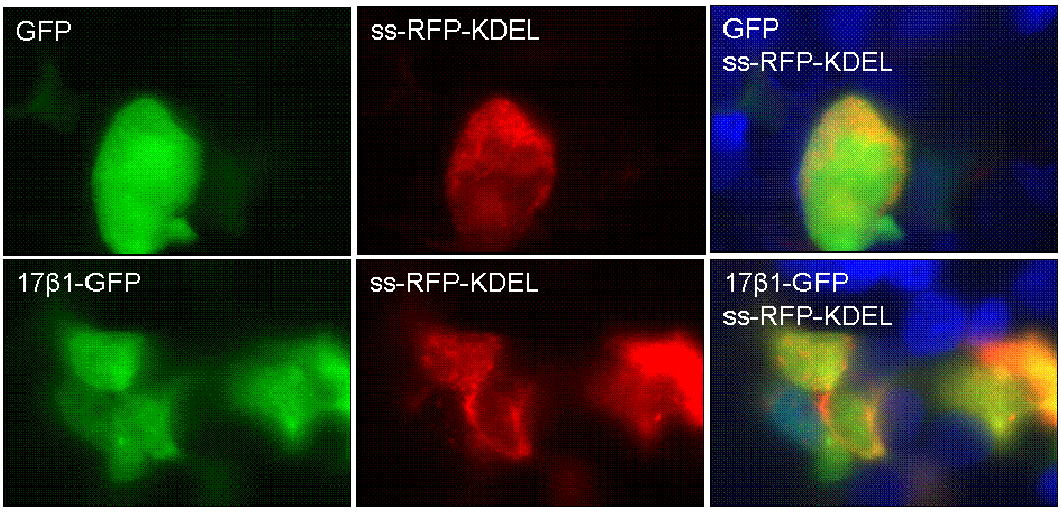

FIGURE 2.23. Fluorescence Microscopy of HEK293T Cells Transfected with GFP and RFP Constructs. The upper panels show GFP co-transfected with ss-RFP-KDEL; the lower panels show 17β1-GFP co-transfected with ss-RFP-KDEL. Individual channels are shown to the left and middle while the merged image is shown on the right.

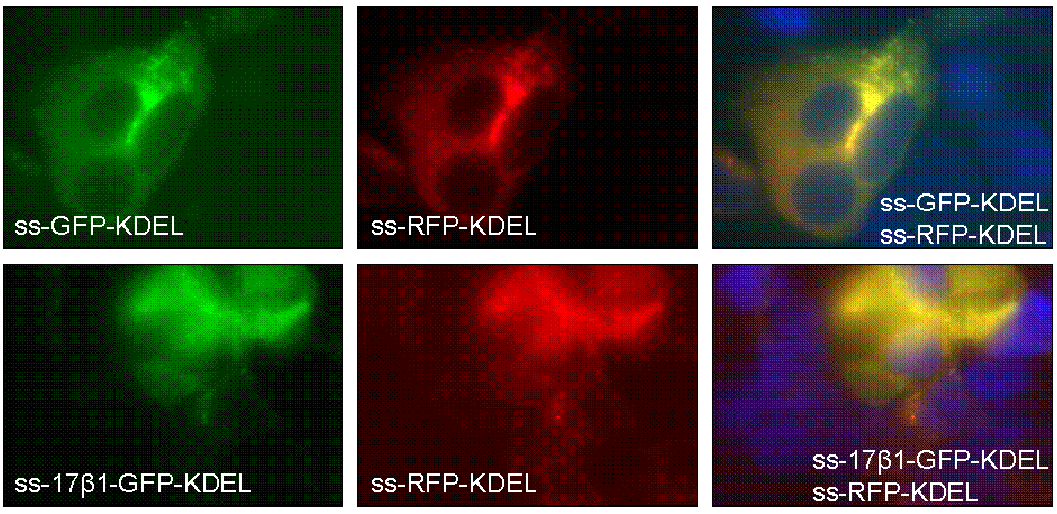

FIGURE 2.24. Fluorescence Microscopy of HEK293T Cells Transfected with ss-17β-HSD1-GFP-KDEL. The upper panels show ss-GFP-KDEL co-transfected with ss-RFP-KDEL; the lower panels show ss-17β1-GFP-KDEL co-transfected with ss-RFP-KDEL. Individual channels are shown to the left and middle while the merged image is shown on the right.

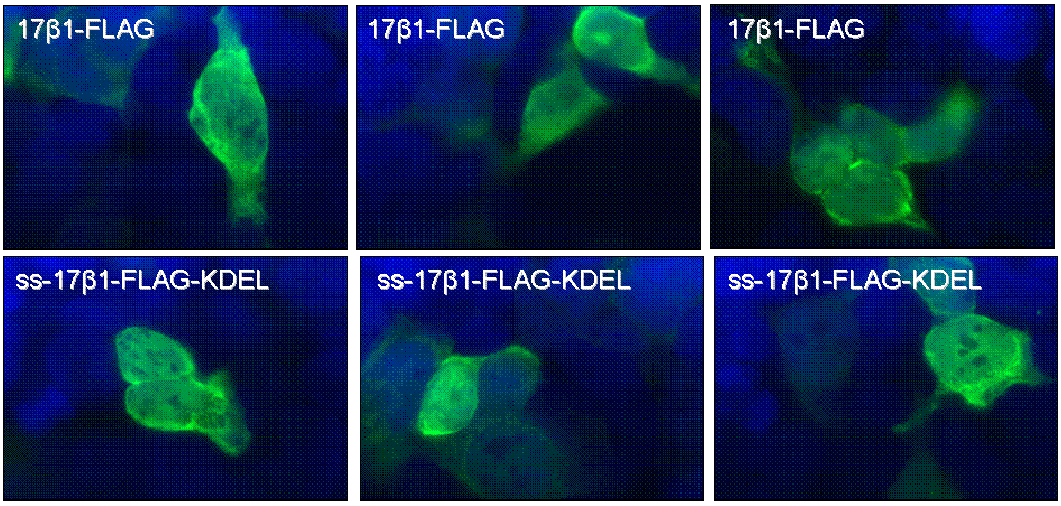

FIGURE 2.25. Immunofluorescence of FLAG constructs 17β-HSD1-FLAG and ss-17β-HSD1-KDEL. Representative images of both are displayed.

To resolve the discrepancies in the fluorescence microscopy experiments, we used cellular fractionation to determine the location of the proteins. We collaborated with Hyeilin Ham from Dr. Kim Orth's laboratory as her lab has extensive experience with cellular fractionation. FIGURE 2.26 shows the 17β-HSD1-F proteins to be restricted to the cytosol, whereas the ss-17β-HSD1FK protein is divided between the ER and cytosol fractions. To understand why 17β-HSD1-F was found in both the P2 and S3 fractions, we first asked whether the 17β-HSD1-F protein detected in these two fractions were the same size (FIGURE 2.28). If the proteins were different sizes, the result might indicate that the N-terminal ER signal sequence and/or KDEL retention sequence was cleaved in one compartment. Identical size proteins would indicate that ER-targeted ss-17β-HSD1-FK was also distributed into the cytosol despite the signal sequence and retention motifs; either an artifact of the fractionation technique or because the

cell was translocating the protein in an ERAD-independent manner. ERAD, Endoplasmic Reticulum Associated Degradation, is the process where misfolded proteins in the ER are translocated across the ER membrane to an awaiting proteasome for protein degradation (Goeckeler 2010). Since we found that in both fractions the proteins are the same size (FIGURE 2.27), we first suspected that the fractionation technique is disrupting the ER membrane, which allows for ER ss-17β-HSD1-FK to leak into the cytosol fraction. The protein used to identify the ER fraction above, calnexin, is an integral ER membrane protein (Michalak 2009) and might fractionate more clearly than a soluble ER luminal protein with a compromised ER membrane. To address this possibility, fractions collected in FIGURE 2.26 were immunoblotted for α-PDI (a protein disulfide isomerase, a soluble ER lumen protein) to assess the integrity of the ER fraction. The α-PDI western blot (FIGURE 2.28) indicates that the soluble contents of the ER were not leaked into the cytosol during the cellular fractionation, confirming that the results were not an artifact of cell disruption.

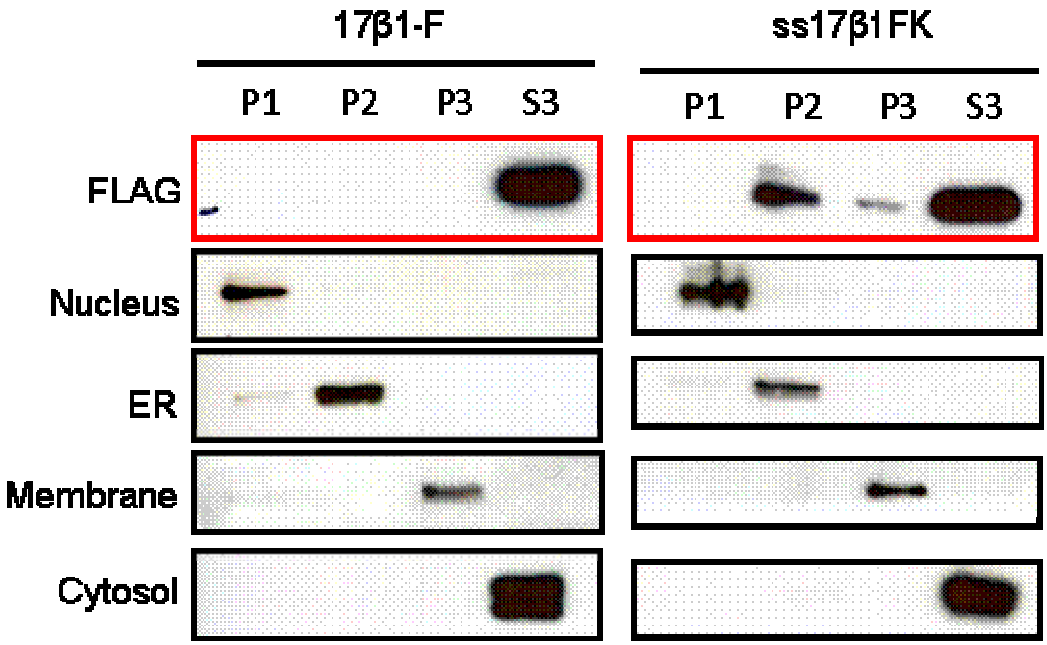

FIGURE 2.26. Cellular Fraction of 17β-HSD1-F and ss17β-HSD1FK. HEK293T cells transfected with expression vectors containing 17β-HSD1-F and ss17β-HSD1FK for 48 hours were fractionated as described in MATERIALS AND METHODS. Total protein concentration in each fraction was measured, and equivalent amounts were resolved by SDS-PAGE for western blotting. The following antibodies were used for each fraction: lamin B (P1, nucleus), calnexin (P2, ER), ATPase B2 (P3, plasma membrane) and aldolase (S3, cytosol).

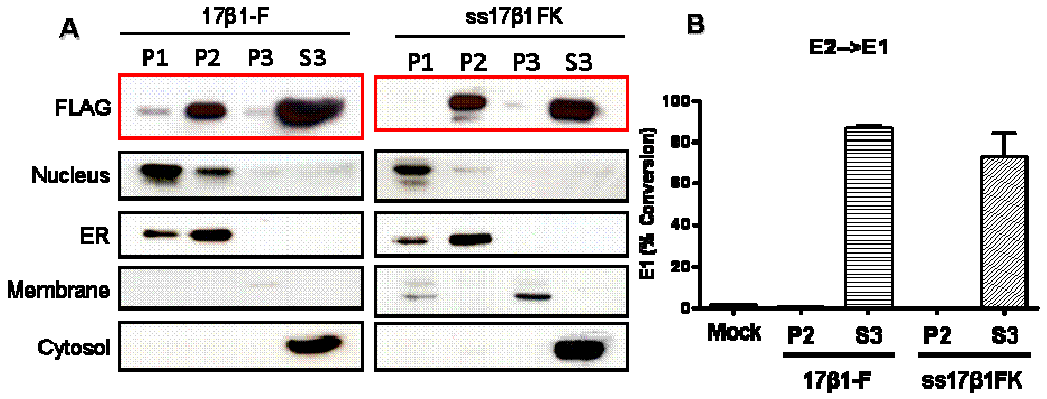

FIGURE 2.27. Cellular Fractionation and Activity Assay of 17β-HSD1-F and ss17β-HSD1FK. A. HEK293T cells transfected with expression vectors containing 17β1-F and ss17β1FK for 48 hours were fractionated as described in MATERIALS AND METHODS. Total protein concentration in each fraction was measured, and equivalent amounts were resolved by SDS-PAGE for western blotting. The following antibodies were used for each fraction: lamin B (P1, nucleus), calnexin (P2, ER), ATPase B2 (P3, plasma membrane) and aldolase (S3, Cytosol). **B.** 5µg of protein was used for an *in vitro* assay to assess protein activity. Aliquots from the cell fractionation were added to 50mM Tris-HCl pH8, 1mM $NADP^+$, 10µM E2 and approximately 280,000 CPM ^{3}H E2 for 1 hour at 37^{o}C. The steroids were extracted, separated on TLC plates, and quantitated by scintillation counting. The data represent the average and standard deviation of three independent experiments.

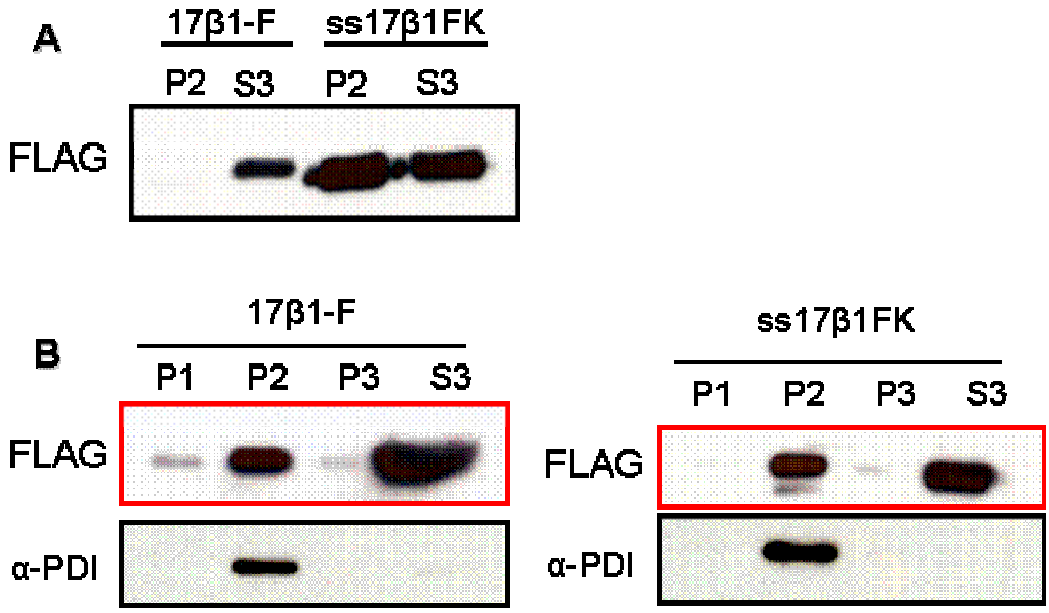

FIGURE 2.28. Western Blots of 17β-HSD1-F and ss17β-HSD1FK in Cellular Fractions. HEK293T cells transfected with expression vectors containing 17β1-F and ss17β1FK for 48 hours were fractionated. Total protein concentration in each fraction was measured, and equivalent amounts were resolved by SDS-PAGE for western blotting. **A.** 17β1-F and ss17β1FK size comparison. **B.** Western blots from Figure 2.26 (anti-FLAG) were stripped and probed for with the soluble ER lumen marker α-PDI with anti-α-PDI antiserum.

Finally, to determine whether the 17β-HSD1-F protein detected in the ER and the cytosol were active, an *in vitro* assay using E2 and exogenous $NADP^+$ was used (FIGURE 2.27). Activity was detected in the S3 (cytosolic) fraction for both the cytosolic and ER-targeted 17β-HSD1-F, whereas no activity was detected in the P2 (ER) fractions. From these data, we conclude that ss-17β-HSD1FK was only partially targeted to the ER lumen, that the ER-retained enzyme was catalytically inactive, and that the cytosolic enzyme alone is responsible for the unaltered directional preference in intact cells.

Since we were only able to target a portion of ss-17β-HSD1-FK to the ER, but not retain it there with a FLAG tag, we reasoned that if 17β-HSD1 is being translocated to the cytosol, avoiding the ERAD pathway (Goeckeler 2010). We reasoned that, if we can prevent 17β-HSD1 from being unfolded, we can prevent this translocation event. GFP is a remarkably stable protein that cannot be degraded by the 26S proteasome (Liu 2003), suggesting that GFP can withstand unfolding and translocation by chaperones in the ER and thus remain in the ER lumen. This prediction is supported by the fluorescence microscopy data in FIGURE 2.24 and 2.25 for 17β-HSD1-GFP and ss-17β-HSD1-GFP-K fusion proteins. To test this prediction, HEK293T cells were transfected with expression vectors containing the cDNA of 17β-HSD1-GFP WT and ss17β-HSD1-GFP-K WT and assayed with E1 and E2. FIGURE 2.29 indicates the behavior of both proteins to be indistinguishable from each other when they were assayed in a high-glucose CM; TABLE 2.4 shows the steroid distributions at pseudo-equilibrium to be identical. We conclude that the GFP tagged 17β-HSD1 constructs have the same directional preference in intact cells as their FLAG-tagged counterparts and are likely to have the same intracellular distributions.

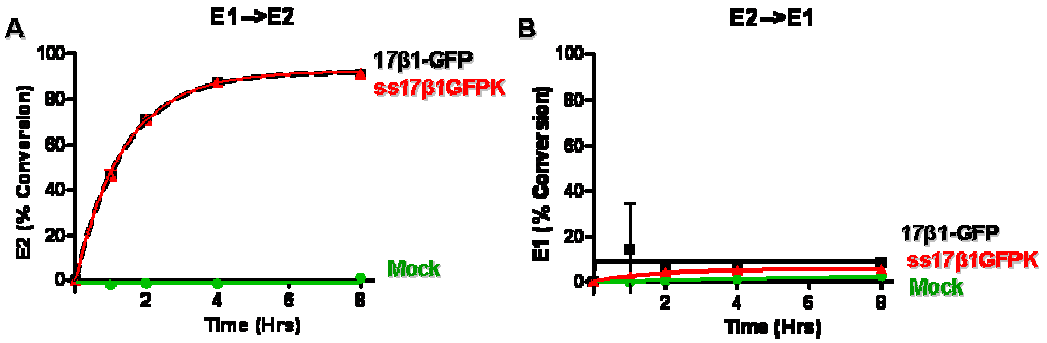

FIGURE 2.29. Activity of Cytosolic and ER Targeted 17β-HSD1-GFP Constructs in High-Glucose Medium. Comparison of E1 and E2 metabolism in high-glucose medium between transient transfections with expression vectors containing cDNA of 17β-HSD1-GFP WT or ss17β1GFPK WT versus control (Mock). **A.** Conversion of E1 (100nM) to E2 by indicated expression vectors is plotted as a function of time. **B.** Conversion of E2 (100nM) to E1 by the same vectors. Data points are means $\pm$ SD of at least three assays; curves are fit to the equation $f(t)=A(1-e^{-kt})$. Equilibrium steroid distributions are derived by setting $t = \infty$ and summarized in Table 2.4.

TABLE 2.4 Steroid Distributions at Pseudo-Equilibrium in HEK-293T cells

	E1→E2		E2→E1	
	%E1	%E2	%E1	%E2
17β1-GFP	8	92	9	91
ss17β1GFPK	8	92	6	94

Chapter 3

AKR1C9 Results

Tagging AKR1C9 with FLAG and GFP

To determine the cellular location of AKR1C9, we added a FLAG peptide sequence or GFP fusion protein, because no antibodies existed for AKR1C9 at the time this research began. A time course showed that FLAG and GFP have no negative impact on AKR1C9 activity (FIGURE 3.1). It should also be noted that the AKR1C9 construct targeted to the ER, ss-AK-FK, was also active, although cells transfected with this construct took longer to reach pseudo-equilibrium than the cytosolic constructs.

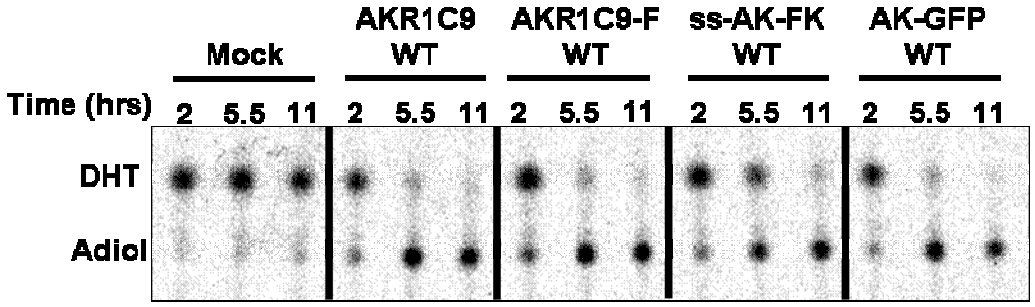

FIGURE 3.1. Assessing AKR1C9-FLAG, ssAKR1C9FK, AKR1C9-GFP Directional Preference. HEK293 cells were transfected with expression vectors containing the cDNA of AKR1C9 WT, AKR1C9-FLAG WT, ss-AKR1C9-FLAG-KDEL WT, AKR1C9-GFP WT and Mock (empty pcDNA3.1 or no DNA) for 48hrs. Cells were then incubated with 100nM DHT. Aliquots were removed at 2, 5.5 and 11hours, extracted, separated on a TLC plate and imaged with a phosphoscreen.

After determining that FLAG does not eliminate AKR1C9 activity, point mutations were introduced to Arginine 276 (R276) in both the cytosolic and ER targeted backgrounds. The crystal structure of rat AKR1C9 shows R276 coordinating the 2'-phosphate group of $NADP^+$ (FIGURE 3.2). Before making stable cell lines with these expression-constructs, we verified that the constructs encoded active proteins. FIGURE 3.3 shows that all eight constructs have activity, converting DHT to Adiol more than the Mock sample, except R276E, which has an oxidative directional preference (Papari-Zareei 2006). FIGURE 3.4 indicates that the FLAG antibody detects proteins with the molecular weight of AKR1C9 (37kDa) using all expression constructs. These data show that our expression constructs are active and encode for proteins of expected molecular weight.

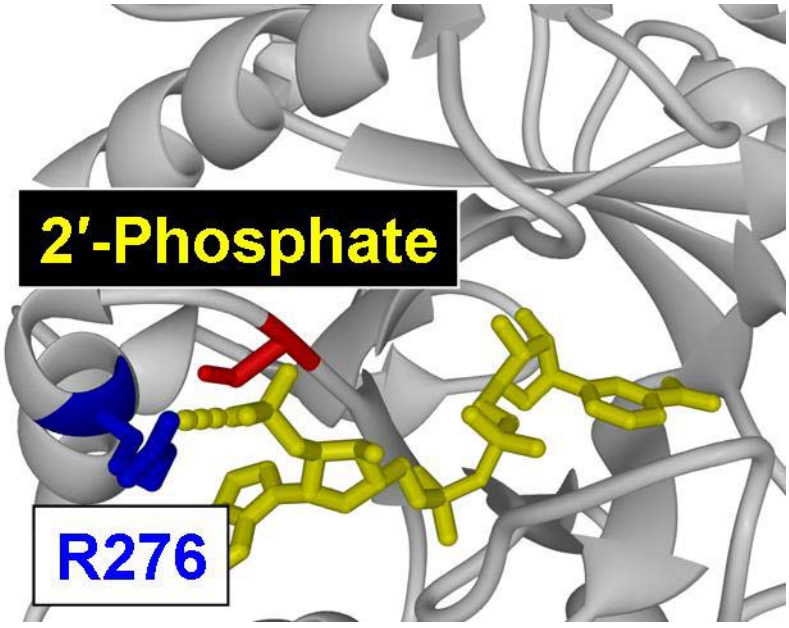

FIGURE 3.2 Crystal Structure of Rat AKR1C9 with $NADP^+$. A partial view of rat AKR1C9 (grey) coordinating $NADP^+$ (yellow). AKR1C9's R276 (blue) forms a salt bridge with the 2'-phosphate group (yellow) of $NADP^+$. Disruption of this salt bridge results in altered steroid distributions. Figure adapted from Mizrachi 2009.

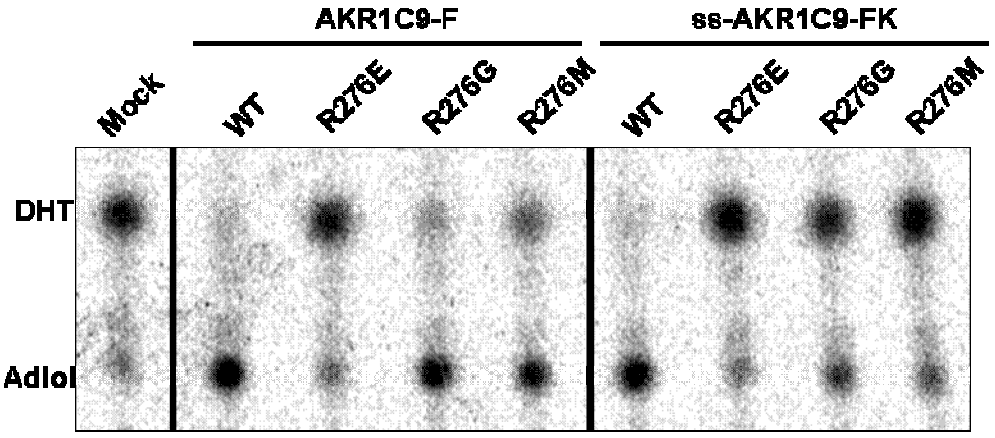

FIGURE 3.3. Assessing AKR1C9-FLAG and ssAKR1C9FK R276 Mutant Activity. HEK293 cells were transfected with expression vectors containing the cDNA of AKR1C9-FLAG WT and R276 mutations, ss-AKR1C9-FLAG-KDEL WT and R276 mutations, and Mock (empty pcDNA3.1 or no DNA) for 48hrs. Cells were then incubated with 100nM DHT. Aliquots were removed after 24 hours, extracted, separated on a TLC plate and imaged with a phosphoscreen.

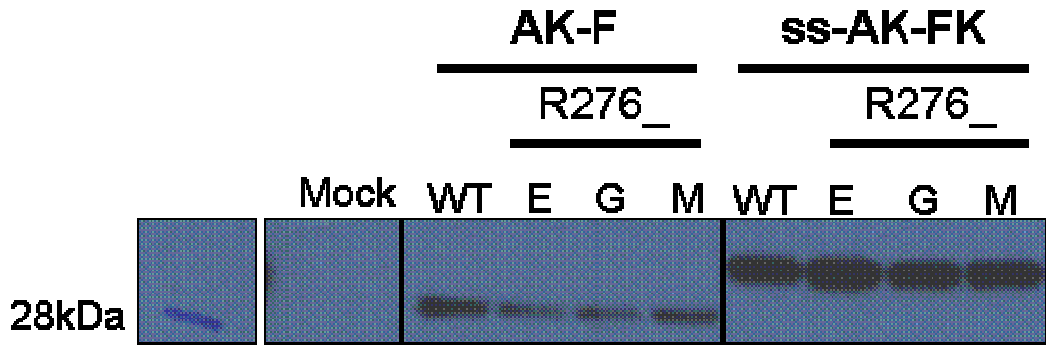

FIGURE 3.4. Anti-FLAG Immunoblot. HEK293 cells were transfected with expression vectors containing the cDNA of AKR1C9-FLAG WT or R276 mutations, ss-AKR1C9-FLAG-KDEL WT or R276 mutations, or Mock-transfected. Cells were lysed, centrifuged, resolved by SDS-PAGE, and western blotted for the FLAG epitope with α-FLAG antibody M2.

Stable Cell Lines

To better assess the affect of the ER lumen on AKR1C9 activity, we chose to make stable cell lines because of the increased signal-to-noise ratio and greater reproducibility that stable cell lines afford over transient transfection. We used the constructs tested in FIGURE 3.3 to make stable cell lines. As was observed with experiments using the ER-targeted 17β-HSD1 expression constructs, every plate transfected with an ER targeted AKR1C9 expression construct gave very few clones

As experienced with the 17β-HSD1 stable lines, we suspected that chronic over-expression of a foreign protein in the ER was toxic to the cells. Consequently, we used Invitrogen's Flp-In T-REx system for inducible protein expression which this required sub-cloning our cDNAs into the pcDNA5 expression constructs, containing a Flp-recombinase site for incorporation into host genome. Before transfecting cells into the Flp-In T-REx HEK293 host cell line to make stable cells, we tested our pcDNA5 expression constructs for activity (FIGURE 3.5) and found that all constructs yielded active enzyme. We transfected our pcDNA5 expression constructs into the host cell line and obtained many clones after several weeks of incubation in selection media. Colonies were not tested for activity; however, as the induction problems encountered with the 17β-HSD1 cell lines were not resolved.

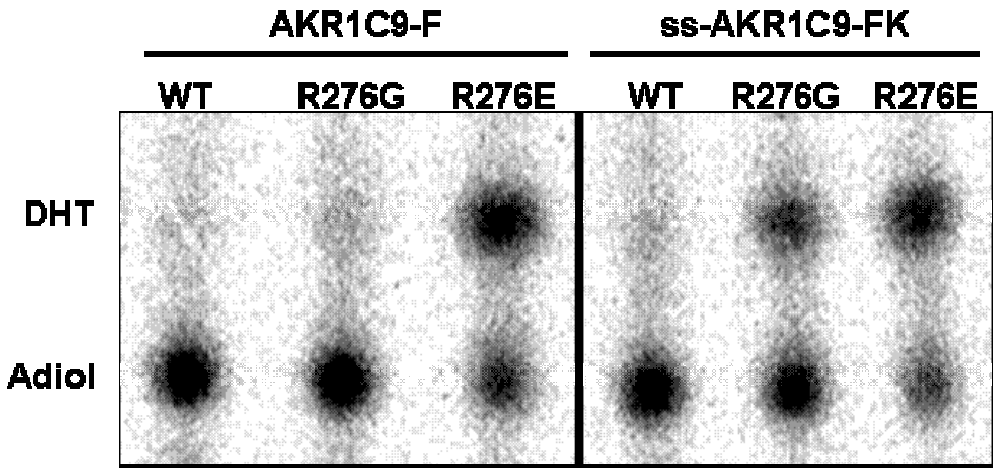

FIGURE 3.5. Assessing AKR1C9-F Activity in pcDNA5. HEK293 cells were transfected with pcDNA5 expression vectors containing the cDNA of AKR1C9-FLAG WT and R276 mutations, or ss-AKR1C9-FLAG-KDEL WT and R276 mutations for 48hrs. Cells were then incubated with 100nM DHT. Aliquots were removed after 24hours, extracted, separated on a TLC plate, and imaged with a phosphoscreen.

Transient Transfections

To determine if the low signal-to-noise ratio and rate of steroid metabolism using transient transfections is adequate for our experiments, we transfected HEK293 cells with 2.5µg of DNA for 48hours, followed by a steroid metabolism time course (FIGURE 3.6). The transient transfections resulted in activity comparable to stable cell lines previously published based on our initial experiment (TABLE 3.1) and indicates that transient transfections could be used if stable cell lines cannot be made.

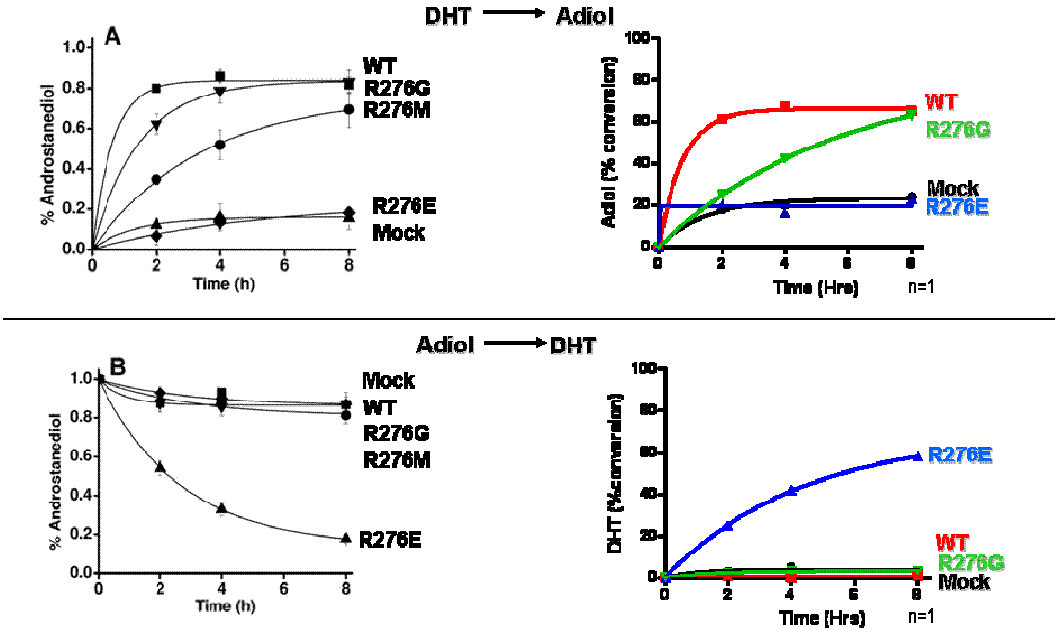

FIGURE 3.6. Comparing Activity of Stable Cell Lines and Transient Transfections. Comparison of DHT and Androstanediol (Adiol) metabolism between HEK293 cell lines expressing AKR1C9 WT or R276 mutations (left hand side of panels, Papari-Zareei 2006) and transient transfections with expression vectors containing cDNA of AKR1C9-FLAG WT and R276 mutations (right hand side of panels). **A.** Conversion of DHT (100nM) to Adiol by cells expressing indicated enzymes is plotted as a function of time. **B.** Conversion of Adiol (100nM) to DHT by the same cells. Data points are from one experiment; curves are fit to the equation $f(t)=A(1-e^{-kt})$. Equilibrium steroid distributions are derived by setting $t = \infty$ and summarized in TABLE 3.1.

TABLE 3.1 Comparison of Steroid Distributions at Pseudo-Equilibrium in Transiently Transfected HEK-293T Cells and Stably-Expressing HEK293 Cell Lines

		DHT → Adiol (%)		Adiol → DHT (%)	
	Enzyme	DHT	Adiol	DHT	Adiol
Transient Transfections in HEK293T cells	AKR1C9-F WT	34	66	1	99
	R276E	80	20	69	31
	R276G	17	83	3	97
Stably expressing HEK293 cells	AKR1C9-F WT	8	92	2	98
	R276E	86	14	80	20
	R276G	13	87	5	95

To assess the affect of the ER lumen on AKR1C9 activity, HEK293 cells were transfected with expression constructs and assayed with both DHT and Adiol (FIGURE 3.7 and TABLE 3.2). These preliminary results are difficult to assess, because high background activity was observed and because cells expressing AKR1C9-F WT converted only ~65% of the DHT to Adiol, rather than the typical >90% conversion. In this pilot experiment, the ER-targeted ss-AKR1C9-FLAG-KDEL WT and R276E mutation demonstrated significant activity above background. Efforts were then focused on the 17β-HSD1 experiments, and AKR1C9 metabolism studies were not pursued further.

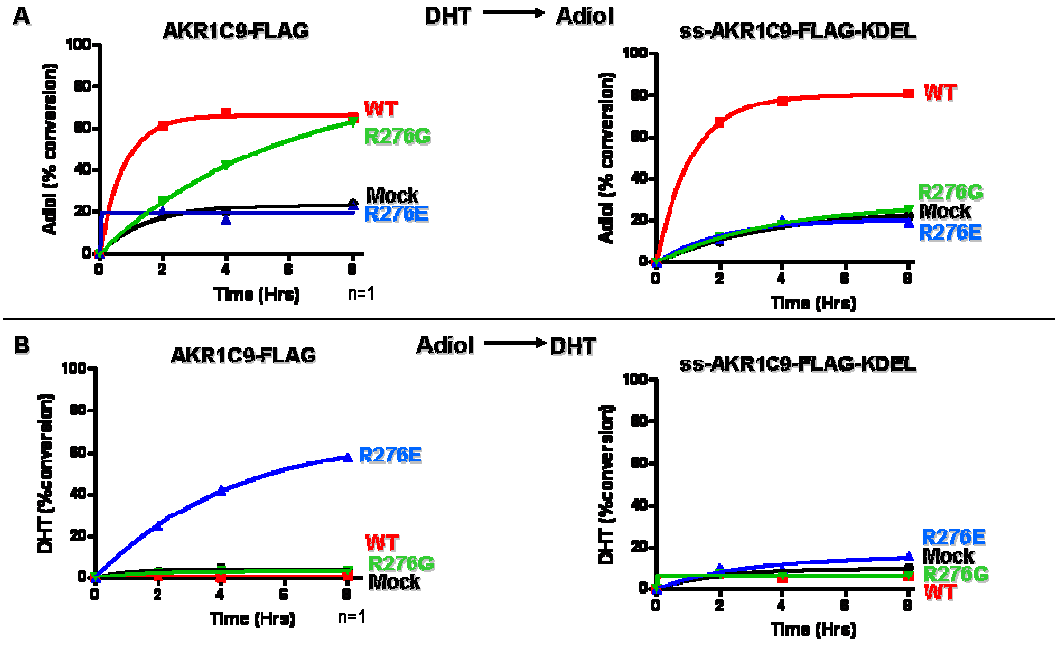

FIGURE 3.7. Activity of Cytosolic and ER-Targeted AKR1C9-F Constructs in High-Glucose Medium. Comparison of DHT and Adiol metabolism in high-glucose medium between transiently transfected HEK293 cells using expression vectors containing cDNA of AKR1C9-FLAG WT and R276 mutations (left hand side of panels) or ssAKR1C9FK WT and R276 mutations (right hand side of panels). **A.** Conversion of DHT (100nM) to Adiol by indicated expression vectors is plotted as a function of time. **B.** Conversion of Adiol (100nM) to DHT by the same vectors. Data points are from one experiment; curves are fit to the equation f(t)=A(1-e-kt). Equilibrium steroid distributions are derived by setting t = ∞ and summarized in TABLE 3.2.

TABLE 3.2 Steroid Distributions at Pseudo-Equilibrium in HEK293T Cells

		DHT → Adiol (%)		Adiol → DHT (%)	
Enzyme		**DHT**	**Adiol**	**DHT**	**Adiol**
AKR1C9-F	WT	34	66	1	99
	R276E	80	20	69	31
	R276G	17	83	3	97
ssAKR1C9-FK	WT	19	81	6	94
	R276E	59	41	37	63
	R276G	49	51	7	93

Determination of Cellular Location

To determine the cellular location of AKR1C9-FLAG and ss-AKR1C9-FLAG-KDEL, HEK293 cells were transfected, fixed to glass slides, permeabilized, probed with anti-FLAG primary antibody and fluorescent-conjugated secondary antibody, and viewed with a fluorescence microscope (FIGURE 3.8). The images obtained were inconclusive; however, AKR1C9-F appears to show diffuse cytosolic localization, whereas ss-AKR1C9-FK has a more granular distribution.

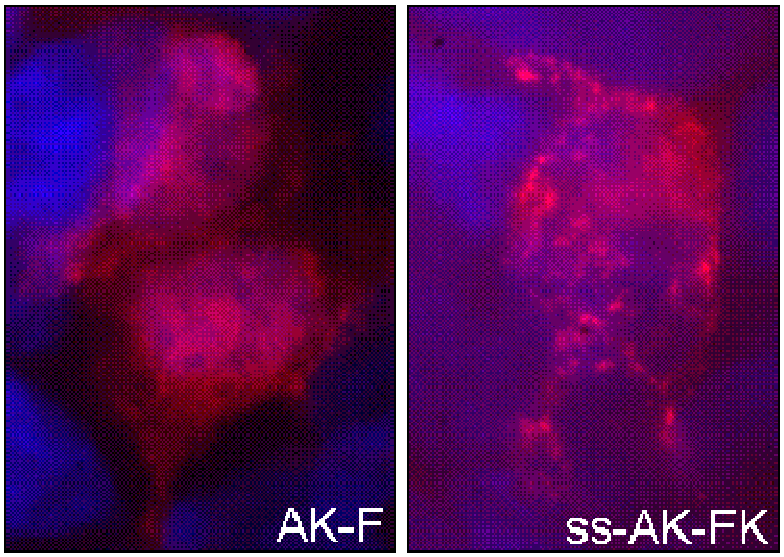

FIGURE 3.8. Immunofluorescence of FLAG Constructs AKR1C9-FLAG (AK-F) and ss-AKR1C9-FLAG-KDEL (ss-AK-FK). Cells were fixed, permeabilized, and probed with anti-FLAG primary and anti-IgG-FITC secondary antibody. Representative images of cells show diffuse localization of fluorescence of both proteins, with ss-AKR1C9-FLAG-KDEL showing more granular pattern.

Chapter 4

11β-HSD1 Results

We intended to generate stable cell lines expressing 11β-HSD1 and engineered variants, with 11β-HSD1 targeted to face inside or outside the ER membrane. HEK293 cells were transfected with expression vectors containing the cDNA of 11β-HSD1-FLAG WT in a pcDNA5 vector, 11β-HSD1-FLAG WT and K5S mutation (faces cytoplasm, FIGURE 4.1), ss-11β-HSD1-FLAG-KDEL WT, 11β1-FLAG cyto, H6PD-HA and G359D mutation (FIGURE 4.2), G6PD WT, ss-G6PD-HA-KDEL, 11β-HSD1-FLAG R66 mutations and 11β-HSD1-FLAG K5S R66 mutations (FIGURES 4.3A and 4.3B), and screened activity by the ability to convert cortisone to cortisol. 11β-HSD1-FLAG WT was assessed in a pcDNA3 vector as well as a pcDNA5 vector for use in making a Flp-In T-REx stable cell line; both constructs are active. Cells transfected with these plasmids showed cortisone reduction only slightly above background at 48h. The K5S point mutation has been shown to reverse the orientation of 11β-HSD1 such that the enzyme is now facing the cytosol instead of the ER lumen (Odermatt 1999); this initial experiment shows poor if any activity in reducing cortisone to cortisol. To determine the effect of the N-terminal transmembrane domain on activity, a soluble ER-targeted 11β-HSD1 construct was made with a signal sequence replacing the N-terminal transmembrane binding domain and the addition of a

KDEL retention signal on the C-terminus (ss11β1FK). To assess the contribution of the ER environment and the N-terminal domain, a soluble cytosolic construct, 11b1 cyto, was made where the N-terminal domain was deleted. No convincing activity could be seen for cells transfected with the K5S, ss11β1FK, or 11b1F cyto constructs. To assess the importance of 11β-HSD1's R66 (Hosfield 2005) in binding NADPH for cortisone reduction, R66 mutants were made in the WT and K5S background. In this pilot experiment, none of the constructs showed convincing activity above background (FIGURE 4.3B).

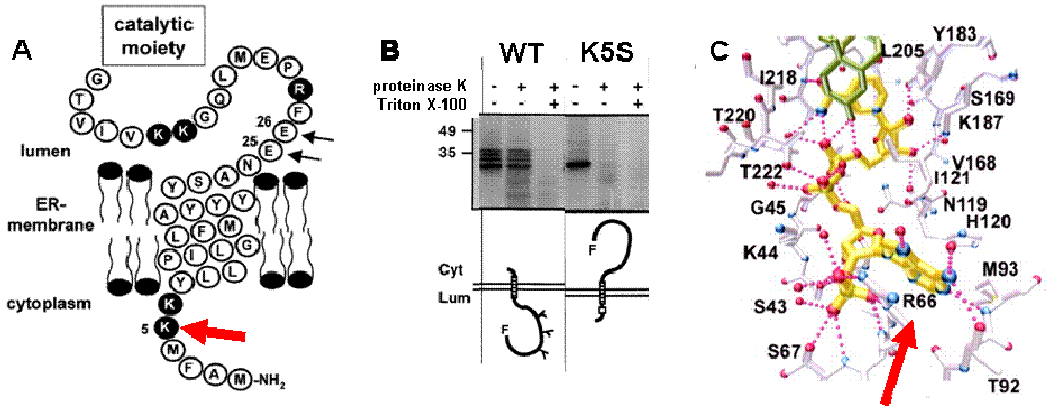

FIGURE 4.1. Key amino acids in 11β-HSD1. A. Secondary structure of 11β-HSD1's N-terminal transmembrane domain (Figure taken from Odermatt 2006). **B**. Protease protection assay of ER microsomes from transiently transfected cells expressing 11β-HSD1-FLAG WT (left hand side) or 11β-HSD1-FLAG K5S (right hand side). The addition of proteinase K without Triton X-100 demonstrates the different orientation of the two proteins (Figure taken and adapted from Odermatt 1999). **C**. Partial view of the human 11β-HSD1 crystal structure (white) shown with $NADP^+$. R66 (red arrow) coordinates the 2'-phosphate group of $NADP^+$.

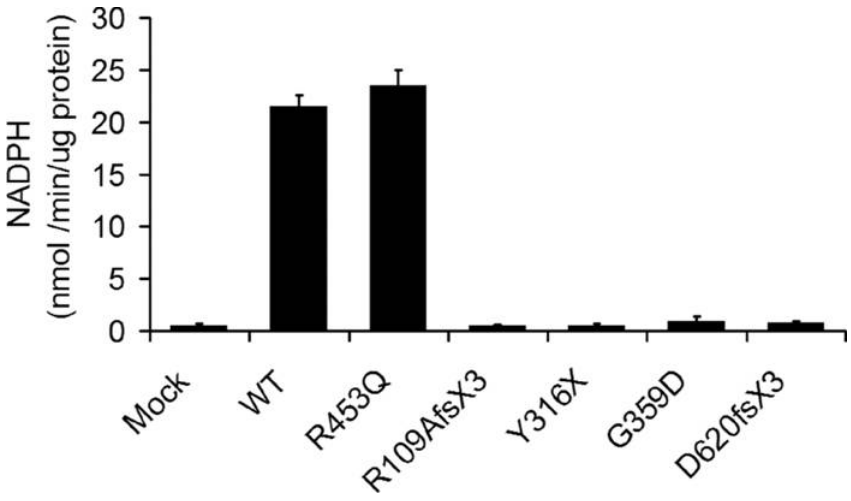

FIGURE 4.2 H6PD G359 NADPH Enzymatic Assay. Patients with reported cortisone reductase deficiency were genotyped and the resulting point mutations in H6PD were reported (Figure taken from Lavery 2008). ER microsomes from stable cell lines were created expressing the above listed H6PD mutations. R109AfsX3, Y316X and D620fsX3 are truncation mutations. G359D is a point mutant that cannot regenerate NADPH *in vitro*.

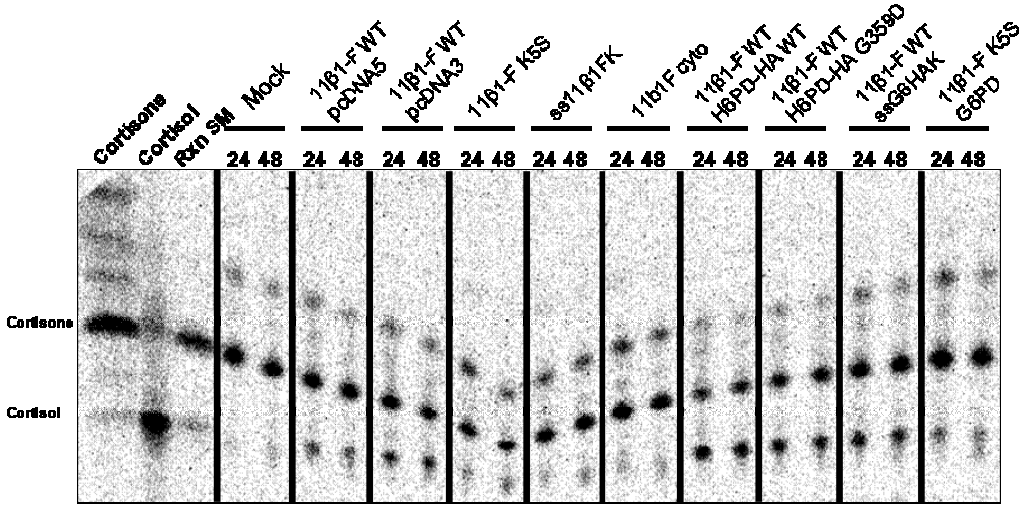

FIGURE 4.3A. Screening 11β-HSD1 Constructs for Activity. HEK293 cells were transfected with expression vectors containing the cDNA of 11β-HSD1-FLAG WT in a pcDNA5 vector, 11β-HSD1-FLAG WT and K5S mutation, ss-11β-HSD1-FLAG-KDEL WT, 11β1-FLAG cyto, H6PD-HA and G359D mutation, G6PD and ss-G6-HA-KDEL. Cells were then incubated with 100nM cortisone. Aliquots were removed after 24 and 48hrs, extracted, separated on a TLC plate and imaged with a phosphoscreen.

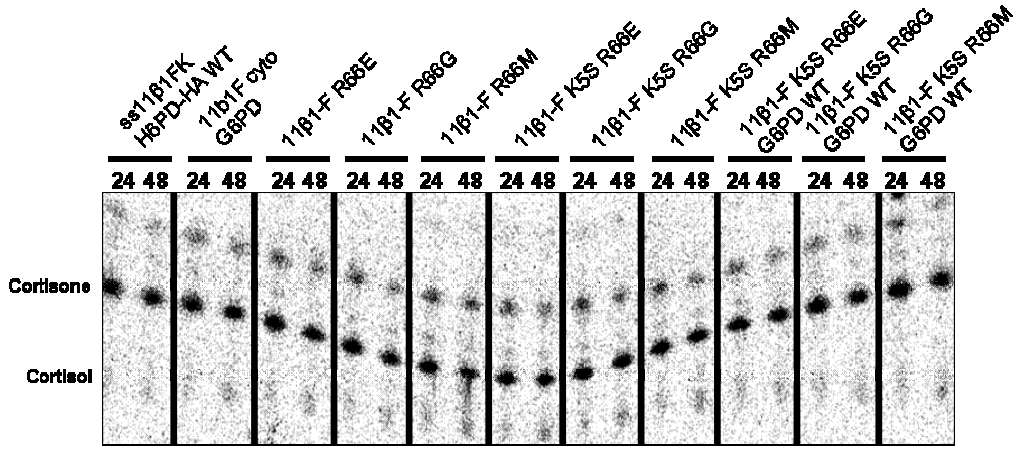

FIGURE 4.3B. Screening 11β-HSD1 Constructs for Activity. HEK293 cells were transfected with expression vectors containing the cDNA of ss-11β-HSD1-FLAG-KDEL + H6PD-HA WT, 11β1-FLAG cyto + G6PD WT, 11β-HSD1-FLAG R66 mutations, 11β-HSD1-FLAG K5S-R66 mutations. Cells were then incubated with 100nM cortisone. Aliquots were removed after 24 and 48hrs, extracted, separated on a TLC plate and imaged with a phosphoscreen.

To efficiently convert cortisone to cortisol, H6PD, which generates NADPH from glucose-6-phosphate in the ER lumen, is required (Atanasov 2004). Addition of WT H6PD to 11β-HSD1-FLAG showed a significant increase in cortisol production, suggesting that our HEK293 cells are relatively deficient in H6PD, which limits cortisone reductive activity in these cells. To further study the important residues in H6PD, numerous point mutations were made, listed in the Materials and Methods section. We decided to use H6PD-HA G359D as a negative control, because this mutation cannot regenerate NADPH (Lavery 2008); however, this mutation appeared to support cortisone reduction as well as WT H6PD. To dissect the contributions of NADPH regeneration on 11β-HSD1 activity, we replaced H6PD with an ER-targeted G6PD, which regenerates NADPH in the cytosol. Our G6PD construct appears to support 11β-HSD1 metabolism similarly to the H6PD WT and G359D constructs. To determine whether this effect was due to the ER location, G6PD was over-expressed with 11β-HSD1 K5S; the cortisone reduction activity is above background in this experiment. In contrast, G6PD did not restore cortisone reductase activity to 11β-HSD1 cyto, suggesting that the N-terminal domain is required for activity.

In summary, we found that only when 11β-HSD1 with intact N-terminal domain was co-expressed with H6PD or G6PD could we obtain good cortisone reduction activity in HEK293 cells. These screening assays were used to identify active constructs, before more extensive kinetic experiments are used to determine the effect of the various mutations on the cortisone:cortisol distribution.

Before we proceeded with experiments involving extensive use of the above assayed expression vectors, we realized that all published data on 11β-HSD1 expression in HEK293 cells assayed initial rates of conversion rather than final steroid distributions. We did not know how cortisone reductase activity varied among cell lines. We have used HEK293 and CHO cells extensively and chose these lines for an initial comparison study. HEK293 and CHO cells were transfected with 11β-HSD1 and H6PD expression constructs to determine directional preference and steady-state steroid distributions. In HEK293 cells, the final steroid distribution actually favors cortisol oxidation, with only 37% cortisol at steady-state compared to 11% in Mock transfected cells (FIGURE 4.4). This result might explain some of the poor metabolism observed in FIGURE 4.3. Co-transfection of H6PD increased cortisone reduction substantially, with 65% cortisol at steady-state. In contrast, CHO cells showed a stronger directional preference with 83% cortisol at steady state, but H6PD co-transfection increased this conversion only to 91%. These data are consistent with low endogenous H6PD expression in HEK293 cells and higher expression in CHO cells. Furthermore, hamster H6PD supports 11β-HSD1 activity.

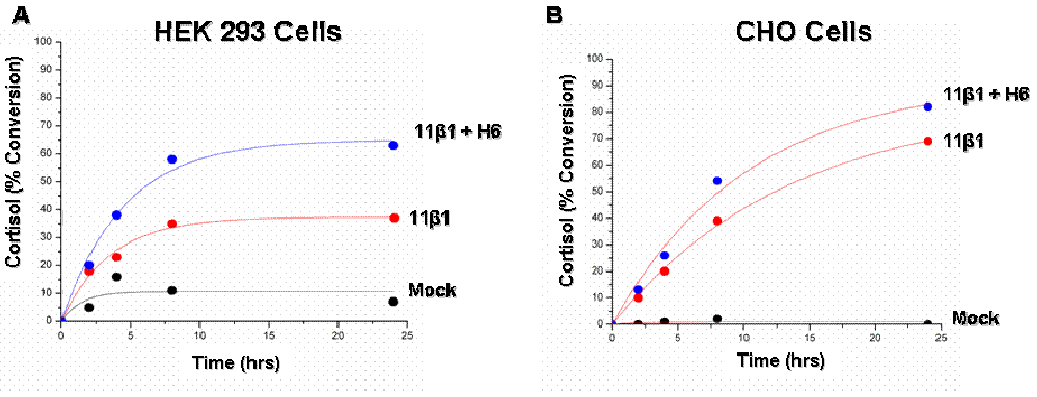

C

	Cortisone→ Cortisol	
	HEK293	CHO
	%Cortisol	%Cortisol
Mock	11	1
11β1	37	83
11β1 + H6PD	65	91

FIGURE 4.4. Time Course of Cortisone Reduction in HEK293 and CHO Cells. HEK293 cells (**A**) and CHO cells (**B**) were transfected with expression vectors containing the cDNA of 11β-HSD1-FLAG with and without H6PD-HA WT. Cells were then incubated with 100nM cortisone. Aliquots were removed after 2, 4, 8 and 24hrs, extracted, separated on a TLC plate, imaged and quantified with a phosphoscreen. **C**. Steroid distributions are tabulated for comparison between the two cell lines. Data points are from one experiment; curves are fit to the equation $f(t)=A(1-e^{-kt})$. Equilibrium steroid distributions are derived by setting $t = \infty$ and summarized. Data derive from one representative experiment which has been repeated twice more.

Before choosing HEK293 or CHO cells for further experiments, we assessed the two cell types with a second time course using the expression constructs containing 11β-HSD1 and H6PD WT and G359D, which cannot regenerate NADPH. The HEK293 samples were inadvertently compromised so only the CHO samples could be assessed. We found little difference in final cortisol conversion whether 11β-HSD1 was expressed alone or with H6PD WT or G359D (FIGURE 4.5). These results convinced us that 11β-HSD1 assays in HEK293 cells afforded us a greater dynamic range than in CHO cells.

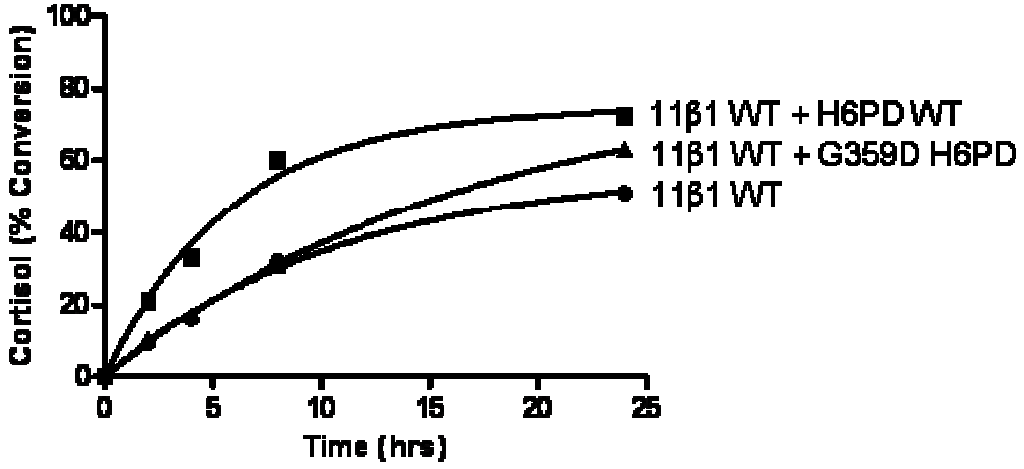

FIGURE 4.5. Cortisone Reduction Time Course in CHO Cells. CHO cells were transfected with expression vectors containing the cDNA of 11β-HSD1-FLAG alone or with H6PD-HA WT or G359D mutation and then incubated with 100nM cortisone. Aliquots were removed after 2, 4, 8 and 24hrs, extracted, separated on a TLC plate, imaged and quantified with a phosphoscreen. Data points are from one experiment; curves are fit to the equation $f(t)=A(1-e^{-kt})$.

To further assess the activity and directional preferences of our constructs, HEK293 cells were transfected with expression vectors containing the various 11β-HSD1 WT cDNAs with or without H6PD and incubated with 100nM cortisone (FIGURE 4.6 Panel A) or 100nM cortisol (FIGURE 4.6 Panel B) for 24hr, with 11β-HSD2 as an oxidation control. Figure 4.6A shows that several constructs showed fair metabolism in the reductive direction, while Figure 4.6B shows that these cells all demonstrated much better conversion in the oxidative direction, nearly as high for 11β-HSD2. This experiment confirms that most of our constructs are active in HEK293 cells, but low endogenous H6PD expression limits cortisone reduction in this cell line.

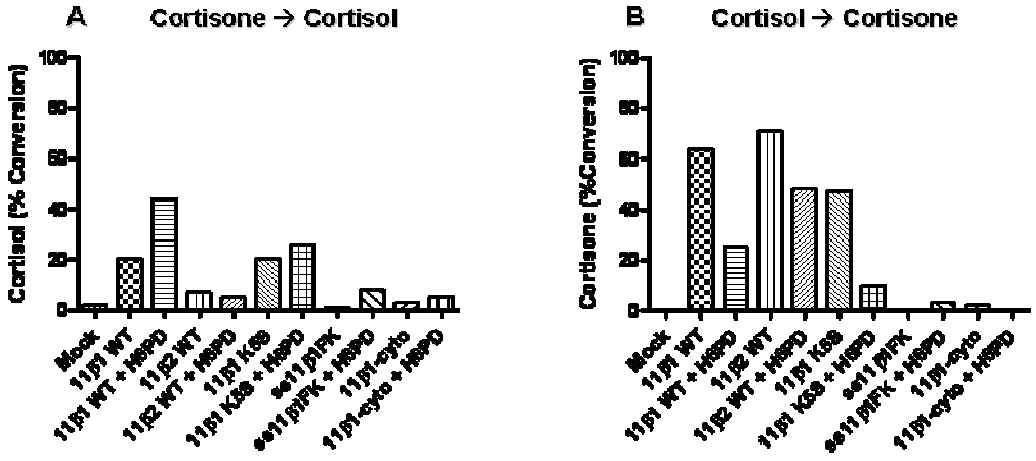

FIGURE 4.6. Exhaustive Metabolism Assay with Cortisone and Cortisol. HEK293 cells were transfected with expression vectors containing the cDNA of 11β-HSD1 WT, 11β-HSD2, H6PD-HA WT, 11β-HSD1-FLAG K5S, ss-11β-HSD1-FLAG-KDEL and 11β1-FLAG cyto as indicated. Cells were then incubated either 100nM cortisone (**A**) or 100nM cortisol (**B**). Aliquots were removed after 24hrs, extracted, separated on a TLC plate, imaged and quantified with a phosphoscreen. Data are from one experiment.

We performed an additional time course experiment for cortisone reduction in HEK293 cells (FIGURE 4.7). This experiment confirmed that only when cells were co-transfected with 11β-HSD1-F and H6PD showed the greatest activity as expected, but the fit of these data to exponential growth curves was poor. In conclusion, studies of 11β-HSD1 directional preference in intact cells are complicated by the abundance of endogenous H6PD, which appears to be higher in CHO cells than HEK293T cells.

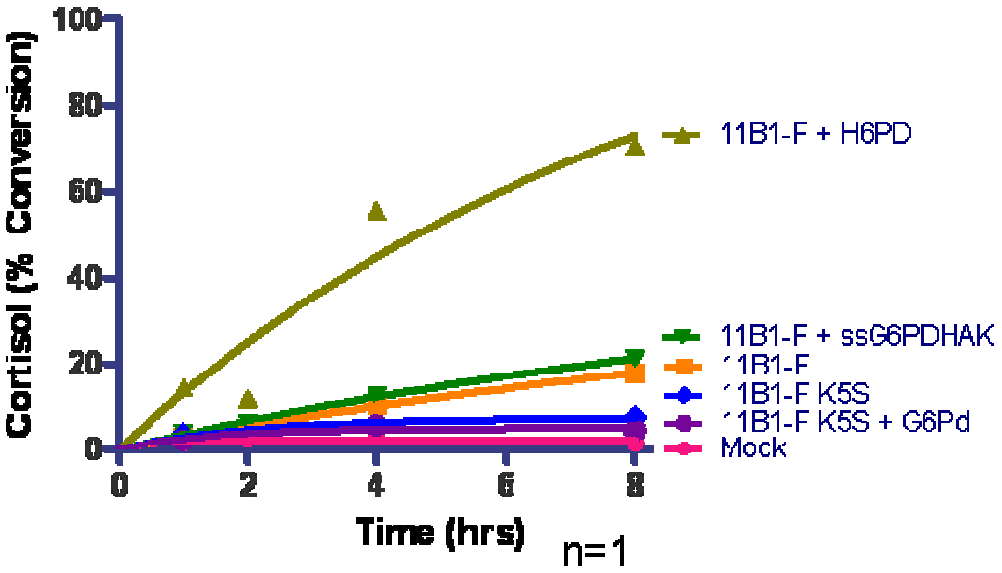

FIGURE 4.7. Time Course of Cortisone Reduction in HEK293T Cells. HEK293T cells were transfected with expression vectors containing the cDNA of 11β-HSD1-FLAG WT and K5S, ssG6PDHAK and H6PD-HA WT and then incubated with 100nM cortisone. Aliquots were removed after 2, 4, and 8 hrs, extracted, separated on a TLC plate, imaged and quantified with a phosphoscreen. Data points are from one experiment; curves are fit to the equation $f(t)=A(1-e^{-kt})$.

Chapter 5

Discussion

17β-HSD1 Discussion

Previous work from our lab has demonstrated the importance of cofactor binding and cofactor concentration ratios on 17β-HSD1 and AKR1C9 directional preference in intact cells. When cofactor binding was compromised by either point mutations or glucose deprivation, the *in vivo* reduction of ketosteroids decreased. *In vitro* kinetic studies with recombinant protein confirmed that mutations designed to impair NADPH binding do reduce NADP(H) affinity (Sherbet 2009, Papari-Zareei 2006). We asked if these principles could be applied to other HSD enzymes with special properties. 11β-HSD1 reduces cortisone to cortisol in the oxidative ER lumen. The previously-mentioned enzymes, 17β-HSD1 and AKR1C9, reduce their respective steroid hormones in the cytosol. We asked, do the same rules for 17β-HSD1 and AKR1C9 apply to 11β-HSD1, and can we learn the factors regulating its directional preference.

To start, we made constructs targeting 17β-HSD1 to the ER lumen and assayed for activity. Initial experiments using transiently transfected cells indicated the ER-targeted 17β-HSD1 had the same activity as the cytosolic version. To confirm our findings, we attempted to derive stable cell lines, to compare the new ER-targeted enzyme to previously published data with cytosolic enzyme. We chose stable cell lines because of the higher signal-to-noise ratios

and better reproducibility than transient transfection experiments. We easily made lines expressing 17β-HSD1 or AKR1C9 with FLAG tags, but we obtained few clones from experiments using the ER targeted constructs, and the few clones obtained exhibited little to no activity and poor viability. This result was repeated several times: lines expressing cytosolic 17β-HSD1 are viable are alive and catalyze E1 reduction, while lines expressing ER-targeted 17β-HSD1 did not survive. This result suggested that over-expression of our ER-targeted 17β-HSD1 construct was toxic to the cells, possibly by inducing ER stress. This posed a dilemma: how can we study the activity of 17β-HSD1 in the ER lumen if its expression in the ER harms cells? The transient transfections used to assess whether the constructs were active or not exhibited activity and protein expression. This dichotomy suggests that chronic over-expression of 17β-HSD1 in the ER is toxic to the cells, whereas short-term over-expression is tolerated. The cells used in making stable lines took weeks to die, more than enough time for us to use them for metabolic experiments. We wanted to take advantage of the high signal to noise ratio and consistency that stable cell lines afford us while not harming the cells with chronic over-expression.

To achieve short-term expression in a stable line, we employed Invitrogen's Flp-In T-REx system to derive tetracycline-inducible stable cell lines. In this case, the protein of interest is only expressed when tetracycline is added, avoiding the toxicity of chronic expression. The Flp-In T-Rex system requires subcloning the cDNAs into the pcDNA5 expression vector, which incorporates a Flp-Recombinase site for single-copy integration. Despite multiple

efforts using tetracycline or doxycycline, we could not achieve protein induction, as evidenced by the lack of E1 reduction. To troubleshoot this issue, we obtained Dr. Frank Lee's Flp-In T-Rex HEK293 FLAG-HIF-2α –P531A cell line (Percy 2008) as a positive control with the same FLAG epitope for western blotting and were able to induce expression in his cell line with doxycycline (Figure 2.14). Our cells were resistant to hygromycin and sensitive to Zeocin, but we were not able to PCR a band with 17β-HSD1 specific primers from genomic DNA, indicating that our cells do not have the 17β-HSD1 cDNA incorporated into their genome. Because the inducible stable cell lines were proving troublesome and the transient transfections with the HEK293Ts yielded results similar to published data from our laboratory, we decided to use transiently transfected HEK293T cells for all experiments.

We noticed that the cytosolic and ER targeted 17β-HSD1 -F constructs exhibited remarkably similar final steroid distributions, contrary to our hypothesis that the lower [NADPH] in the ER lumen would disfavor the E1 reduction. We found the same final steroid distributions in both the high glucose medium and in glucose-free medium with 2-deoxyglucose (Table 2.2). We considered the possibility that the rates of E1 reduction and/or E2 oxidation were slower in the ER than in the cytosol, despite similar final steroid distribution in either cellular location. Using double-isotope scrambling experiments starting with the final steroid distribution observed in the previous time course experiments, we found no difference in the oxidation and reduction rates observed between the cytosolic and ER-targeted 17β1-F constructs.

All the thermodynamic and kinetic data both indicate no difference in activity between 17β1-F in the cytosol and ER lumen. This surprising result prompted us to question whether our ER-targeted constructs successfully isolated the engineered 17β-HSD1 to the ER lumen. To determine the cellular location of our 17β1-F constructs, we made use of our GFP- and FLAG-tagged constructs to track subcellular location with fluorescence microscopy experiments. We compared their location to known cytosolic GFP and ER-targeted RFP constructs. 17β1-GFP and ss-RFP-KDEL clearly reside in different compartments, while ss17β1GFP-KDEL and ss-RFP-KDEL overlap, as evidenced by the yellow color (FIGURE 2.22 and 2.23). The FLAG-tagged constructs yielded inconclusive information, possibly because FLAG localization requires cell permeabilizing and antibody probing before fluorescence microscopy. The inconsistent results did not enable us to conclude that 17β-HSD1 was successfully targeted to the ER lumen.

To resolve these discrepancies from fluorescence microscopy experiments, we used cellular fractionation to determine the cellular location of our constructs. We acknowledge the contributions of graduate student Hyeilin Ham from the Orth Lab, who performed these experiments. The first fractionation indicated that all of the cytosolic 17β1-F was in the cytosol, as expected, while the ER-targeted 17β1-F was split between the ER and cytosolic fraction (Figure 2.26). If this result is true, then the identical final steroid distributions for cells expressing the two enzymes means that either the enzyme in the ER catalyzes the same steroid distribution as that in the cytosol, or that these cells have much more enzyme in the cytosol. Alternatively, the enzyme in the ER could be misfolded and inactive.

To determine whether the protein isolated in the ER fractions was active, an *in vitro* assay using the cellular fractions was performed. Although subsequent fractionations were less pure than the first experiment, activity was found only in the cytosolic fractions. This result was observed several times, with no activity ever recovered in the ER fraction. To determine if the 17β-HSD1-F and ss17β1 -FLAG-KDEL recovered from different fractions were processed, a side-by-side western blot failed to reveal a convincing size difference in these proteins. We concluded that the ER-targeted ss17β-HSD1-FLAG-KDEL was trafficking through the ER, since some protein was recovered from the ER fraction, but cleavage of the ss signal sequence and possibly KDEL ER-retention motif translocated the majority of the protein to the cytosol, with the same mass as native 17β-HSD1. 17β-HSD1-F does not have any N-glycosylation sites as an independent confirmation of ER processing. Nevertheless, we needed to exclude the potential artifact that the fractionation technique itself caused the ER-targeted 17β-HSD1-F to leak into the cytosolic fraction. Calnexin, an integral ER membrane protein, was used in the previous experiments to assess purity of the ER fraction, but soluble proteins are more vulnerable to spillage from an organelle. We therefore hypothesized that if the ER membrane is somewhat compromised, allowing its contents to partially mix with the cytosol, a membrane protein marker would remain in the ER fraction, but a lumen protein such as disulfide isomerase (α-PDI), which resembles our protein, would mix with the cytosol. Western blots clearly showed that α-PDI was distributed exclusively in the ER fraction, indicating that the procedure did not significantly compromise

the ER membrane integrity and that ss17β-HSD1-FK indeed existed intracellularly in both compartments. Therefore, the reason that our experiments with ER-targeted 17β-HSD1 failed to show a difference in final steroid distribution is that the enzyme partially resides in the cytosol and that only cytosolic enzyme is active.

We concluded that either over-expression processing or an intrinsic property causes ss-17β-HSD1-FK to be transported out of the ER. Preliminary experiments by Hyeilin Ham suggest that ss-17β-HSD1-FK is found mostly in the cytosolic fraction 24 hours after transfection (not shown). We hypothesized that if we could prevent the translocation of ss17β-HSD1-FK from the ER to the cytosol, then we could determine its true directional preference in the ER. Because protein unfolding is required for translocation, we predicted that if we could prevent 17β-HSD1 from unfolding, we could prevent its translocation. We recaptured GFP's stability and resistance to unfolding, and we fused GFP to 17β-HSD1, to assess whether this fusion with GFP would retain 17β-HSD1 in the ER. Initial the fluorescence microscopy images strongly indicate that ss-17β-HSD1-GFP-KDEL remains in the ER lumen (FIGURE 2.23), yet metabolism experiments show that cells expressing 17β1-GFP and ss17β1GFPK exhibit the same directional preference as 17β1-FLAG constructs. We could not conclude why 17β1-GFP and ss17β1GFPK, and the possible explanations include that ss17β1GFPK translocate into the cytosol at later time points, that enzyme in the ER still catalyzes the same final steroid distribution despite lower [NADPH]. Or that enzyme retained in the

ER is inactive. Fractionation experiments as performed for 17β-HSD1-F are required to resolve these discrepancies.

17β-HSD1 Future Directions

We were able to target 17β-HSD1 to the ER, but we were not able to retain it there as evidenced by the fluorescence microscopy and cellular fractionation. This phenomenon explains why the directional preference of ER-targeted and cytosolic 17β-HSD1 *in vivo* are indistinguishable, because both constructs yield active cytosolic enzyme. What causes 17β-HSD1 to be translocated out of the ER and into the cytosol? To dissect this problem, a construct that reports whether 17β-HSD1 has been trafficked through the ER would be a useful tool. I propose to add an N-glycosylation site or domain to the C-terminus (Bano-Polo 2011). If the protein was successfully targeted to the ER lumen, it should be glycosylated and thus migrate slower on SDS-PAGE before and faster after being treated with Endoglycosidase H (EndoH) to remove the carbohydrate.

If vigorous over-expression due to the strong CMV promoter was the reason our protein was not retained in the ER, we could use a weaker promoter than CMV. Even a commercially available construct for targeting proteins to the ER (Invitrogen's pShooter) uses a CMV promoter, which raises the concern that such constructs are not reliable for ER-targeting experiments. The problems we have encountered could also be attributed to poor solubility, altered disulfide bond formation, or toxicity of misfolded proteins and ER stress. We tried to address the

toxicity previously by using the inducible Flp-In T-REx system, but technical challenges prevented this approach. To address the potential errant disulfide bond formation, I examined the crystal structure (pdb id 1FDU) of human 17β-HSD1 (Mazza 1998) shows five of the six cysteines buried in the protein and only C55 solvent-exposed. To test whether the ER targeted 17β-HSD1 has undergone errant disulfide bond formation, a non-reducing or native gel can be used to determine whether the ER-targeted 17β-HSD1 migrates faster or slower than native cytosolic 17β-HSD1. Alternatively, iodoacetamide treatment, which labels free sulfhydryl groups, can be performed before and after reduction with DTT, to determine the number of free sulfhydryls. This experiment is normally performed with [^{14}C]-iodoacetamide followed by assessing radioactivity incorporation per μg protein, or by mass spectrometry. If these studies indicate that the ER-targeted 17β-HSD1 is indeed forming errant disulfide bonds, we can use point mutagenesis to mutate the cysteines to a serine or to glycine to maintain the polar interactions but abolish the ability to form disulfide bonds. If these studies indicate that ER-targeted 17β-HSD1 is not forming errant disulfide bonds and forms a normal dimer, the protein is likely to be exerting a toxic effect in the ER, either due to its catalytic activity, the process of expression, or misfolding. A catalytically dead mutant can be generated by mutating the 17β-HSD1 catalytic triad residues, S142, Y155 and K159 (Negri 2010) to alanine and repeating the above ER-targeting experiments. If the catalytic triad mutants behave the same as the 17β-HSD1 WT constructs, we can at least conclude that the translocation out

of the ER, and/or cytotoxicity are inherent features of 17β-HSD1 expression, rather than due to its enzymatic activity.

To better assess the effect of the redox environment on 17β-HSD1 activity, we can prepare a membrane-bound fusion protein to anchor 17β-HSD1 in the ER, which might prevent cleavage and translocation to the cytosol. For example, we have made a fusion protein consisting of 11β-HSD1's N-terminal transmembrane domain fused to 17β-HSD1, with a C-terminal KDEL retention signal. We decided to use the 11β-HSD1 transmembrane domain because we can reverse the orientation from intralumenal to cytosolic with a single point mutation, K5S (Frick 2004). To confirm the location and orientation of the constructs, we can use cellular fractionation followed by a protease protection assay, so following fractionation, the protease treatment would degrade protein facing the cytosol, while protein facing into the ER lumen is protected from degradation. Once the orientation is confirmed, we can assay the constructs and determine the effect of the ER lumen environment on directional preference. The cytosolic facing construct serves as a positive control, to demonstrate that the transmembrane domain does not affect activity. If the ER facing construct is active, we can make conclusions based on its activity or directional preference. If the ER-lumenal and cytosolic facing constructs have the same directional preferences, the ER [NADPH] is adequate for strong reduction preference. If the directional preference activity is attenuated or reversed, we would conclude that either the [NADPH] or additional factors in the ER lumen is insufficient to support preferential E1 reduction. If we observe an attenuated directional

preference, we would co-express H6PD and attempt to rescue its shift to E2 oxidation. If co-expression of H6PD fails to restore preferential E1 reduction, we would conclude that H6PD selectively supports 11β-HSD1 catalyzed-reduction of cortisone to cortisol in the ER lumen.

AKR1C9 Discussion and Future Direction

The results from the AKR1C9 experiments mirror the 17β-HSD1 results. The constructs are expressed and the encoded proteins are active. The ER-targeted protein migrates higher on a Western blot than the cytosolic version, indicating that the full-length protein is expressed but is either modified by a post-translational modification or that the signal sequence is not cleaved in the ER. A closer look at the DNA sequence reveals a mutation in the signal peptidase cleavage site; AEA was inadvertently mutated to AEE, which might explain this result..

The *in vivo* data reflect the results observed for 17β-HSD1, in that the ER-targeted and cytosolic constructs gave the same final steroid distributions. To interpret these data, AKR1C9's cellular location should be determined with the fluorescence microscopy and cellular fractionation techniques used for 17β-HSD1. If AKR1C9 is successfully targeted and retained in the ER, we can determine its directional preference catalyzed in the ER lumen. If ER-targeted AKR1C9 is translocating out of the ER lumen like 17β-HSD1, we can use the above mentioned techniques, including GFP fusion and tethering the enzyme

to11β-HSD1's N-terminal transmembrane domain, to study the effect of the redox environment on its directional preference.

11β-HSD1 Discussion

To address a hypothesis set forth in the beginning of this body of work, that H6PD channels NADPH to 11β-HSD1 in the ER lumen through specific interactions, we prepared and screened numerous constructs, and we found that only some constructs were active, with poor cortisone reduction in HEK293 cells. Co-expressing H6PD, however, doubled the final portion of cortisol generated by the active constructs, suggesting that the cells are relatively deficient in H6PD. In contrast, the active constructs yielded more cortisone reduction when expressed in CHO cells with approximately 10% more cortisone reduction for 11β-HSD1-H6PD co-transfections. We conclude that HEK293 cells afford us a greater dynamic range for mechanistic studies of 11β-HSD1-H6PD interactions than CHO cells. The presumed higher H6PD expression in CHO than HEK293 cells can be confirmed with western blot or RT-PCR.

The preliminary experiments confirm that 11β-HSD1 requires H6PD for high cortisone reduction should be repeated before embarking on subsequent studies, but time constraints precluded further work. Once the cortisone:cortisol ratio is established with 11β-HSD1 +/- H6PD, we can proceed to ask how the ER lumen environment and H6PD interaction domains affect the reaction. Preliminary data shown in Figure 4.5 indicate that cytosolic K5S 11β-HSD1 has very little reductive ability in the highly reducing cytosol and that co-expressing

NADPH-regenerating G6PD did not increase cortisone reduction. The poor steroid metabolism in both directions by cells expressing 11β-HSD1 mutation K5S suggests that either this mutation has poor intrinsic catalytic activity or that physical interaction with H6PD is required for high cortisone reduction activity. This proposal is supported by our data, which show that unlike H6PD co-expression, the co-expression of either native G6PD or ER-targeted G6PD failed to increase cortisone reduction in HEK293 cells. While this result contrasts with data in other systems (McCormick 2006), our data support the model that H6PD is specifically required for efficient cortisone reduction by 11β-HSD1 in the ER lumen.

To further assess the importance of H6PD for cortisone reduction, we studied the H6PD mutation G359D. This mutation was identified in a patient with cortisone reductase deficiency and shown to be deficient in regenerating NADPH (Lavery 2008). If H6PD's main function is to regenerate NADPH in the ER lumen, a construct deficient in this activity should not support cortisone reduction by 11β-HSD1and serve as a good negative control. Contrary to our predictions, co-expressing H6PD mutation G359D with 11β-HSD1 appeared to produce greater amounts of cortisol than 11β-HSD1 alone but less than 11β-HSD1 with H6PD. Although this result suggests that the NADPH-regeneration activity of H6PD is not required to increase cortisone reduction, the result must be repeated and performed under different conditions before drawing conclusions.

The N-terminal transmembrane domain of 11β-HSD1 has been shown to co-immunoprecipitate with H6PD (Atanasov 2008). To study the importance of

this transmembrane domain on complex formation and cortisone reduction, we made a soluble version of 11β-HSD1 targeted to the ER lumen and screened for cortisone reduction with and without H6PD. HEK293 cells expressing this soluble 11β-HSD1 enzyme reduced negligible cortisone to cortisol and the addition of H6PD increased its activity above the Mock control. These cells also poorly oxidized cortisol to cortisone, suggesting poor intrinsic activity, but this experiment was done only once. With the immunoprecipitation data, the transmembrane region appears to be required for efficient cortisone reduction *in vivo*, perhaps serving to induce association of 11β-HSD1 with H6PD.

11β-HSD1 Future Directions

H6PD comprises two large domains, a dehydrogenase domain and a lactonase domain (Senesi 2010). The dehydrogenase domain is highly homologous to G6PD while the lactonase domain is highly homologous to 6-phosphogluconolactonase (6PGL) (Senesi 2010). G6PD and 6PGL catalyze the first two steps in the pentose phosphate pathway, and enzymes catalyzing the subsequent steps in the pathway have also been identified in the ER lumen (Bublitz 1988). If substrate channeling of NADPH, from H6PD to 11β-HSD1 occurs, then one or both domains might perform this function. To determine the contribution of the dehydrogenase domain to the cortisone reduction-reaction, we would mutate residues in each domain important for catalysis. *In vitro* studies with Leuconostoc Mesenteroides G6PD identified D177, H178 and H240 as the catalytic triad for proton transfer during catalysis (FIGURE 5.1, Cosgrove 1998).

A sequence alignment between these residues and human G6PD revealed that the corresponding three residues are D230, H231 and H293. A subsequent sequence alignment between G6PD and H6PD showed D203, H204 and H267 to be the catalytic triad for the dehydrogenase domain of H6PD. A sequence alignment between all three enzymes identified of the same H6PD residues. We mutated each of these residues (D230A, H231A and H293A) but have not tested their influence on 11β-HSD1 catalysis *in vivo*.

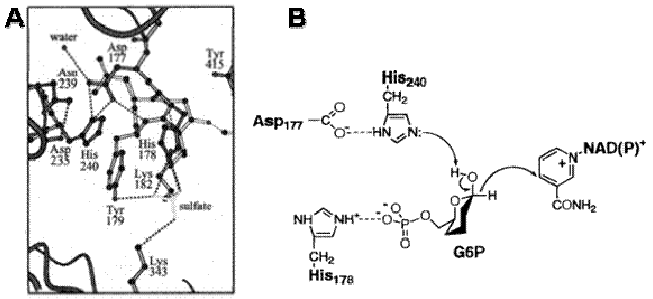

G6PD		H6PD
Leuconostoc Mesenteroides	Human	Human
D177	D230	D203
H178	H231	H204
H240	H293	H267

FIGURE 5.1. G6PD and H6PD Dehydrogenase Domain Catalytic Residues. A. Crystal structure of Leuconostoc Mesenteroides G6PD (dark grey) active site with G6P (light grey) (Figure Taken from Cosgrove 1998). **B.** Proposed mechanism for G6P oxidation, highlighting D177, H178, and H240 (Figure taken from Cosgrove 1998). **C.** Results of aligning L. Mesenteroides G6PD with Human G6PD and H6PD.

A similar approach was taken to identify important residues in H6PD's lactonase domain. The structure of 6PGL from Trypanosoma brucei (Duclert-Savatier 2009) has been solved, and 6PGL residues interacting with the lactone have been identified (FIGURE 5.2). A sequence alignment between T. brucei and H6PD revealed conservation among the active-site residues. Six of these eleven H6PD residues identified in this alignment were mutated to probe the lactonase domain. By comparing the consequences of mutations that selectively impair the dehydrogenase and lactonase domains of H6PD, which catalyzes both of these steps, the contributions of each step and domain in supporting cortisone reduction by 11β-HSD1 can be deduced.

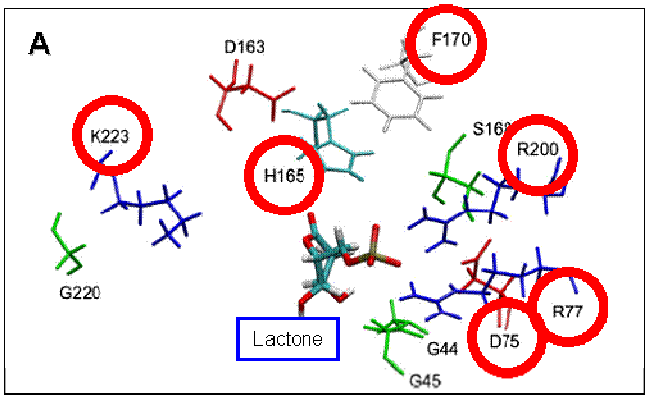

B

T. brucei Lactonase	Human H6PD
D75	D620
R77	R622
H165	H698
F170	F703
R200	R728
K223	K751

FIGURE 5.2. H6PD Lactonase Domain Residues. A. Crystal structure of T. brucei Lactonase active site with lactone (Figure taken from Duclert-Savatier 2009). Important catalytic residues are illustrated. **B.** Results of a sequence alignment between T. brucei Lactonase and Human H6PD to identify corresponding residues in Human H6PD's Lactonase domain.

Protein glycosylation is important for ER protein folding, trafficking and protein-protein interactions. H6PD has three N-glycosylation sites, N157, N282 and N683 (FIGURE 5.3). It is not known which of these three sites are glycosylated and if glycosylation is important for catalysis and/or interacting with 11β-HSD1. To address these questions, we mutated each site individually, in pair wise combinations, and all three residues together, but we have not assayed these mutants. To determine which sites are glycosylated, WT H6PD can be isolated by immunoprecipitation, treated with and without EndoH, analyzed by SDS-PAGE to determine its sizes. If there is a uniform size reduction after EndoH treatment, then H6PD is glycosylated, and the above experiments with these 3 asparagine mutations will enable us to deduce which residues are glycosylated and which are important for catalysis and/or interacting with 11β-HSD1 and altering its reductive directional preference.

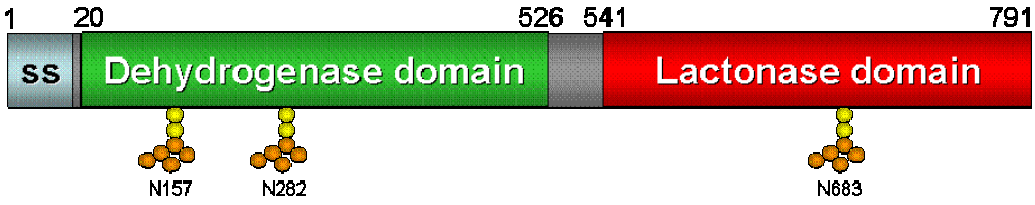

FIGURE 5.3. H6PD Glycosylation Residues. N-glycosylation residues are illustrated at positions N157, N282 and N683. We mutated each site singly, in pair wise combinations, and all three residues together. (Figure adapted from Senesi 2010).

In addition to the above mentioned mutagenesis and deglycosylation experiments, one can use protein-protein docking software such as ClusPro (Kozakov 2010, Kozakov 2006, Comeau 2004, Comeau 2004) for use as a model in predicting important contact residues for complex formation with H6PD and 11β-HSD1. The disadvantage of this approach is that, if the membrane-spanning regions are part of the transition, the crystal structures of the proteins or models used for these exercises do not contain the membrane-spanning domains. Cross-linking experiments might be feasible but suffer from technical challenges and non-specific artifacts.

The activity of H6PD is required for 11β-HSD1 to maintain its strong directional preference in intact cells. In addition to determining the importance of each domain and glycosylation size of H6PD in supporting cortisone reduction, we likewise intend to determine the residues in 11β-HSD1 necessary for high NADPH affinity. 17β-HSD1 and AKR1C9 have an arginine, which coordinates the 2'-phosphate group of NADPH and thus confers reductive directional preference *in vivo.* Based on sequence alignment, we predict that R66 of 11β-HSD1 also coordinates the 2'-phosphate group of NADPH, but the data from pilot experiments were inconclusive and complicated by low expression of 11β-HSD1 in HEK293 cells. Experiments probing the NADPH binding of 11β-HSD1 might benefit from using HEK293 cell lines stably expressing high amounts of H6PD or CHO cells, or some other cell such as yeast with high endogenous or engineered H6PD expression.

We believe that we have made the appropriate constructs to initiate a rigorous study into the regulation and identification of important catalytic and interaction residues in both 11β-HSD1 and H6PD. These studies can help in elucidating the mechanism and determining the biochemical factors that regulate 11β-HSD1 cofactor usage and directional preference in intact cells.

Chapter 6

Materials and Methods

Cloning 17β-HSD1-FLAG and AKR1C9-FLAG

Directional Cloning and TA cloning (Invitrogen's TA Cloning Kit) were used to add the FLAG epitope (DYKDDDDK, 5-GATTACAAGGATGACGAC GATAAG-3) to the C-terminus of human 17β-HSD1 and rat AKR1C9 in pcDNA3.1 (Invitrogen); these formed the background constructs used for further cloning. PcDNA5 constructs were made by excising the 17β-HSD1-F WT or AKR1C9–F WT ORF from pcDNA3.1 constructs and ligating into a pcDNA5 vector after restriction enzyme digest (BamH1 and EcroR1 for 17β-HSD1, Kpn1 and Xho1 for AKR1C9). Point mutations were made using Agilent's Quickchange mutagenesis process. All constructs in TABLE 6.1 were sequenced for final verification and validation.

TABLE 6.1 17β-HSD1-FLAG and AKR1C9-FLAG Constructs

Construct	**Vectors**	
17β-HSD1-F WT	pcDNA3.1	pcDNA5
17β-HSD1-F R38D	pcDNA3.1	
17β-HSD1-F R38E	pcDNA3.1	pcDNA5
17β-HSD1-F R38G	pcDNA3.1	pcDNA5
17β-HSD1-F R38K	pcDNA3.1	
AKR1C9-F WT	pcDNA3.1	pcDNA5
AKR1C9-F R276E	pcDNA3.1	pcDNA5
AKR1C9-F R276G	pcDNA3.1	pcDNA5
AKR1C9-F R276M	pcDNA3.1	
-F : FLAG Tag epitope		

Cloning ss-17βHSD1-FLAG-KDEL and ss-AKR1C9-FLAG-KDEL

Two step overlapping PCR (Sambrook 2001) and TA cloning first added the signal sequence (ss), the first 20 amino acids of BiP (MKLSLVAAMLLLLSAARAEE, 5-ATGAAGCTCTCCCTGGTGGCCGCGA TGCTGCTGCTGCTCAGCGCGGCGCGGGCCGAGGAG-3) followed by addition of the KDEL (5-AAGGACGAACTG-3) ER-retention signal to the AKR1C9 constructs (Blobel 1975, Teasdale 1996, Munro 1987). An ER targeted 17β-HSD1-KDEL construct using the first 18 amino acids of pre-proalbumin (MKWVTFWLLLFISVSAFSAEAGSG, 5-ATGAAATGGGTTACTTTTTGGT TACTTCTCTTTATTTCTGTTTCTGCTTTTTCTGCTGAAGCCGGATCAGGT -3)as a signal sequence for ER targeting followed by a AEA peptidase cleavage

site and GSG linker was kindly provided to us by Dr. Alex Odermatt (University of Basal in Switzerland). Quickchange mutagenesis was used to correct a point shift mutation in the N-terminus while, overlapping PCR and TA cloning were used to add a FLAG epitope to the C-terminus. Point mutations were made using Agilent's Quickchange mutagenesis process. All constructs in TABLE 6.2 were sequenced for final verification and validation.

TABLE 6.2 ss-17βHSD1-FLAG-KDEL and ss-AKR1C9-FLAG-KDEL Constructs

Construct	**Vectors**	
ss-17βHSD1-FK WT	pcDNA3.1	pcDNA5
ss-17βHSD1-FK R38D	pcDNA3.1	
ss-17βHSD1-FK R38E	pcDNA3.1	pcDNA5
ss-17βHSD1-FK R38G	pcDNA3.1	pcDNA5
ss-17βHSD1-FK R38K	pcDNA3.1	
ss-AKR1C9-FK WT	pcDNA3.1	pcDNA5
ss-AKR1C9-FK R276E	pcDNA3.1	pcDNA5
ss-AKR1C9-FK R276G	pcDNA3.1	pcDNA5
ss-AKR1C9-FK R276M	pcDNA3.1	
-F: FLAG Tag		
ss: signal sequence for ER targeting		
KDEL: ER retention signal		

GFP fusion protein constructs with 17β-HSD1, 17β-HSD2 and AKR1C9

Directional cloning into Clontech's pEGFP-C1 vector added GFP to the N-terminus of 17β-HSD1 and AKR1C9. Dr. Melissa Rasar Young used directional cloning, over-lapping PCR and Clontech's pEGFP-N1 to add GFP to the C-terminus of 17β-HSD1. A two-step approach using overlapping PCR and TA cloning added the signal sequence and retention signal to 17βHSD1-GFP. To facilitate future C-terminal GFP-tagged constructs as well as serve as a positive control for an ER-localized protein in fluorescence microscopy experiments, an ER-targeting, multiple cloning site (MCS) construct was made using the above mentioned overlapping PCR and TA cloning. The ss-RFP-KDEL plasmid (Altan-Bonnet 2006) was generously provided by Dr. Anil Agarwal. All constructs in TABLE 6.3 were sequenced for final verification and validation.

TABLE 6.3 GFP and RFP Constructs

Construct	**Vector**	
GFP-17βHSD1	pEGFP-C1	
GFP-17βHSD2	pEGFP-C1	
GFP-AKR1C9	pEGFP-C1	
17βHSD1-GFP	pEGFP-N1	pcDNA3.1
ss-17βHSD1-GFP-K		pcDNA3.1
ss-MCS-GFP-K		pcDNA3.1
ss-RFP-KDEL		pcDNA3.1

Cloning 11β-HSD1 Constructs

FLAG-tagged human 11β-HSD1 and human 11β-HSD2 were generously provided by Dr. Alex Odermatt. Quickchange mutagenesis was used to make the R66 (Hosfield 2005) mutations. Dr. Dario Mizrachi used overlapping PCR to successfully clone the K5S mutation. Overlapping PCR, directional cloning and TA cloning were used to replace 11β-HSD1's N-terminal membrane domain (Odermatt 1999) with a signal sequence and to add a KDEL retention signal to the C-terminus to make ss-11βHSD1-FK. The same procedure was employed to delete the N-terminal membrane domain to make a soluble-cytosolic 11β1F protein, 11β1F-cyto. All constructs in TABLE 6.4 were sequenced for final verification and validation.

TABLE 6.4 11β-HSD1 Constructs

Construct	Vector
11β-HSD1-F WT	pcDNA3.1
11β-HSD1-F R66E	pcDNA3.1
11β-HSD1-F R66G	pcDNA3.1
11β-HSD1-F R66M	pcDNA3.1
11β-HSD1-F K5S	pcDNA3.1
11β-HSD1-F K5S R66E	pcDNA3.1
11β-HSD1-F K5S R66G	pcDNA3.1
11β-HSD1-F K5S R66M	pcDNA3.1
11β-HSD2-F WT	pcDNA3.1
ss-11βHSD1-FK	pcDNA3.1
11β1F-cyto	pcDNA3.1

Cloning H6PD Constructs

Human H6PD cDNA was ordered from Open Biosystems (Catalog EHS1001-5742733, Clone ID 5266232, Accession: BC081559). The CDNA received was not WT but a common R453D mutation (Lavery 2009). Directional cloning was used to add the HA (YPYDVPDYA) epitope to the C-terminal. Quickchange mutagenesis was used for all point mutations. Directional and TA cloning were used to make the ssH6D (H6PD's signal sequence and H6PD's dehydrogenase domain) and ssH6L (H6PD's signal sequence and H6PD's lactonase domain). The first 20 amino acids of H6PD (MWNMLIVAMCLALLGCLQAQ) were fused to GFP-KDEL with directional cloning and use of the previously made ss-MCS-GFP-KDEL construct. All constructs in TABLE 6.5 were sequenced for final verification and validation

TABLE 6.5 H6PD Constructs

Construct	Vector
H6PD-HA WT	pcDNA3.1
H6PD-HA D203N	pcDNA3.1
H6PD-HA H204N	pcDNA3.1
H6PD-HA H267N	pcDNA3.1
H6PD-HA D620A	pcDNA3.1
H6PD-HA R622A	pcDNA3.1
H6PD-HA H698A	pcDNA3.1
H6PD-HA F703A	pcDNA3.1
H6PD-HA R728A	pcDNA3.1
H6PD-HA K751A	pcDNA3.1
H6PD-HA N157D	pcDNA3.1
H6PD-HA N282D	pcDNA3.1
H6PD-HA N683D	pcDNA3.1
H6PD-HA N157D N282D	pcDNA3.1
H6PD-HA N157D N683D	pcDNA3.1
H6PD-HA N282D N683D	pcDNA3.1
H6PD-HA N157D N282D N683D	pcDNA3.1
H6PD-HA G359D	pcDNA3.1
H6PD-HA R453D	pcDNA3.1
ssH6-GFP-KDEL	pcDNA3.1
ssH6D (Dehydrogenase Domain)	TA pCR2.1
ssH6L (Lactonase Domain)	TA pCR2.1

Cloning of G6PD Constructs

G6PD-FLAG (Pan 2009) was kindly given to us by Dr. Bradford Berk (University of Rochester). Directional cloning allowed us to add a HA tag as well as a signal sequence and KDEL retention signal. All constructs, TABLE 6.6, were sent to sequencing for final verification and validation

TABLE 6.6 G6PD Constructs

Construct	Vector
G6PD-HA WT	pcDNA3.1
ssG6PD-HAK WT	pcDNA3.1

Generating Stable HEK293 Cell Lines using pcDNA3

Unless otherwise stated, the following materials constitute the complete media (CM) used for all tissue culture experiments: DMEM (Dulbecco's Modified Eagle Medium, High Glucose 1x, Gibco), 10mg/ml Penicillin-Streptomycin Solution (Mediatech Inc Cellgro 30-002-CI) and 10% Fetal Bovine Serum (Mediatech Inc Cellgro 35-010-CV).

Briefly, HEK293 cells are seeded in a 100mm tissue culture dish (BD Falcon 353003) and transfected with 1µg DNA (as measured in an Amersham Biosciences Ultrospec 2100 Pro UV/Vis Spectrophotometer) and 3µl FUGENE6 (Roche). The medium was changed 48 hours later and cells recovered for 24 hours, then harvested with trypsin and diluted 1:25 into a 150mm tissue culture plate (Corning 430599). The media is changed the following day to CM with G-418 (0.5mg/ml) for selections and colonies appeared after 14-21 days. The

colonies were isolated with firm pressure and suction using a P200 pipette tips, allowed to attach in a 6-well plate, and split between two plates: one for assay and the other for propagation. For colonies with good activity from the assay plates, the corresponding cells in the propagation plate were expanded in T-75 flasks, and one flask of cells was frozen in FBS with 10% DMSO at -80^{o}C for storage.

Generating Tetracycline-Inducible Stable HEK293 Cell Lines

Invitrogen's T-REx System was used for making cell lines with inducible protein expression (FIGURE 6.1). Briefly, the host HEK293 cells are transfected with two plasmids, a blasticidin-resistant tetracycline-repressor protein (TetR) expressing plasmid and a Zeocin-resistant, FRT-site containing plasmid. After successful integration into the host cell genome, the host cells now constitutively express TetR and have a FRT site for exogenous gene integration. These cells are now considered to be Flp-In T-REx HEK293 cells (Invitrogen 51-0026).

The cDNA of interest, YFG = "Your Favorite Gene", is subcloned into a pcDNA5 plasmid containing a FRT site and hygromycin resistance gene. This pcDNA5 plasmid is co-transfected with a Flp-recombinase encoding plasmid, Invitrogen pOG44, into the T-REx cells. After homologous recombination, YFG expression is regulated by two tetracycline repressor binding elements, $TetO_2$. YFG expression is repressed because TetR is bound to $TetO_2$, preventing transcription. TetR binds tetracycline added to the media, undergoes a conformational change and no longer binds TetO2, allowing for YFG expression.

To generate inducible stable cell lines expressing our 17β-HSD1, AKR1C9 and 11β-HSD1 proteins of interest, we seeded Flp-In T-REx cells into a 6-well plate. The next day, we transfected cells with the following: 1 (1μg YFG), 1:10 (1μg YFG, 10μg pOG44), 1:20 (1μg YFG, 20μg pOG44). After a 48hr transfection, the cells were transferred to a 100mm plate. We changed the media to CM supplemented with hygromycin for selection and colonies appeared after 21-28 days. Colonies were isolated and transferred as previously mentioned. Cells were allowed to attach to a 6-well plate, and split between two plates: an assay plate and a propagation plate. All colonies were frozen in FBS with 10% DMSO and stored at -80^{o}C. Dr. Frank Lee sent a positive control expressing HIF-2α-FLAG (Percy 2008).

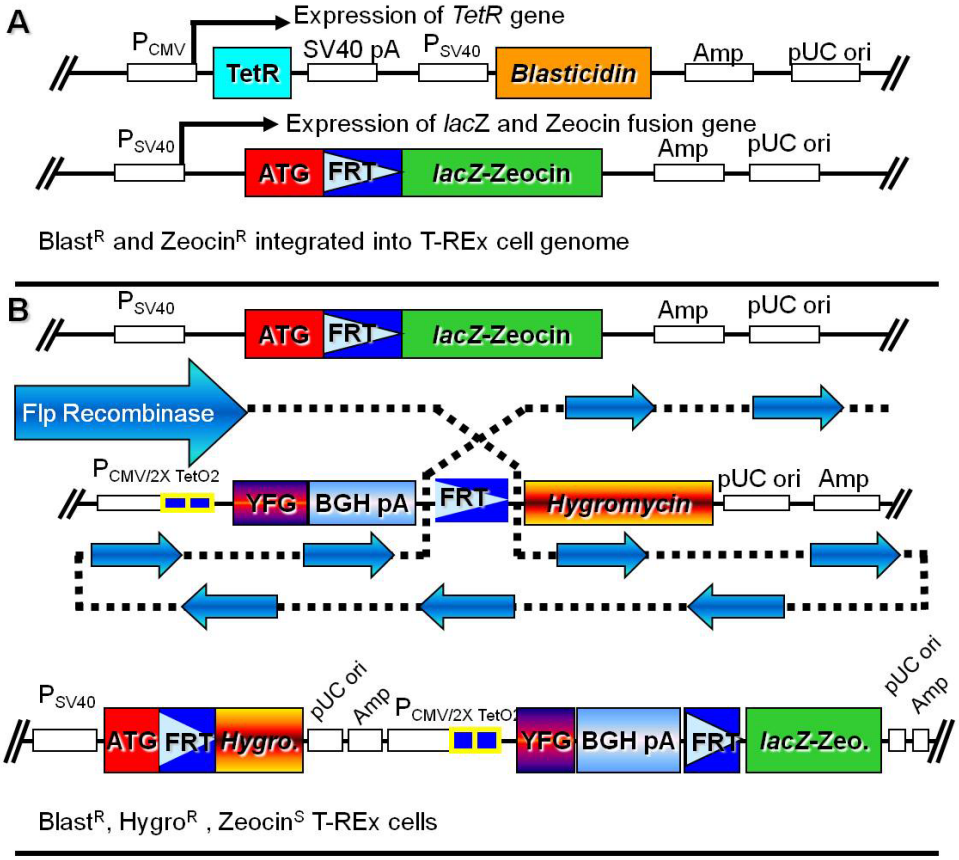
A
Expression of TetR gene
P CMV
TetR
SV40 pA
P SV40
Blasticidin
Amp
pUC ori
P SV40
Expression of lacZ and Zeocin fusion gene
ATG
FRT
lacZ-Zeocin
Amp
pUC ori
Blast R and Zeocin R integrated into T-REx cell genome
B
P SV40
ATG
FRT
lacZ-Zeocin
Amp
pUC ori
Flp Recombinase
P CMV/2X TetO2
YFG
BGH pA
FRT
Hygromycin
pUC ori
Amp
P SV40
ATG
FRT
Hygro.
pUC ori
Amp
P CMV/2X TetO2
YFG
BGH pA
FRT
lacZ-Zeo.
pUC ori
Amp
Blast R, Hygro R , Zeocin S T-REx cells

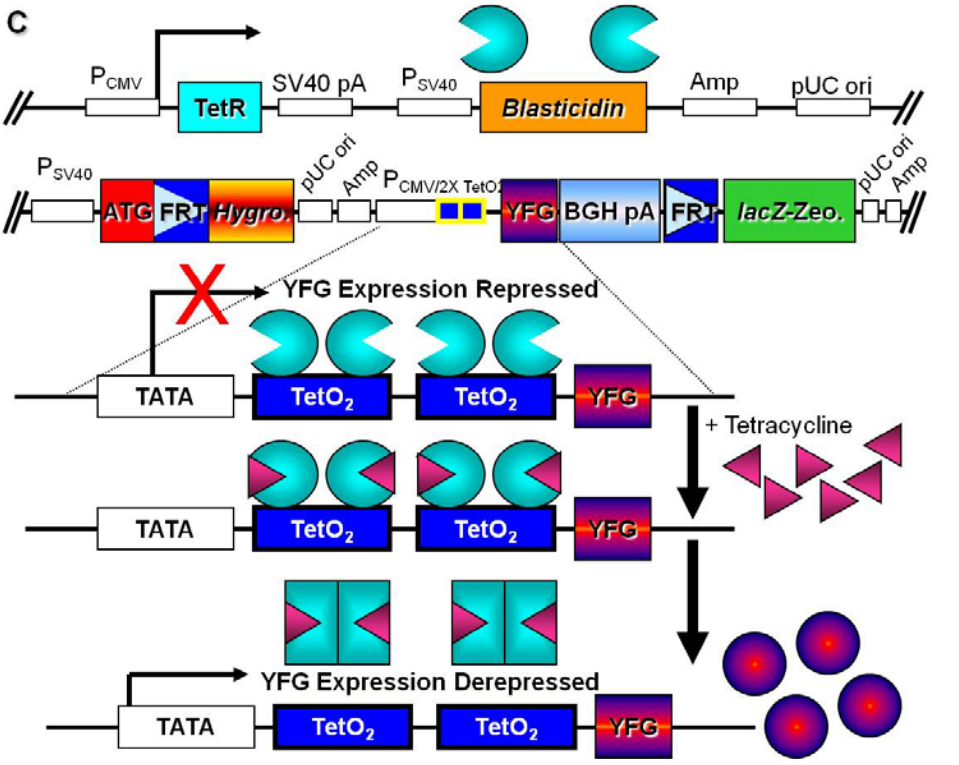
C
P CMV
TetR
SV40 pA
P SV40
Blasticidin
Amp
pUC ori
P SV40
ATG
FRT
Hygro.
pUC ori
Amp
P CMV/2X TetO2
YFG
BGH pA
FRT
lacZ-Zeo.
pUC ori
Amp
YFG Expression Repressed
TATA
TetO2
TetO2
YFG
+ Tetracycline
TATA
TetO2
TetO2
YFG
YFG Expression Derepressed
TATA
TetO2
TetO2
YFG

FIGURE 6.1 Invitrogen's Flp-In T-REx System for Inducible Protein Expression. A. Maps of the plasmids integrated into the host genome. The Blasticidin plasmid constitutively expresses the Tet-repressor protein (TetR); the Zeocin plasmid has a FRT site for future exogenous gene incorporation. **B**. The gene of interest (YFG = "Your Favorite Gene") subcloned into the Hygromycin resistant plasmid pcDNA5 is co-transfected with the pOG44 plasmid, which encodes a Flp Recombinase protein (large light blue arrow). The top map shows the host genome FRT site before transfection and the bottom map shows the same host genome map after transfection with the Hygromycin YFG pcDNA5 and pOG44. The host cell is now resistant to Hygromycin but now sensitive to Zeocin. **C**. TetR protein binds to a $TetO_2$ binding site just upstream of YFG, conferring repression. TetR relieves repression when tetracycline is added to the media; TetR binds tetracycline, undergoes a conformational change and no longer binds the $TetO_2$ binding site.

Fluorescence Microscopy

Glass cover slips (Deckgläser 12mm) were soaked in 0.1mg/ml poly-lysine (poly-K) in a 6-well plate for at least one hour at 37^{o}C. The poly-K solution was removed; cells, approximately 10% of a 100% confluent T-75 flask, were added in 2ml CM and allowed to attach over night. Cells were transfected with FUGENE6 as described above and imaged after 48 hours for optimal protein expression and imaging.

For GFP-tagged proteins, the complete media was aspirated, and cells were washed once with DPBS (Mediatech cellgro Dulbecco's Phosphate-Buffered Saline 21-031-CV). The cells were fixed with 4% PFA (Sigma HT501128-4L) for 10min at 4^{o}C. Cells were washed again with DPBS and mounted on slides (Fisherbrand Plain Microscope Slides 12-549-3) with Vectashield (Vector Laboratories, Hard Set Mounting Medium with DAPI H-1500).

For FLAG-tagged proteins, cells were fixed for 15min at room temperature (RT) followed by a 10min methanol incubation and 1 min acetonitrile incubation, both at -20^{o}C. Cells were washed twice with DPBS and incubated with a blocking solution (DPBS, 0.1% Triton X-100, 1% BSA, 0.3M glycine) for 30min on a shaker at RT. Cells were washed twice with DPBS and incubated with a primary antibody (Sigma Monoclonal ANTI-FLAG M2, F1804, 1:1000 dilution) at 4^{o}C overnight. Cells were washed three times with DPBS and then incubated with the secondary antibody (Invitrogen Rabbit anti-mouse IgG Alexa Fluor 488, A-21204, 1:500) for an hour in the dark. Cells were washed with DPBS and mounted on slides as described for GFP imaging. Images were acquired in the Live Cell Imaging Core Facility (L5.108A) on a Zeiss AxioObserver motorized microscope.

Cell Culture Equilibrium and Double-Isotope Scrambling Experiments

All equilibrium and kinetic experiments were performed in 6 well plates. Cells were divided, counted with a hemocytometer, and seeded at approximately one million cells per well. Cells were transfected with FUGENE6 as described, 48hours later, fresh CM was added to the cells along with 100nM steroid substrate with at least 50,000 CPM per time point of [^{3}H]-tracer steroid. Aliquots of CM were removed, extracted with 1ml of 1:1 ethyl acetate:isooctane, and dried under a nitrogen stream. Samples were resuspended with 30µl methylene chloride, applied to a TLC plate (Whatman PE SIL G/UV), and separated with 3:1 chloroform/ethyl acetate (Sherbet 2009, Khan 2004) for estrogens and androgens;

cortisone and cortisol were separated with 92:8 chloroform/ethanol solvent (Myers 2007). TLC plates were then exposed to a phosphoscreen (Fuji Imaging Plate, BAS-IP TR 2040) overnight and imaged on a Storm840 Scanner (Amersham Biosciences). For some experiments, 50nmol of each steroid was added before the samples were dried for visualization under UV light or I_2 vapor. After the TLC plate was developed, iodine chamber exposure revealed the steroid locations. Substrate and product were excised from of the plate, mixed with Budget-Solve (Research Products International), and quantified by liquid scintillation counting using a Beckman Coulter LS 6500 Multi-Purpose Scintillation Counter or a Beckman LS 1801 Scintillation Counter using one or two channels. Excel and GraphPad Prism were used for data analysis.

Radiolabeled Cortisone Preparation with Mouse Liver Microsomes

Mouse Liver Microsome Preparation

Dr. Liliana Carbajal Hernandez (Professor Stephen Hammes laboratory) sacrificed four wild-type Black 6 mice and generously provided the livers to our laboratory. The livers were minced and placed into a 30ml Dounce homogenizer with 10ml cold buffer (10mM Tris Buffer pH 7.5, 5mM EDTA, 0.25M Sucrose). The livers were homogenized with costrokes until uniform in color and appearance, transferred to a centrifuge tube, and pelleted at approximately 10,000x g for 10min at 4^{o}C in a fixed rotor on an Eppendorf 5810 R Centrifuge.

The supernatant was collected, transferred to a high-speed centrifuge tube with 40ml more cold buffer and centrifuged at 35,000RPM for 1hr at 4^{o}C in a

45Ti Rotor on a Beckmann Optima L-70K ultracentrifuge. The supernatant was discarded. The pellet was resuspended with 2ml of cold buffer containing 20% glycerol, aliquoted, and stored at -80^{o}C.

Making Radiolabeled Cortisone from Radiolabeled Cortisol

To test conditions for making radiolabeled cortisone from cortisol, we performed a time course with increasing amounts of mouse liver microsomes, which contain endogenous 11β-HSD1 (FIGURE 6.2A). The microsomes were incubated at 37^{o}C with 50mM Tris-HCl pH8, 1mM $NADP^{+}$, 10nM cortisol, with 200,000 CPM [^{3}H]-cortisol tracer in a 200µl reaction. To stop the reactions at the indicated time points, 1ml of a 1:1 ethyl acetate:isooctane solution was added. Steroids were extracted and separated on TLC as indicated in the previous section.

To scale up radiolabeled cortisone production, we increased the volume to 500µl, keeping all concentrations and proportions the same but now with pure [^{3}H]-cortisol (400 million CPM, ~10nmol). Cortisone was extracted with 1:1 ethyl acetate:isooctane and dried under a nitrogen stream. A 5ml glass pipette packed with fine silica gel in hexanes was used to purify the product. The dried reaction was resuspended in 120µl of hexanes with 10% ethyl acetate and 17% methylene chloride and applied to the silica column. The column was washed with increasing concentrations of ethyl acetate in hexanes to elute the product cortisone (0-100% ethyl acetate). From 2-4ml fractions, radioactivity was determined on 2µl of each fraction by scintillation counting to quantify the radioactivity of each

sample; 50,000 CPM was spotted on a TLC plate followed by phosphoscreen imaging to determine which fractions contained the cortisone product.

The first purification result is indicated in FIGURE 6.2B. Since the preparation yielded low purity and radioactivity (700000 CPM, 0.2% yield), we repeated the reaction (FIGURE 6.2C). Fractions 6 and 7 were pooled and dried, yielding 500000 CPM, 0.15% yield. The procedure was repeated several times consistently yielded 450000 to 750000 CPM (0.14% to 0.23% yield). Better results were obtained using 100µl microsomes, 10mM $NADP^+$, keeping other concentrations the same and overnight incubation at 37^{o}C. The reaction was quenched and dried as previously indicated, and the product was extremely clean by phosphoscreen (FIGURE 6.2D); less than 1% cortisol is present. To assess that the resulting product was cortisone and not an artifact, we ran a short reaction with the mouse liver microsomes (FIGURE 6.2E). The band from the overnight reaction runs identically to the band produced from the short time course reaction, confirming the product purified is cortisone and not an artifact; we did not have a radiolabeled cortisone standard for comparison.

We extracted [^{3}H]-cortisone with 2ml 1:1 ethyl acetate:isooctane, dried under a nitrogen stream, and resuspended in 100% ethanol. This overnight reaction resulted in a much cleaner product with significantly more radioactivity (100 million CPM, 30% yield). This overnight reaction and short clean-up procedure were used in all subsequent *in vivo* experiments.

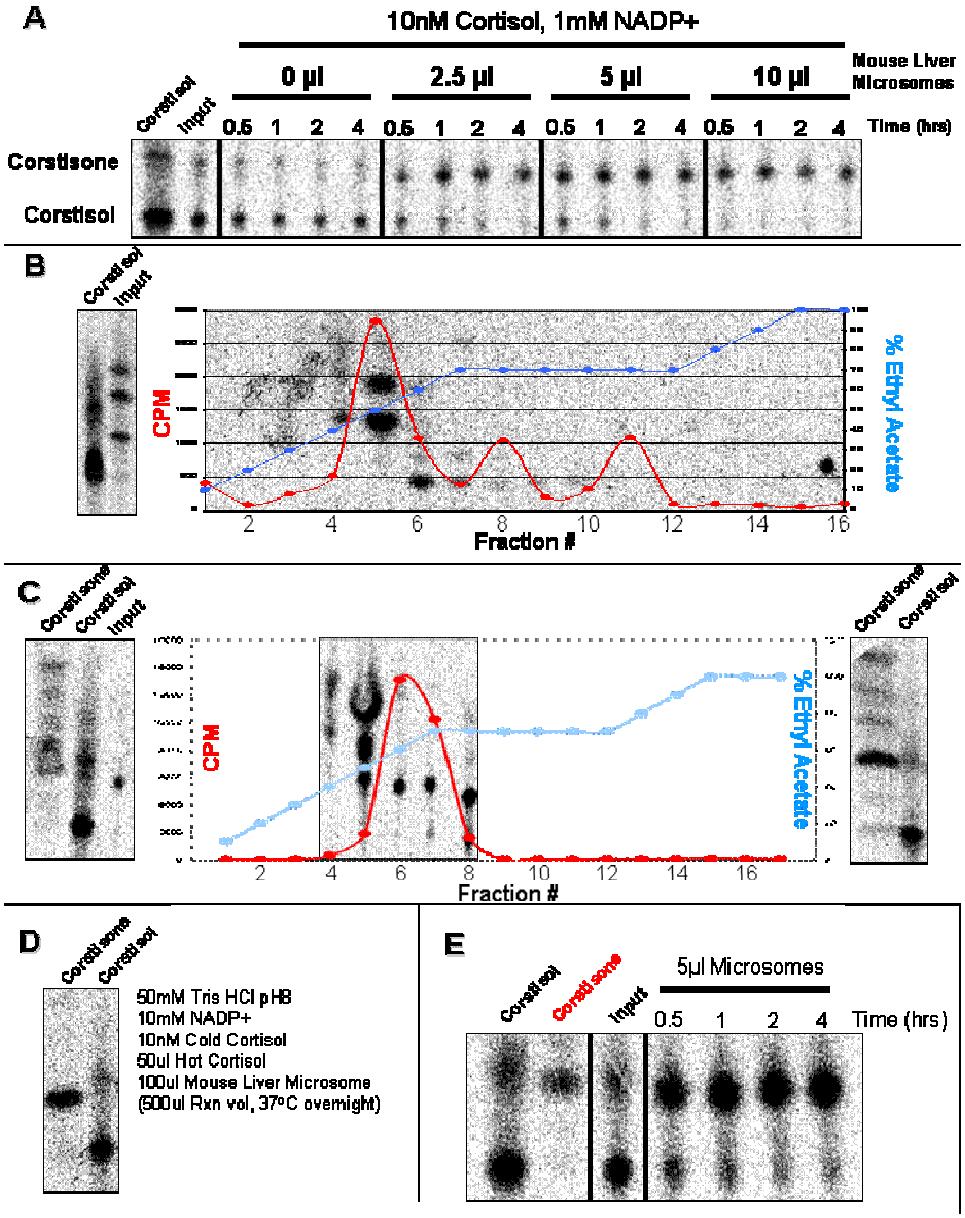

FIGURE 6.2 Making ^{3}H Cortisone. A. Initial reaction optimization using a time course and increasing amounts of mouse liver microsomes. Reactions were analyzed by TLC separation and phosphoscreen imaging. **B.** The first purification scheme for the [^{3}H]-cortisone reaction. An ethyl acetate-hexane gradient was used to purify [^{3}H]-cortisone. Fractions were separated with TLC and quantitated with scintillation counting. **C.** A subsequent purification scheme highlighting the impurities acquired during the process (notice the far right panel). **D.** Representation of the results achieved with the improved protocol. **E.** Confirmation that the purified product from D. was cortisone and not an artifact.

Cellular Fractionation

HEK293T cells were seeded in a 100mm Petri dish. Cells were transfected with 1.5µg plasmid for 48hours using FUGENE6, and unless otherwise stated, pelleted and delivered to Hyeilin Ham (Professor Kim Orth laboratory) for cellular fractionation. Cell pellets were resuspended in cold HNMEK lysis buffer (1 mini-protease inhibitor cocktail tablet, 20mM NaF, 20mM β-glycerol phosphate, 1mM DTT, 0.5mM sodium vanadate, 0.5mM EGTA brought to volume with HNMEK buffer, consisting of 20mM HEPES pH 7.6, 150mM NaCl, 2mM $MgCl_2$, 2mM EDTA, 10mM KCl). Resuspended cell pellets were lysed using nitrogen cavitation. Total cell lysate was centrifuged for 10min at 500g, resulting in the S1 supernatant and P1 pellet containing the nuclei and cellular debris. S1 was centrifuged at 10,000g for 10min to yield the S2 supernatant and P2 pellet containing the mitochondria, Golgi, ER and lysosomes. S2 was further centrifuged at 100,000g for one hour resulting in the S3 supernatant containing cytosolic proteins and the P3 pellet containing the plasma membrane and vesicle membranes.

Each fraction's protein concentration was determined with a Bradford assay, and equal protein amounts were separated by SDS-PAGE and analyzed with Western blots. The following antibodies were used to determine the purity of cellular fractionations: lamin B (P1, nucleus), calnexin (P2, ER), ATPase B2 (P3, membrane) and aldolase (S3, cytosol). α-PDI was used as a soluble ER lumen protein marker for some experiments. Sigma's M2 FLAG antibody was used to identify17β-HSD1-FLAG.

REFERENCES

Agarwal, A. K. and R. J. Auchus (2005). "Minireview: cellular redox state regulates hydroxysteroid dehydrogenase activity and intracellular hormone potency." Endocrinology 146(6): 2531-8.

Altan-Bonnet, N., R. Sougrat,β et al. (2006). "Golgi inheritance in mammalian cells is mediated through endoplasmic reticulum export activities." Mol Biol Cell 17(2): 990-1005.

Atanasov, A. G., L. G. Nashev, et al. (2008). "Direct protein-protein interaction of 11β-hydroxysteroid dehydrogenase type 1 and hexose-6-phosphate dehydrogenase in the endoplasmic reticulum lumen." Biochim Biophys Acta 1783(8): 1536-43.

Atanasov, A. G., L. G. Nashev, et al. (2004). "Hexose-6-phosphate dehydrogenase determines the reaction direction of 11β-hydroxysteroid dehydrogenase type 1 as an oxoreductase." FEBS Lett 571(1-3): 129-33.

Avvakumov, G. V., A. Cherkasov, et al. (2010). "Structural analyses of sex hormone-binding globulin reveal novel ligands and function." Mol Cell Endocrinol 316(1): 13-23.

Banner, D. W., A. C. Bloomer, et al. (1975). "Structure of chicken muscle triose phosphate isomerase determined crystallographically at 2.5 angstrom resolution using amino acid sequence data." Nature 255(5510): 609-14.

Bano-Polo, M., F. Baldin, et al. (2011). "N-glycosylation efficiency is determined by the distance to the C-terminus and the amino acid preceding an Asn-Ser-Thr sequon." Protein Sci 20(1): 179-86.

Bennett, M. J., B. P. Schlegel, et al. (1996). "Structure of 3α-hydroxysteroid/dihydrodiol dehydrogenase complexed with NADP+." Biochemistry 35(33): 10702-11.

Blobel, G. and B. Dobberstein (1975). "Transfer of proteins across membranes. I. Presence of proteolytically processed and unprocessed nascent immunoglobulin light chains on membrane-bound ribosomes of murine myeloma." J Cell Biol 67(3): 835-51.

Bosland, M. C. (2000). "The role of steroid hormones in prostate carcinogenesis." J Natl Cancer Inst Monogr(27): 39-66.

Bublitz, C. and S. Steavenson (1988). "The pentose phosphate pathway in the endoplasmic reticulum." J Biol Chem 263(26): 12849-53.

Chen, W. Y. (2008). "Exogenous and endogenous hormones and breast cancer." Best Pract Res Clin Endocrinol Metab 22(4): 573-85.

Comeau SR, G. D., Vajda S, Camacho CJ. (2004). "ClusPro: an automated docking and discrimination method for the prediction of protein complexes." Bioinformatics.

Comeau SR, G. D., Vajda S, Camacho CJ. (2004). "ClusPro: a fully automated algorithm for protein-protein docking." Nucleic Acids Research.

Cooper, W. C., Y. Jin, et al. (2007). "Elucidation of a complete kinetic mechanism for a mammalian hydroxysteroid dehydrogenase (HSD) and identification of all enzyme forms on the reaction coordinate: the example of rat liver 3α-HSD (AKR1C9)." J Biol Chem 282(46): 33484-93.

Cosgrove, M. S., C. Naylor, et al. (1998). "On the mechanism of the reaction catalyzed by glucose 6-phosphate dehydrogenase." Biochemistry 37(9): 2759-67.

Day, J. M., P. A. Foster, et al. (2008). "17β-hydroxysteroid dehydrogenase Type 1, and not Type 12, is a target for endocrine therapy of hormone-dependent breast cancer." Int J Cancer 122(9): 1931-40.

Duclert-Savatier, N., L. Poggi, et al. (2009). "Insights into the enzymatic mechanism of 6-phosphogluconolactonase from Trypanosoma brucei using structural data and molecular dynamics simulation." J Mol Biol 388(5): 1009-21.

Fortunati, N., M. G. Catalano, et al. (2010). "Sex Hormone-Binding Globulin (SHBG), estradiol and breast cancer." Mol Cell Endocrinol 316(1): 86-92.

Frick, C., A. G. Atanasov, et al. (2004). "Appropriate function of 11β-hydroxysteroid dehydrogenase type 1 in the endoplasmic reticulum lumen is dependent on its N-terminal region sharing similar topological determinants with 50-kDa esterase." J Biol Chem 279(30): 31131-8.

Geck, M. K. and J. F. Kirsch (1999). "A novel, definitive test for substrate channeling illustrated with the aspartate aminotransferase/malate dehydrogenase system." Biochemistry 38(25): 8032-7.

Goeckeler, J. L. and J. L. Brodsky (2010). "Molecular chaperones and substrate ubiquitination control the efficiency of endoplasmic reticulum-associated degradation." Diabetes Obes Metab 12 Suppl 2: 32-8.

Griffin, J. E. O., Sergio R. (2004). Textbook of Endocrine Physiology.

Heyns, W. and P. De Moor (1974). "A 3(17)β-hydroxysteroid dehydrogenase in raterythrocytes. Conversion of 5α-dihydrotestosterone into 5α-androstane-3β,17β-diol and purification of the enzyme by affinity chromatography." Biochim Biophys Acta 358(1): 1-13.

Hosfield, D. J., Y. Wu, et al. (2005). "Conformational flexibility in crystal structures of human 11β-hydroxysteroid dehydrogenase type I provide insights into glucocorticoid interconversion and enzyme regulation." J Biol Chem 280(6): 4639-48.

Huang, X., H. M. Holden, et al. (2001). "Channeling of substrates and intermediates in enzyme-catalyzed reactions." Annu Rev Biochem 70: 149-80.

Khan, N., K. K. Sharma, et al. (2004). "Human 17β-hydroxysteroid dehydrogenases types 1, 2, and 3 catalyze bi-directional equilibrium reactions, rather than unidirectional metabolism, in HEK-293 cells." Arch Biochem Biophys 429(1): 50-9.

Kotelevtsev, Y., M. C. Holmes, et al. (1997). "11β-hydroxysteroid dehydrogenase type 1 knockout mice show attenuated glucocorticoid-inducible responses and resist hyperglycemia on obesity or stress." Proc Natl Acad Sci U S A 94(26): 14924-9.

Kozakov, D., D. R. Hall, et al. (2010). "Achieving reliability and high accuracy in automated protein docking: ClusPro, PIPER, SDU, and stability analysis in CAPRI rounds 13-19." Proteins 78(15): 3124-30.

Kozakov D, B. R., Comeau SR, Vajda S. (2006). "An FFT-based protein docking program with pairwise potentials." Proteins.

Lavery, G. G., E. A. Walker, et al. (2006). "Hexose-6-phosphate dehydrogenase knock-out mice lack 11β-hydroxysteroid dehydrogenase type 1-mediated glucocorticoid generation." J Biol Chem 281(10): 6546-51.

Lavery, G. G., E. A. Walker, et al. (2008). "Steroid biomarkers and genetic studies reveal inactivating mutations in hexose-6-phosphate dehydrogenase in patients with cortisone reductase deficiency." J Clin Endocrinol Metab 93(10): 3827-32.

Liu, C. W., M. J. Corboy, et al. (2003). "Endoproteolytic activity of the proteasome." Science 299(5605): 408-11.

Luu-The, V., Y. Zhang, et al. (1995). "Characteristics of human types 1, 2 and 3 17β-hydroxysteroid dehydrogenase activities: oxidation/reduction and inhibition." J Steroid Biochem Mol Biol 55(5-6): 581-7.

Ma, B. G., L. Chen, et al. (2008). "Characters of very ancient proteins." Biochem Biophys Res Commun 366(3): 607-11.

Mazza, C., R. Breton, et al. (1998). "Unusual charge stabilization of NADP+ in 17β-hydroxysteroid dehydrogenase." J Biol Chem 273(14): 8145-52.

McCormick, K. L., X. Wang, et al. (2006). "Evidence that the 11β-hydroxysteroid dehydrogenase (11β-HSD1) is regulated by pentose pathway flux. Studies in rat adipocytes and microsomes." J Biol Chem 281(1): 341-7.

Meyer, A. J. and T. P. Dick (2010). "Fluorescent protein-based redox probes." Antioxid Redox Signal 13(5): 621-50.

Miles, E. W., S. Rhee, et al. (1999). "The molecular basis of substrate channeling." J Biol Chem 274(18): 12193-6.

Miller, W. L. and R. J. Auchus (2011). "The molecular biology, biochemistry, and physiology of human steroidogenesis and its disorders." Endocr Rev 32(1): 81-151.

Mizrachi, D. and R. J. Auchus (2009). "Androgens, estrogens, and hydroxysteroid dehydrogenases." Mol Cell Endocrinol 301(1-2): 37-42.

Moore, C. C., S. H. Mellon, et al. (1993). "Structure and function of the hepatic form of 11β-hydroxysteroid dehydrogenase in the squirrel monkey, an animal model of glucocorticoid resistance." Endocrinology 133(1): 368-75.

Munro, S. and H. R. Pelham (1987). "A C-terminal signal prevents secretion of luminal ER proteins." Cell 48(5): 899-907.

Myers, M., M. C. Lamont, et al. (2007). "Role of luteal glucocorticoid metabolism during maternal recognition of pregnancy in women." Endocrinology 148(12): 5769-79.

Negri, M., M. Recanatini, et al. (2010). "Insights in 17β-HSD1 enzyme kinetics and ligand binding by dynamic motion investigation." PLoS One 5(8): e12026.

Odermatt, A., P. Arnold, et al. (1999). "The N-terminal anchor sequences of 11β-hydroxysteroid dehydrogenases determine their orientation in the endoplasmic reticulum membrane." J Biol Chem 274(40): 28762-70.

Odermatt, A., A. G. Atanasov, et al. (2006). "Why is 11β-hydroxysteroid dehydrogenase type 1 facing the endoplasmic reticulum lumen? Physiological relevance of the membrane topology of 11β-HSD1." Mol Cell Endocrinol 248(1-2): 15-23.

Pan, S., C. J. World, et al. (2009). "Glucose 6-phosphate dehydrogenase is regulated through c-Src-mediated tyrosine phosphorylation in endothelial cells." Arterioscler Thromb Vasc Biol 29(6): 895-901.

Papari-Zareei, M., A. Brandmaier, et al. (2006). "Arginine 276 controls the directional preference of AKR1C9 (rat liver 3α-hydroxysteroid dehydrogenase) in human embryonic kidney 293 cells." Endocrinology 147(4): 1591-7.

Pelham, H. R. (1990). "The retention signal for soluble proteins of the endoplasmic reticulum." Trends Biochem Sci 15(12): 483-6.

Percy, M. J., P. W. Furlow, et al. (2008). "A gain-of-function mutation in the HIF2A gene in familial erythrocytosis." N Engl J Med 358(2): 162-8.

Rosner, W., D. J. Hryb, et al. (2010). "Interactions of sex hormone-binding globulin with target cells." Mol Cell Endocrinol 316(1): 79-85.

Sambrook, J. a. R., David W. (2001). Molecular cloning : A Laboratory Manual. Cold Spring Harbor, N.Y.

Sawicki, M. W., M. Erman, et al. (1999). "Structure of the ternary complex of human 17β-hydroxysteroid dehydrogenase type 1 with 3-hydroxyestra-1,3,5,7-tetraen-17-one (equilin) and NADP+." Proc Natl Acad Sci U S A 96(3): 840-5.

Schröder, M. (2008). "Endoplasmic reticulum stress responses." Cell Mol Life Sci. 65(6): 862-94.

Senesi, S., M. Csala, et al. (2010). "Hexose-6-phosphate dehydrogenase in the endoplasmic reticulum." Biol Chem 391(1): 1-8.

Sherbet, D. P., O. L. Guryev, et al. (2009). "Biochemical factors governing the steady-state estrone/estradiol ratios catalyzed by human 17β-hydroxysteroid dehydrogenases types 1 and 2 in HEK-293 cells." Endocrinology 150(9): 4154-62.

Teasdale, R. D. and M. R. Jackson (1996). "Signal-mediated sorting of membrane proteins between the endoplasmic reticulum and the golgi apparatus." Annu Rev Cell Dev Biol 12: 27-54.

Thoden, J. B., H. M. Holden, et al. (1997). "Structure of carbamoyl phosphate synthetase: a journey of 96 A from substrate to product." Biochemistry 36(21): 6305-16.

Veech, R. L., L. V. Eggleston, et al. (1969). "The redox state of free nicotinamide-adenine dinucleotide phosphate in the cytoplasm of rat liver." Biochem J 115(4): 609-19.